Defect and fracture detection using Acoustic Emission Monitoring

By

Gerswynn Mckuur

A dissertation submitted to the Faculty of Engineering and the Built Environment in partial fulfilment of the degree of Master of Science in Engineering.

Department of Mechanical Engineering
University of Cape Town
2006

Declaration

I know that plagiarism is wrong. Plagiarism is to use another's work and pretend that it is one's own.

Each significant contribution to, and quotation in this report from the works of other people has been attributed, cited and referenced.

This report is my own work.
I have not allowed and will not allow anyone to copy my work with the intention of passing it off as their own.

Gerswynn Mckuur

Signed by candidate

SYNOPSIS

This thesis is a consolidation of work that investigates the flaw detection capabilities of Acoustic Emission (AE) technology applied to metal alloys and composite materials. The thesis explores the background to AE and how it is applied to flaw detection and fracture characterisation.

In preliminary tests, a steel pressure vessel and a filament wound composite pressure vessel were used in hydro proofing tests. Each of the vessels had existing flaws/defects in them. The locations of these flaws were known. Acoustic emission sensors were placed on the surface of the vessels, the vessels were subjected to a pressurising programme, and the AE equipment was used in order to confirm the locations of these flaws.

The results showed that the locations of the flaws could be confirmed with AE. The flaws were detected within ±4% uncertainty in the steel vessel, and within ±14% in the composite vessel. The larger uncertainty in the composite as opposed to the steel vessel shows that the composite emits more acoustic activity in the area of the flaw due to possible sources of matrix cracking, fibre breakage or interfacial friction. These mechanisms are not present in the steel vessel.

To investigate the fracture characterisation capabilities of the AE system, two sets of tests were conducted. Fracture toughness tests were conducted on a steel alloy, ROQ-

tuf AD 690 whilst monitored with AE equipment. In the second set of tests, glass fibre composite specimens were monitored with AE equipment during tensile tests. In these tests two lay-up configurations were used, i.e., transverse and longitudinal lay-ups.

The results showed that the AE activity during a fracture toughness test followed a predictable trend. The stages of crack development namely, Linear Elastic extension, Plastic blunting and Crack tearing, were clearly defined. The AE results surprisingly indicated that the blunting phase produced up to seven times more AE activity than the tearing phase.

The composite testing showed that fibre breakage and matrix cracking have two distinct AE activity traces associated with them. The most notable difference is however, that fibre breakage produces up to ten times more AE activity than matrix cracking.

ACKNOWLEDGEMENTS

The author wishes to thank the following people for their contributions towards the completion of this thesis.

Professor J. Gryzagoridis, my supervisor, whose knowledge, perseverance and guidance were invaluable to the completion of this work and Professor R.B. Tait for his extensive input into the fracture toughness testing and theory.

Mr. Hubert Tomlinson and the workshop staff in the Department of Mechanical Engineering for the impeccable work they delivered in the preparation of specimens and apparatus. Furthermore, I wish to thank them for their continued encouragement during this process.

Messrs. K. Mokolobate, C. Masekoameng and A. Runciman, who were all instrumental in the compilation of this work.

I wish to thank my family for their continued support, encouragement and prayers to make this achievement possible.

TABLE OF CONTENTS

LIST OF ABBREVIATIONS

AE	Acoustic Emission
BS	British Standard
COD	Crack tip Opening Displacement
dB	Decibels
EPFM	Elastic Plastic Fracture Mechanics
ESH	Electronic Servo Hydraulic
HFVF	High Fibre Volume Fraction
kHz	Kilo Hertz
kN	Kilo Newton
LEFM	Linear Elastic Fracture Mechanics
LFVF	Low Fibre Volume Fraction
MARSE	Measured Area Under the Rectified Signal Envelope
NDT	Non Destructive Testing
Pa	Pascal
PAC	Physical Acoustics Corporation
SEN	Single Edge Notch
wt %	Weight percentage

1. Introduction

Industry is always looking to find cost-effective ways to increase the life span of its plant and to ensure that it remains serviceable. A method that has been used successfully to help to do this is Non Destructive Testing (NDT). NDT inspection of pressure vessels for defects is a good example.

NDT includes a number of different techniques, one of which is Acoustic Emission (AE) Monitoring. Research in AE monitoring started in the 1950's [1] and was successfully implemented as an industrial NDT method in the 1970's [1, 2]. The technique is therefore relatively new when compared to the other, more established, techniques such as Pulse-Echo Ultrasonic Inspection, Eddy Current Testing, and X-Ray Radiography, to name but a few [1-3].

An acoustic emission, sometimes called a Stress Wave Emission, is an elastic stress wave released in a material when there is permanent plastic deformation due to the application of a load [1, 2]. This emission is an indication that there has been a microscopic change. The method depends on the detection and evaluation of these emissions to indicate the presence of active flaws and their significance, e.g. twinning, slip, micro crack formation, and crack tearing [4, 5]. Piezo-electric transducers in contact with the surface of the test piece monitor the level of this activity by sensing the surface movement caused by the impinging stress wave [2]. The received signals are processed and finally displayed as shown in the Fig. 1.1.

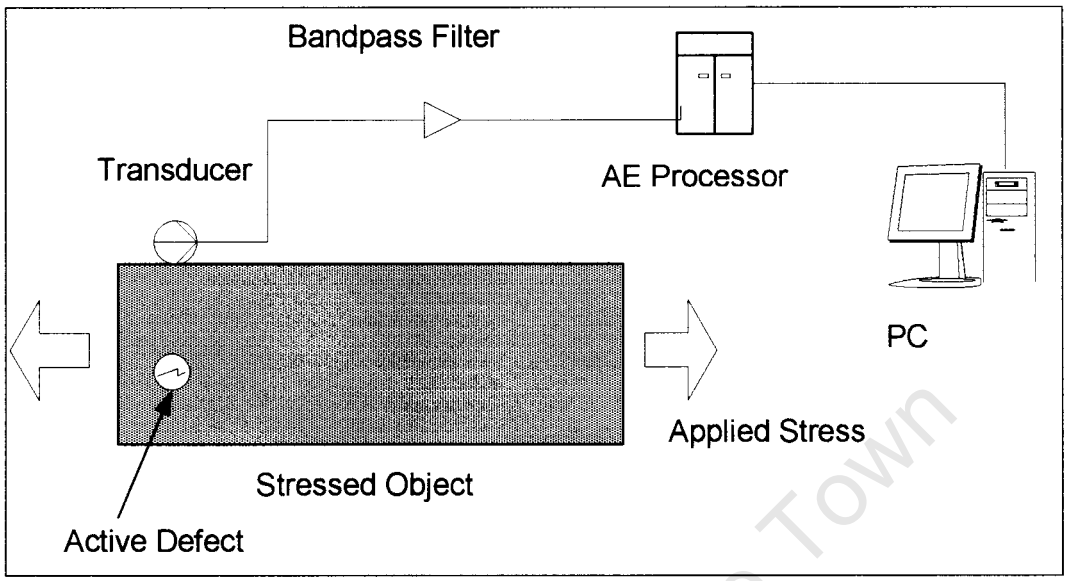

Figure 1.1 Test setup for detecting and monitoring an Acoustic Emission.

AE is able to examine a large area, e.g. the complete surface area of a pressure vessel, at a time, and it is possible to locate as well as assess active flaw sites [1, 2]. Over the years, the emphasis in industry has been on the location of, rather than the assessment, of these active sites.

When locating material defects, AE technology uses linear interpolation or triangulation algorithms to do so. This requires the use of two, in the former case, or more sensors, in the latter to pin point the location of such active sites [2-4]. In the case of metal structures, these defect sites are found relatively easily. On the other hand composite materials, by their very nature are noisy, which makes detection more challenging [5].

Recently, research has been directed towards monitoring and evaluating the fracture processes in materials such as metals and composites [6]. This new approach uses AE as a tool for component life prediction by looking at the quantity and characteristics of the activity arising from flaw sites [5, 6].

From the study of Linear Elastic Fracture Mechanics (LEFM) and Elastic Plastic Fracture Mechanics (EPFM) it has been shown that metal specimens with atomically sharp cracks, subjected to a monotonically rising load, fail in a predictable way [7-10]. This fracture process can be categorized in the manner shown in Fig. 1.2. Other studies [11-23] have hinted that this fracture process can be characterized as a repeatable AE trace.

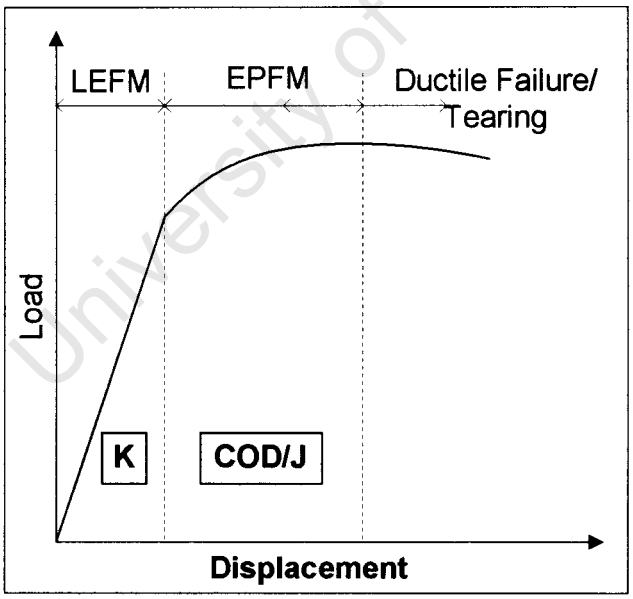

Fig 1.2 A typical load deflection curve for a structural steel

Similarly, in the case of composites, if the modes of failure due to a monotonically rising load can be isolated and monitored by AE, the same inference may be made.

It is therefore, my intention to explore whether AE can be used as a reliable tool to characterize the fracture process for these materials. If successful, this model will serve as a predictive tool for the fracture process in steels. In the case of composites it may serve to show what the AE characteristics for each mode of failure may be [24, 25].

This thesis starts by introducing the technology of AE, the science of Fracture Mechanics and that of composite materials. It then looks at previous studies that have investigated the relationship between material fracture and AE. Preliminary experiments were done in both metal and composite structures to show the flaw/defect detection capability of the system. Then, various standardized Composite material tests and Fracture Toughness tests were done in order to show the repeatability of the AE outputs. The test results are presented, discussed and finally conclusions are drawn from the analyses.

2. Background and Literature Review

2.1 Historical Background and Principles of Acoustic Emission Testing

2.1.1 Introduction

In 1950 J. Kaiser initiated the theoretical work for Acoustic Emission (AE) monitoring; it was first used by industry in 1964, but really only came of age in the late 1970's. AE is thus one of the least mature of the NDT methods but is now being used as a routine method [2, 3]. The technique has been successfully applied in a number of areas, for example in corrosion detection inside cylinders, detecting problems in composite components and structural testing of aircraft, bridges, railroad tank cars, and rotating machinery [1-5].

When a solid is stressed to a certain level, discreet acoustic wave packets, emanating from processes such as micro-crack formation and twinning, are generated that can be detected by transducers placed on it [4]. In the 1960's when this new non-destructive testing technology was born it was found that growing flaws in pressure vessels could be picked up by monitoring their acoustic wave packets. The phenomenon, that causes the generation of sound in materials under stress, was termed acoustic emission (AE), or Stress Wave Emission. Included in the materials that exhibit this phenomenon are the well-known metallic alloys such as steels [1].

AE monitoring relies on the detection and quantification of transient elastic stress waves caused by sudden deformation, such as localised yielding, in a stressed

material. These waves travel from the source to the mounted transducers where they are converted to electrical signals that can be stored, processed and manipulated for interpretation by the operator [2].

In some materials, such as wood and rock, signals are often audible. However, in many other engineering materials, like metals and composites, the signals are inaudible and require more sensitive AE detection devices.

The major difference between AE and most other NDT techniques is that it detects microscopic movements, not geometric discontinuities. AE is unique in that it can identify damage in real time, i.e. when damage initiates or as it propagates. Furthermore, AE equipment does not introduce energy into the test piece like ultrasound does, for example. It is therefore a passive NDT method.

Typical applications for AE include [1]:

- Fracture Mechanics testing
- Fatigue Mechanics monitoring
- Composite tank testing
- Nuclear Plant monitoring
- Leak detection
- General weld monitoring
- Buried pipeline monitoring

2.1.2 Stressing the Structure and the Kaiser Effect

A distinguishing aspect of AE is that the inspected component requires the application of some kind of stimulus. This stimulus may take the form of a mechanical loading, pressure, or even a thermal gradient. Therefore, the loading programme is essential to the success of an AE test.

Structures will emit acoustically only when they are loaded above any previously applied load. This phenomenon is known as the Kaiser Effect [1, 3]. The principle is that on the first loading, a structure will undergo permanent plastic deformation especially at regions of stress concentration; but thereafter the material will behave elastically, not giving any more emission, until the load is taken higher. The Kaiser effect is an important principle and serves as a fundamental starting point for most AE testing procedures.

2.1.3 Traditional AE Monitoring and Measurement Parameters

When an acoustic emission wave front impinges on the surface of a test object, minute movements (of the order of nanometres) of the surface molecules occur. The transducers on the surface of the test object detect the motion and convert the detected motion into data in the form of a voltage-time signal. These data are used in subsequent steps of the technique [1-3].

AE transducers are very sensitive piezoelectric sensors that detect the surface movement caused by an emission. The AE sensors are usually resonance sensors, which means, they are only very sensitive to a certain frequency. Since the AE signals are very weak, a preamplifier is employed right after the AE transducer to prevent the signal loss [2].

The voltage-time signals pass through a filter to remove electronic interference, whilst the main amplifier enlarges the signals before they are sent to the signal conditioner. Thereafter, certain features are extracted and stored for further analysis. During investigations, other parameters, such as load, deformation, pressure, and temperature, can also be recorded [2].

A typical AE signal/event, as well as the commonly measured parameters as detected, is shown in Figure. 2.1. Health monitoring of a structure is usually carried out in the presence of continuous background noise and therefore a threshold detection level is set somewhat above the background level to serve as a reference for the waveform properties.

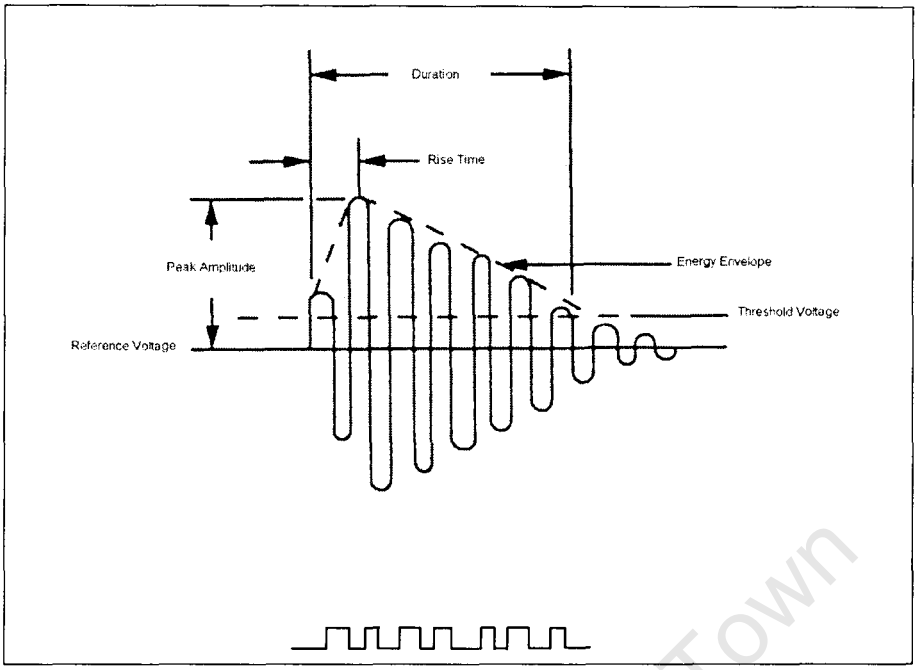

Figure 2.1 AE signal and Measured Parameters [2]

2.2 Historical Background and Principles of Fracture Mechanics

The fracture toughness of a material can be described as a material's resistance to cracking. We are able to relate fracture toughness to the stress applied to the material and the flaw size within the material by a relationship defined as the triangle of integrity. This concept forms the basis of the discipline known as a fracture mechanics [7].

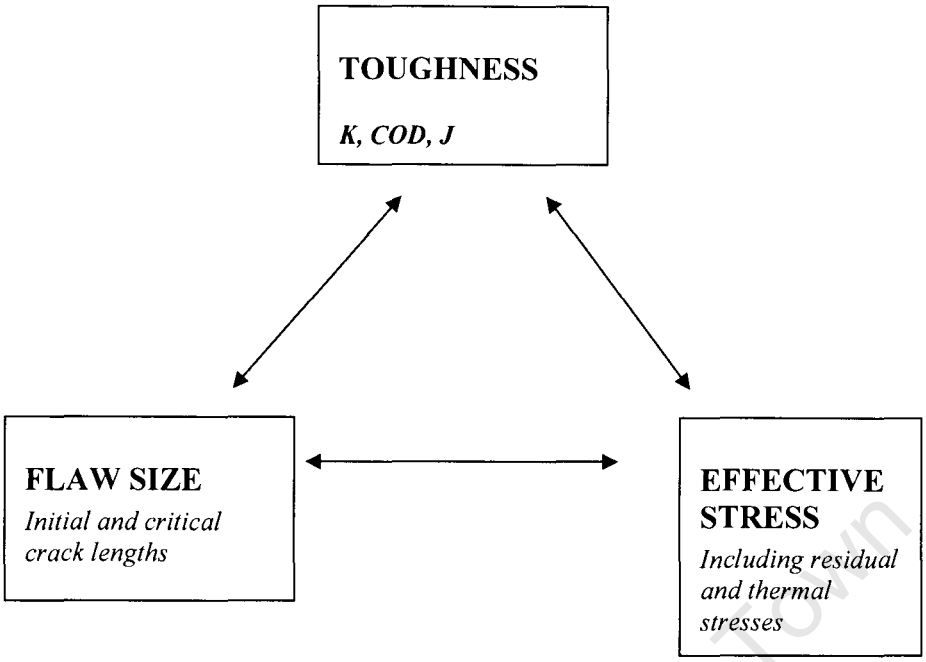

Figure 2.2 Triangle of Integrity describing the interrelationship between materials design and fabrication [7]

2.2.1 The Foundations of Linear Elastic Fracture Mechanics (LEFM)

During the course of experimental procedures in the early twentieth century it was found that a discrepancy existed between the actual strength of brittle materials and the theoretical estimates. The reason for this discrepancy was thought to be the flaws that exist in materials and subsequently decrease the strength of the materials by magnifying the local stresses in the material.

The first quantitative evidence of the effect of flaws on material properties was provided by Inglis 1913, who considered the effect of local stresses caused by elliptical holes formed in flat plates [9].

In 1920, Griffith furthered the development of the fracture theory in brittle flawed materials, by balancing the stored energy and the surface energy of the material [10]. He considered the total change of energy of a cracked body as the crack length increased and used both surface and internal cracks acting as stress concentrations. His explanations equated the rate at which the crack grows (work done) to the elastic strain energy released to supply the surface energy of the newly formed crack surface. He therefore found that,

$$\sigma_f = \sqrt{\frac{2\gamma_s E}{\pi a}} \qquad (1)$$

Where σ_f, is the applied stress, γ_s is the surface energy of the newly formed crack surfaces per unit area, **E** is the Young's modulus for the material, and **a** is the crack length [9].

In 1934 Irwin modified Griffith's equation to account for local plasticity and developed the concept of an energy release rate (G) as the driving force for crack propagation [9]. This driving force was then compared to the material resistance (due to elastic and plastic work required to form two new surfaces) to determine whether the crack would propagate, thus resulting in the following equation,

$$\sigma_f = \sqrt{\frac{2(\gamma_s + \gamma_p)E}{\pi a}} \qquad (2)$$

Where γ_p is the work done in plastic deformation, per unit area of the crack surface.

The above equation gives a simple basis for fracture. The defining parameter for fracture being $\sigma\sqrt{\pi a}$ which is known as the stress intensity factor, denoted by **K,** and has dimensions of MPa m $^{1/2}$. If the value of **K** should exceed a given value for a particular material the crack becomes unstable and fracture occurs [7]. This parameter is the critical fracture toughness $\mathbf{K_{IC}}$.

In cases where there is an increase in the ductility of the material and there is significant crack tip plasticity, this analysis by LEFM becomes invalid and other fracture toughness parameters pertaining to elastic-plastic fracture mechanics need to be considered.

2.2.2 The Development of Elastic Plastic Fracture Mechanics

Elastic plastic fracture mechanics applies to materials, which exhibit plastic deformation and two elastic-plastic toughness parameters are introduced

Crack tip opening displacement (**COD**), and

The **J** contour integral

The origin of these parameters can be attributed to A. A. Wells and J. R. Rice, respectively [9].

A.A. Wells found that the results he obtained during his experimentation could not be characterised by linear elastic fracture mechanics. Wells noticed during his experiments that the crack faces of his specimens moved apart prior to fracture and the plastic deformation of the specimens blunted the initially sharp crack. Wells also discovered that the degree of crack blunting increased in proportion to toughness of material [10]. It was this observation which led him to propose that the opening of a crack tip was a measure of fracture toughness and it is this which is known today as crack tip opening displacement (COD). Wells presumed that the COD is an appropriate crack tip characterising parameter when linear elastic fracture mechanics is no longer valid.

Further development of elastic plastic fracture mechanics led J.R. Rice to assume that non-linear elastic behaviour may be valid for an elastic-plastic material [9, 10]. Rice applied the deformation theory of plasticity that relates the total strains to the stresses in a material and is equivalent to non-linear elasticity. J.W. Hutchinson, G.F. Rosenberg and J.R. Rice also showed, through further experimentation, that the **J – integral** uniquely characterises crack tip stresses and strains in non-linear material [9, 10]. Therefore the **J**-integral can be viewed as both and energy parameter where it can be equated to **G** for LEFM cases, and a stress intensity factor similar to **K** in LEFM.

2.2.3 Crack Growth Resistance Curves

In this thesis, **COD** was used as the fracture toughness parameter. Materials with high toughness do not fail catastrophically at any specific value of **COD**, but fail by micro-void coalescence, the associated fracture mechanism for ductile metals. High toughness also increases the amount of work hardening occurring in the material and this also resists crack growth. [9, 10]

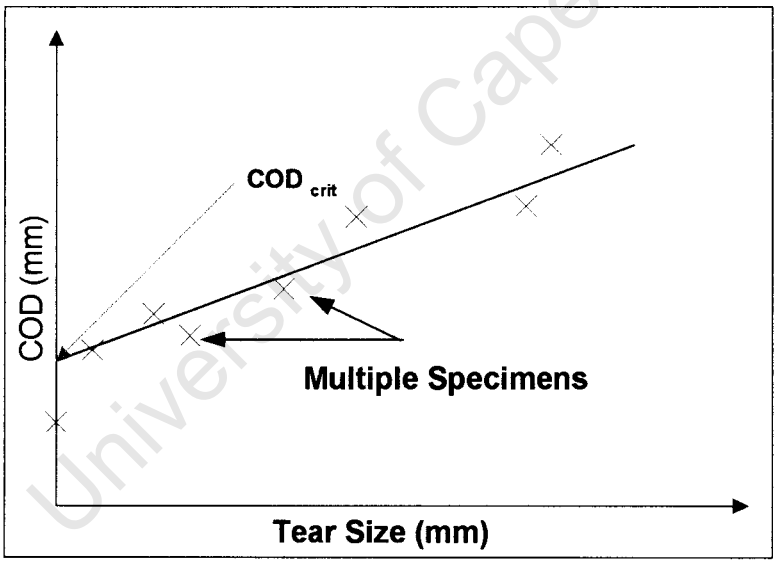

Fig 2.3. Crack Growth resistance curve, showing definition of COD_{crit} for crack initiation and for crack growth [8]

The concept of crack growth resistance has in the past been shown as a **COD** – resistance curve. The curve shown in Fig 2.3 describes the three stages of crack development.

The initial stages of deformation show the **Resistance (R)** curve to be vertical, representing small amounts of crack blunting. When the local stresses at the crack tip become large enough, the crack begins to advance. The point is known as crack initiation and is labelled $\mathbf{COD_{crit}}$. The crack then develops by stable crack growth.

2.2.4 Experimental Methods Applied for COD Measurements

The multiple specimen technique used to determine $\mathbf{COD_{crit}}$ involves loading many, nominally equal, specimens to different loads, heat tinting the specimens and then breaking them open to measure the crack lengths. The results are then plotted on graphs of **COD** – integral vs. tear size and then analysed [8].

Since AE is associated with the plastic deformation of a material, the potential exists to use acoustic emission to monitor crack growth development.

2.3 Acoustic Emission in Fracture Mechanics Principles

The presence of flaws and notches in a stressed material causes localised plastic deformation at stresses below the yield stress of the material.

2.3.1 Energy generated during Deformation of steel

According to Palma and Stafford [13], and others [14-23], energy is released during the fracture process of metals in two forms viz. energy released during the processes of crack initiation and propagation.

It was further observed that in stationary cracks, emissions could be generated only under rising loading conditions due to the Kaiser Effect [1-3]. Palma and Stafford said this about crack growth; "The crack growth was due to the coalescence of plasticity induced voids. The fracture surfaces confirmed this by exhibiting shear dimples. Although the continuation of these tests produced weak AE activity, the ultimate failure process was identified by an increasing stress wave count" [13].

2.3.2 Acoustic Emission in the Fracture Process

The main source of acoustic emission in loaded metals was found to be plastic deformation as mentioned above. During the initiation of plastic deformation, at or near the yield stress, a high level of acoustic emission activity will be observed. This was found at the onset of macro plastic deformation resulting from simultaneous motion of many dislocations [14].

Jones and Brown [23] conducted a study to assess the usefulness of AE for determining the plane strain fracture toughness. The results showed definite acoustic indications of pop-in, which were too small to pick up with compliance gauges. The K_{IC} values based on the AE were usually slightly lower than those based on

compliance gauges due to the higher sensitivity of AE. This showed the advantage of AE for use in this type of testing. A major disadvantage of the method at the time was its susceptibility to extraneous noise, which could be confused with actual pop-in.

Baker [22] investigated the limiting sensitivity for reliably detecting crack initiation and or growth in high strength steels using the Stress Wave Analysis Technique (SWAT) or AE. Certain samples were heat treated to provide both conditions of high strength-low fracture toughness, and low strength –high fracture toughness. This study indicated that that the material type and heat treatment appeared only to affect the type of micro cracking that occurred, but did not appreciably alter the minimum detectable crack size.

Hartbower [17] conducted tensile tests on single edge notched (SEN) specimens of HY-80 and HY-150 and D6aC low alloy high strength steel to correlate AE characteristics with crack instability. He indicated that plane stress instability was always accompanied by an increasing emission rate generally starting at approximately at the plane strain pop-in point. Highly brittle D6aC fractured immediately after plane strain pop-in with only two or three intervening emission bursts. From this investigation the conclusions were that crack growth could reliably be detected by SWAT and that AE was capable of providing recognizable, reproducible data that could serve to identify plane strain instability and the onset of plane stress instability

Aero-jet investigators, in the same way as Dunegan [12], attempted to develop a quantitative relationship between AE and flaw size. In the investigation they concluded that the analysis of the frequency spectrum was a powerful tool. The results of these tests re-emphasized the need for laboratory studies to characterise the crack growth process of specific materials when AE will be used for structural monitoring applications.

2.4 Background on Composite Materials

2.4.1 Definitions

A composite material is a combination of two or more materials which retain their individual characteristics as they act together. The combination of the constituent materials produces properties and characteristics that are different from those of the constituents.

One of these constituents forms a continuous phase and is called the matrix. The other major constituents are reinforcement in the form of fibres or particulates. The reinforcement forms a discontinuous phase and serves to improve the matrix properties. The matrix of a composite may be a polymer, a metal, or a ceramic. Composite materials are named depending on the type of matrix material it has, e.g., polymer matrix composite or metal matrix composite [24, 27].

"The primary effect of the reinforcement in a composite depends somewhat on the matrix used for example; polymers have very low modulus and strength compared to the reinforcing fibers used in polymer matrix composites."[27] Thus, in these composites, the addition of fibers serves to increase the modulus and strength of the polymer matrix. Fibers are the more commonly used reinforcements in polymer matrix composites [24].

Laminated composites are composites with multiple layers, which can have different fiber type, fiber orientation and fiber architecture. Each layer is called a lamina or a

ply. "The order in which the laminae with different fiber orientations are stacked is called the stacking sequence and is engineered to obtain the desired stiffness and/or strength for the laminate." [27] Laminates in which the fiber orientation is the same in all laminae are called the unidirectional laminate.

Failures in composites initiate from flaws in the material. Failure/Damage in composite materials occurs in the basic forms of matrix cracking, fiber-matrix interfacial debonding, fiber fracture, and fiber pull-out [24].

2.4.2 Failure Modes in Composites

2.4.2.1 Matrix cracking

Matrix cracking is one of the first forms of damage that occurs in a fiber-reinforced composite. "The formation of matrix cracks is influenced strongly by the laminate's internal and external geometries, including laminae fiber orientations, laminae thickness and laminae stacking sequence." [27] Matrix cracking is mostly observed in 90^0 plies during axial loading in the 0° direction. These micro cracks are called transverse cracks because they are transverse to the loading direction.

2.4.2.2 Fibre/Matrix interfacial debonding

When a matrix crack approaches the neighbouring fibres, the stress field ahead of the crack tip will induce shear stress at the fibre/matrix interface." [27] If

the interface debonds relatively easily, the interfacial debonding will occur in a zone ahead of the crack tip.

2.4.2.3 Fibre Breakage

This failure mode occurs at the final stages of laminate failure. As the matrix crack develops, there is nothing transferring loads between fibres. Some fibres will carry most of the load, resulting in them breaking under the load.

2.4.2.4 Fibre pull-out matrix/fibre

This failure occurs in certain composites, in which the matrix/fibre interfacial bonds are weak. Due to the weak interfacial bonds, the fibres pull-out of the matrix.

3. Experimental Procedure

3.1 The Acoustic Emission Set up

The AE system used for testing was the 8000 Spartan AT (a product of the *Physical Acoustics Corporation (PAC))*. The system is computerized and stores, analyzes and displays captured data. The data captured are the acoustic signals from the loaded test specimen. As stated before, these signals are converted to electrical signals by the sensors, amplified and measured.

For the experimental work, the *PAC* R15 and R15I sensors were used. These are very practical resonant type sensors. The difference between the two is the integral pre amplifier that is housed in the R15I (Figure 3.1). These sensors have one or more preferred frequencies of oscillation. The waveform and the spectrum are therefore dominated by these preferred frequencies [2].

Figure 3.1 Picture of the R15I and R15 sensors

The above mentioned sensors are recommended for use on small specimens [2] and are resonant at 150 kHz. Furthermore the system is fitted with band pass filters for the range 100-300 kHz.

In addition to the selection of sensor and filters, it is important that the settings of Threshold and Gain are such that the effects of a noisy environment are negated. Therefore, for medium to low sensitivity Threshold values between 40 and 50dB were chosen as well as a Gain of 20-30 dB [2]. Also there are certain timing constants that can be set:

- Peak Definition Time (PDT) – Enables the determination of the true peak of the signal
- Hit Definition Time (HDT) – When a signal first crosses the threshold voltage, the hit/event is registered. The HDT determines how long the system will wait to register the hit as complete
- Hit Lock-out Time (HLT) – The minimum delay after a hit has ended, before which a new hit can be registered.

The acoustic emission properties of the sensors are given in Table 3.1.

Table 3.1 Acoustic properties of the AE sensors used [2]

Small size, stainless steel construction
Operation range -45°C to 80°C
Good RFI/EMI immunity
Wide dynamic range (>80dB)
Low noise preamp (<1.0μV)
Single BNC input/output (Power/Signal)
Interchangeable with existing preamp/sensors
Ideal for Field/Lab testing

As described before, it is possible to measure various parameters associated with an AE waveform. Therefore measurements of Hit Rate, Count Rate, Energy Rate (or

MARSE) and Peak Amplitude can be taken for each test. These parameters are presented in readable displays that stem from the associated software package (*SU-DAQ.EXE*, also a *PAC* product). The programme allows Threshold and Gain, as well as various display types to be set.

Once these parameters have been loaded, the tests are conducted as outlined in the sections below.

3.2 Preliminary Tests for Defect Location

Preliminary tests were done to show the detection capabilities of the AE system. These comprised hydro-proof testing of pressure vessels in a similar manner to those of Barthelemy, et al [29-33]. A steel pressure vessel was pressurised in a manner simulating an actual in service test, i.e. the pressure was increased and decreased to a set programme [29, 34] shown in the table.

Table 3.2 A typical pressurisation sequence for defect location

Pressure (kPa)	0-500	500-0	0-1000	1000-0	0-1500	1500-0	0-2000
Time Elapsed (s)	0-30	30-60	60-90	90-94	94-120	120-131	131-135

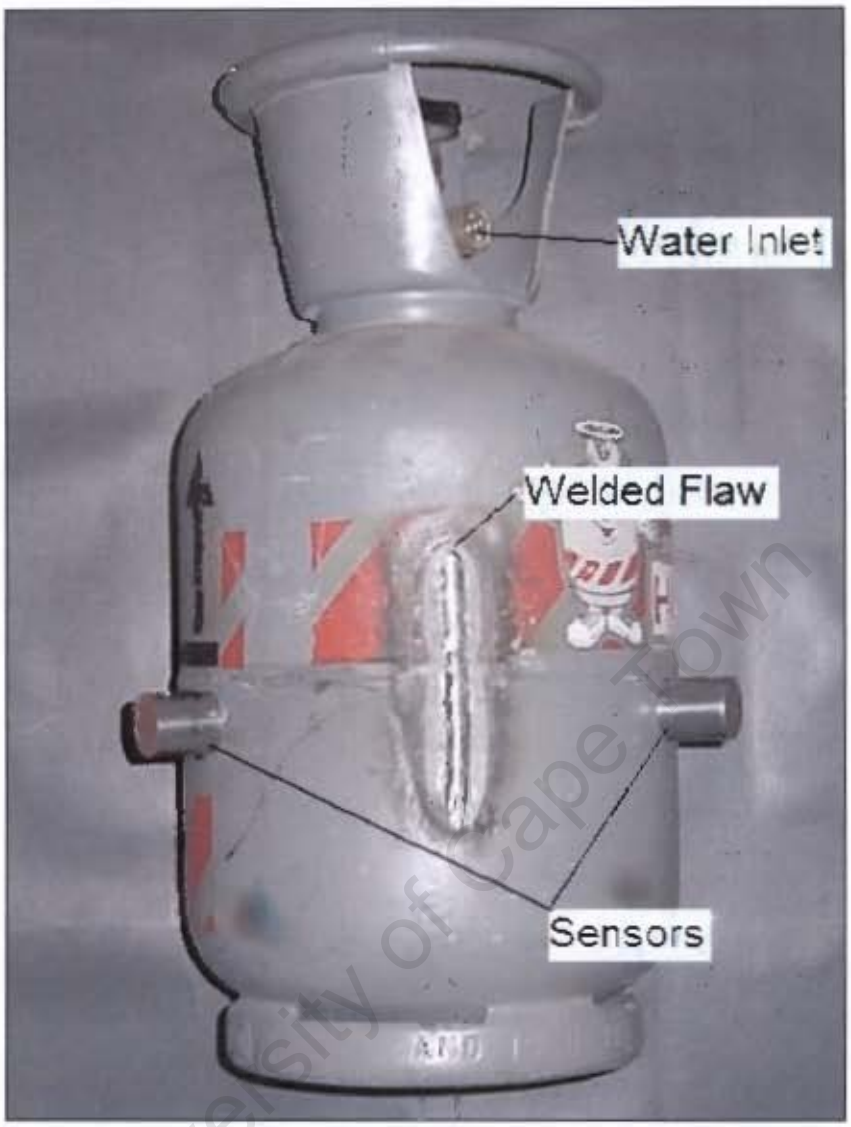

Figure 3.3 Photograph of a similar steel pressure vessel with two sensors attached and the welded flaw

Typically, two R151 sensors were mounted on either side of an existing flaw, a set distance apart, perpendicular to the flaw in an in-line arrangement as in Figure 3.3.

A steel pressure vessel with the following dimensions was used:

- Outer diameter – 185mm
- Height – 350mm

An existing flaw was welded shut to the following dimensions:

- Weld height from surface - 1.7mm
- Weld length - 130mm.

The composite pressure vessel comprised filament wound pressure vessel that was pressurised in a similar way to the steel vessel [30-32].

Figure 3.4 Photograph of a similar composite pressure vessel with two sensors attached

The dimensions were as follows:

- Inner diameter – 176.5mm
- Outer diameter – 179.8mm
- Height – 200mm

An artificial flaw was machined into the outer surface.

The penny-shaped flaw was typically 18mm long and 1.2mm deep.

3.3 Fracture Toughness Testing in a Structural Steel

3.3.1 Test material for Fracture Toughness Tests

The material used for the fracture toughness tests was a tough, high strength low alloy structural steel (ROQ-tuf AD 690). The chemical composition of this steel is given in Table 3.4.

Table 3.4: Material composition (wt. %) of ROQ-tuf AD 690 using Scanning Electron Microscopy

Grade	C	Mo	Mn	Si	σ_y MPa	σ_{UTS} MPa
ROQ-tuf AD 690	0.12	0.5	0.45	0.2	690	760-895

The dimensions of the specimens are shown in the appendix. All specimens tested were in L-T orientation (according to British Standard BS 7448 Part1:1991).

3.3.2 Fatigue Pre-Cracking of Specimens

Fracture mechanics theory applies to cracks, which are infinitely sharp prior to loading. Fatigue crack growth is the most efficient way to produce such sharp cracks in laboratory testing. The fatigue cracking procedure is designed to initiate a crack at the tip of a machined notch and to grow that crack to an approximate length of between 0.45 and 0.55 of the measured specimen width. Controlling the cyclic loading conditions of the specimen grows the crack. By maintaining a constant crack growth rate of between 1×10^{-4} and 2×10^{-4} mm/cycle, the crack tip has the desired small plastic zone surrounding the crack tip.

Once the Electronic Servo-Hydraulic (ESH) testing machine is set-up for fracture toughness testing, the specimens are placed in the ESH machine individually and then ramped in compression for bend specimens. As the load is slowly increased beyond the material's elastic range the crack tip begins to open. The resulting increase in crack opening and load produces a plot.

The experimental arrangement used is shown schematically in Figure 3.5 below.

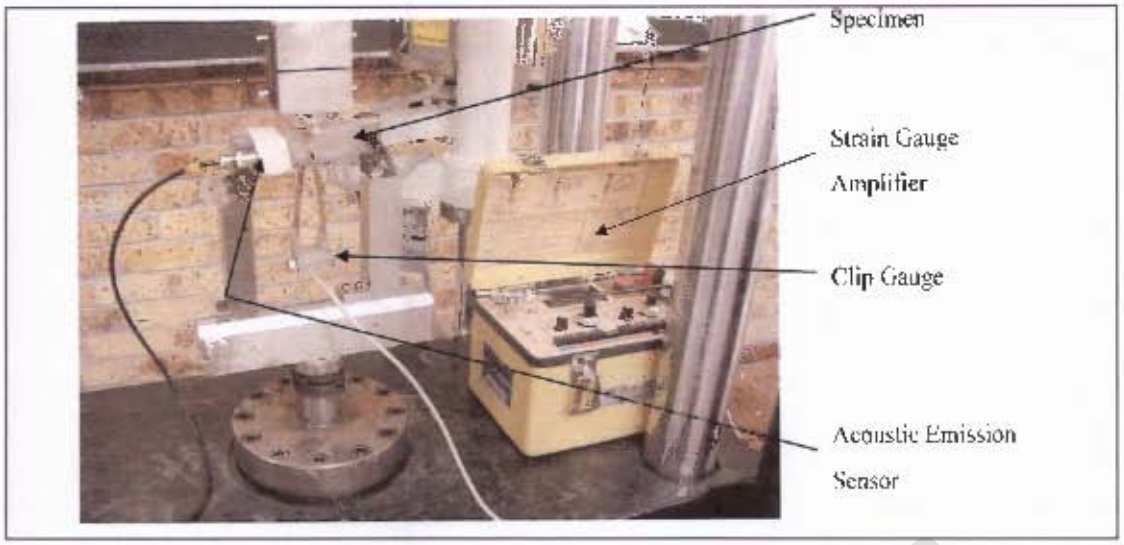

Figure 3.5 Experimental arrangement for a three point bend (TPB) specimen

The multi-channel 8000 Spartan AT system and PC for data storage were used in conjunction with the ESH machine.

3.3.3 Heat Tinting And Exposing The Fracture Surfaces.

Heat tinting is a method used to increase the visibility of the different crack propagation fronts. The test specimens are removed from the testing rig and placed in the oven at approximate temperature of 550°C for between 5 and 10 minutes until the metal begins to turn slightly blue in colour. The specimens are then removed and placed on a ceramic table and allowed to cool at room temperature.

Once the specimens have cooled to room temperature, they are placed in liquid nitrogen. This is to change the ductile fracture mode to brittle fracture mode by lowering the temperature of the metal to well below the materials ductile to brittle

transition temperature. At this temperature the specimens can be cleanly broken at the crack by loading the specimens in the ESH machine. The specimens are then dried off to remove any condensation, which could cause corrosion of the fracture surfaces.

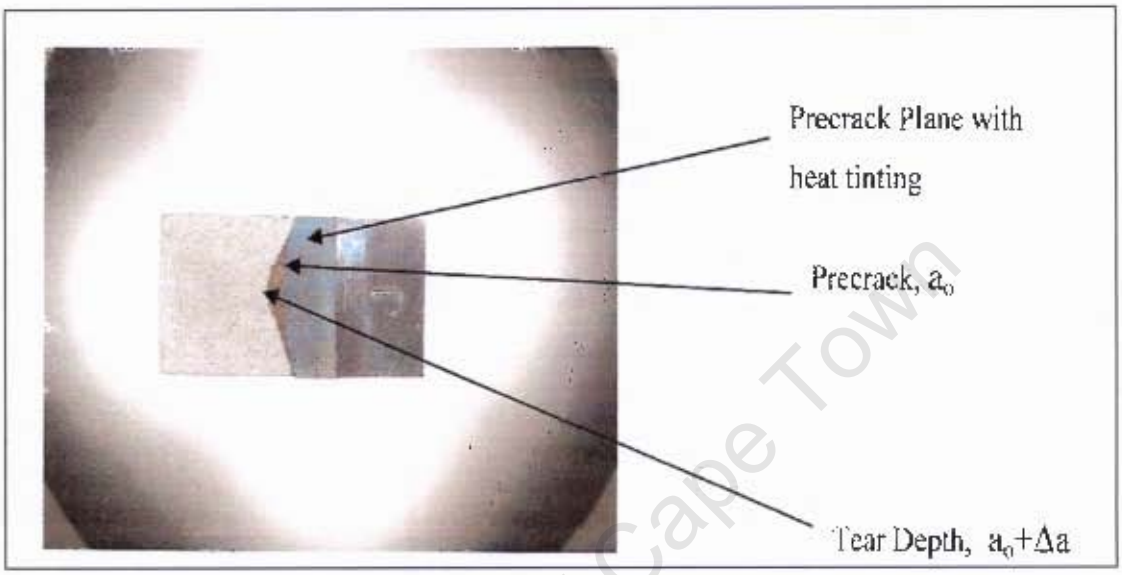

Figure 3.6 Picture of the Fracture Surface after Heat Tinting

The specimens typically show a blue pigment in the region of fatigue crack growth and a darker region for the ductile tearing region. The change in colour aids in the measurement of the specimens crack lengths for the calculation of the fracture toughness of the individual specimen.

3.3.4 Crack Measurements

Once the specimens have been broken, the specimens are measured to determine the fatigue crack growth length and the crack tearing length. The cracks are measured at 6-9 equally spaced intervals across the width of the specimen. These measurements when completed are used in the calculations of COD.

3.4 Composite Testing

3.4.1 Specimen Preparation for Composite Testing

Two laminates, with a different fibre volume fraction, were prepared. The first laminate had a low fibre volume fraction (LFVF), high resin content, and the second laminate had a high fibre volume fraction (HFVF), low resin content. Specimens with two different lay-up configurations were used. Six specimens, of the $[0°]_{6s}$ (0° direction to the load-6 layer) and $[90°]_{6s}$ (90° direction to the load-6 layer) configurations were produced from the HFVF epoxy/glass fibre laminate. Six further specimens of the $[0°]_{6s}$ and $[90°]_{6s}$ lay-up configurations were produced from the LFVF epoxy/glass fibre laminate.

In order to achieve a uni-axial state of stress which is necessary for the subsequent evaluation of mechanical properties, test specimens of uniform width were employed. The specimens, made from the LFVF laminate, had a total length of 150 mm and a width (W) of 10 mm. The HFVF specimens had a total length of 150 mm and a width (W) of 17.4 mm

Tabs of the same material as the specimens were glued to the specimens' ends as shown in Figure 3.7. These tabs serve to reduce the stress concentrations at the grips, by increasing the cross sectional area there. The axial load is transferred into the specimen through shear; the tabs will ensure that the specimen breaks at the middle rather than at the grips.

stress concentrations, due to the geometric discontinuity at the gage end of each tab. In order to minimize this latter source of stress, the tabs are tapered at the ends. Since load is transferred into the specimen by gripping the ends of the specimen; the tabs also serve to protect the composite from being damaged by the metal grips. The tabs also decrease noise in the signal due to the gripping of the specimen.

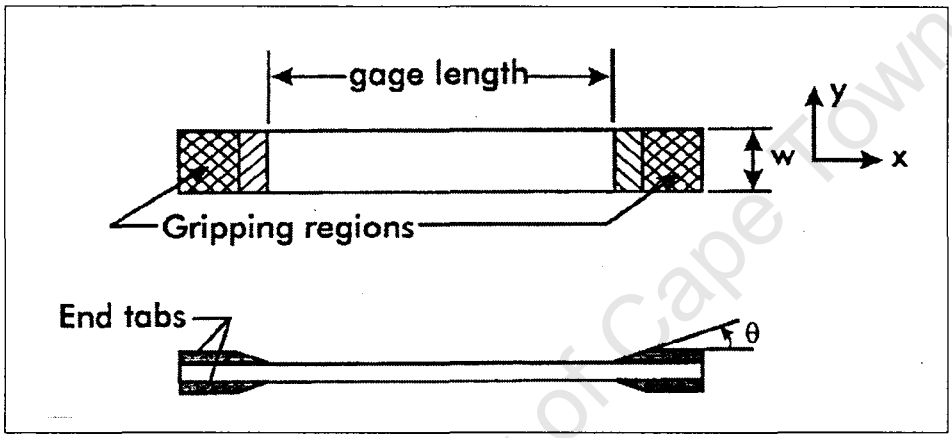

Figure 3.7 Configuration of the Composite Test specimen

The tabs were 25 mm in length, 10 mm width for the LFVF and 17.4 mm width for the HFVF specimens. The tabs had the same thickness as the specimen.

3.4.2 Tensile Tests of Composite

Load was applied to the specimens using a Zwick 1484 tensile testing machine, manufactured by Wirsam, Scientific & Precision Equipment (Pty) LTD. The tensile tester which is controlled by a computer, automatically records the load and displacement data and has a maximum tensile force of 200 kN,

4. Experimental Results, Observations and Discussions

4.1 Preliminary Investigation into AE Detection in Pressure Vessels

In the initial investigation to establish the detection capability of the 8000 Spartan AT equipment, both filament wound composite vessel and steel vessel were looked at. These were loaded according to a pressurization programme, and artificial flaws were introduced as indicated in Chapter 3. Typical examples of the findings are presented here.

4.1.1 AE Monitoring of the Steel Vessel

Sensors were placed 100mm apart.

The AE monitoring parameters for the loading programme were as follows:

Gain (dB)	Threshold (dB)	PDT (μs)	HDT (μs)	HLT(μs)
30	30	700	1400	1400

The pressurization regime that was applied was as follows:

Pressure (kPa)	0-500	500-0	0-1000	1000-0	0-1500	1500-0	0-2000
Time Elapsed (s)	0-30	30-60	60-90	90-94	94-120	120-131	131-135

In the figure below, it can be seen that the energy released from the vessel's material and the flaw increases with every incremental increase in pressure. This is an indication of the Kaiser Effect in that the material and flaw emits at or near the previous maximum pressure [29, 33].

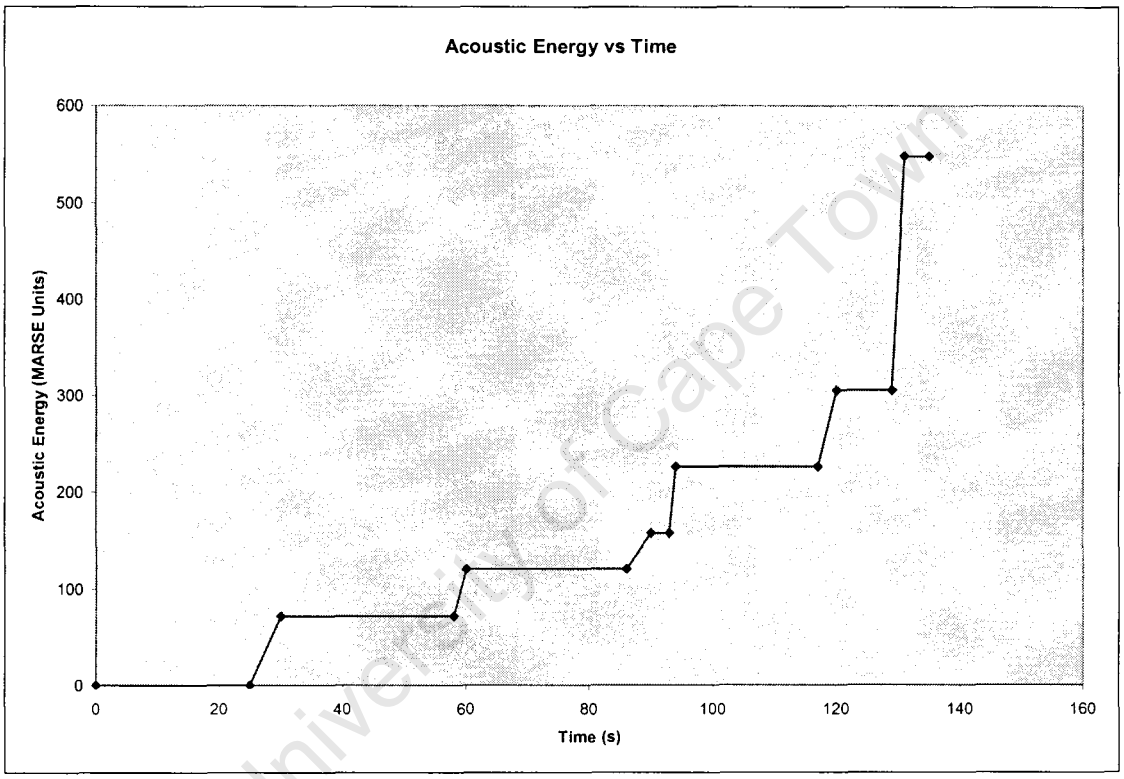

Figure 4.1 Graph of Acoustic Energy vs. Time during the Loading of the Steel Pressure Vessel

During the first 2 stages of pressurization (positive pressure gradient), there is no clear indication of the location of the flaw, since hits are registered across the test area due to noise associated with material strain or due to the testing procedure [29, 33] (see Figure 4.2).

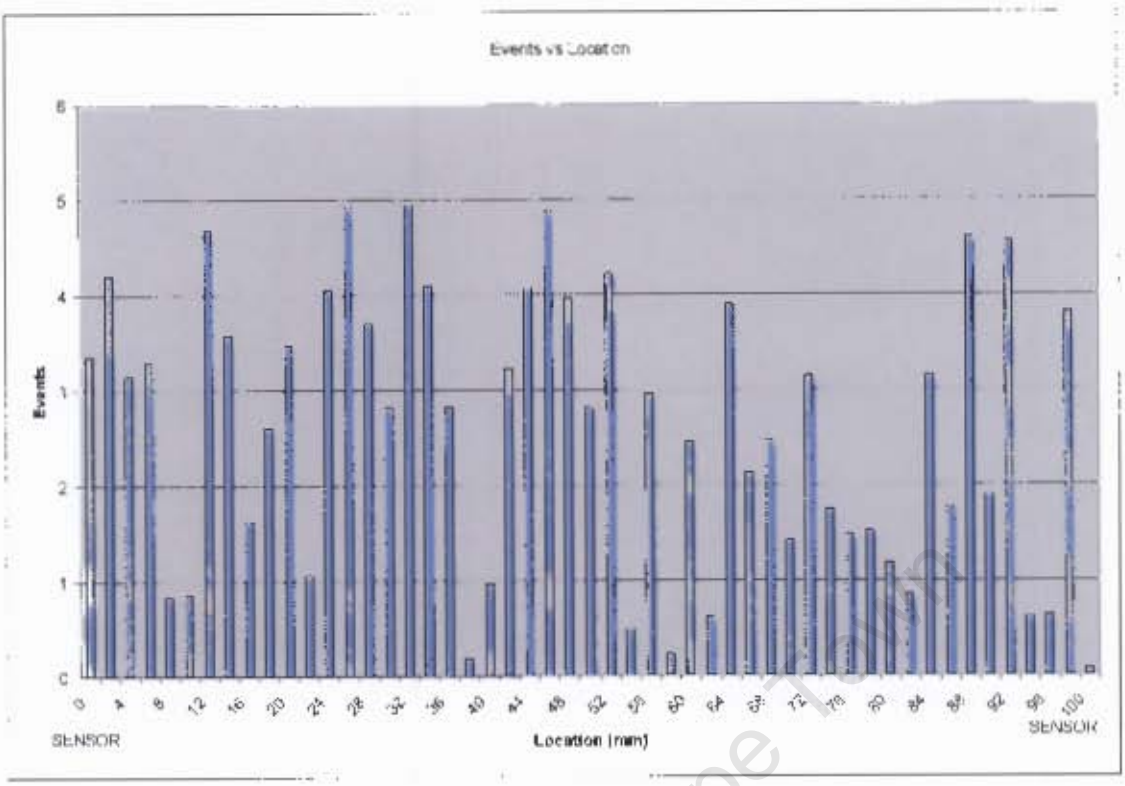

Figure 4.2 Graph of AE Events vs. Location (Stage 2)

After the third loading, the location of the defect becomes apparent as the emissions associated with defect propagation exceed the background noise significantly. At this stage the highest number of events viz., 19 events, is registered at a location 48 mm from Sensor 1 as shown in Figure 4.3.

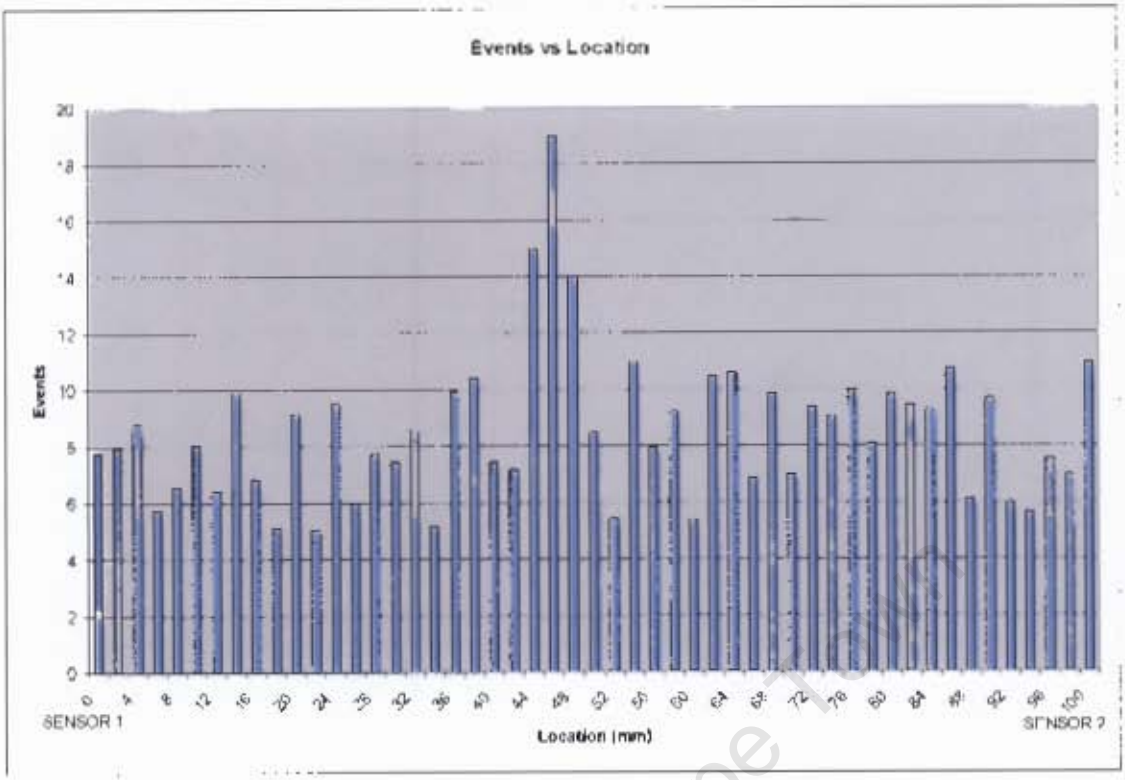

Figure 4.3 Graph of AE Events vs. Location (Stage 3)

At the final stage of the loading programme the location of the flaw is clearly indicated. The graph in Figure 4.4 shows that the flaw is clearly situated 46 ± 4mm from Sensor 1 (at the zero position).

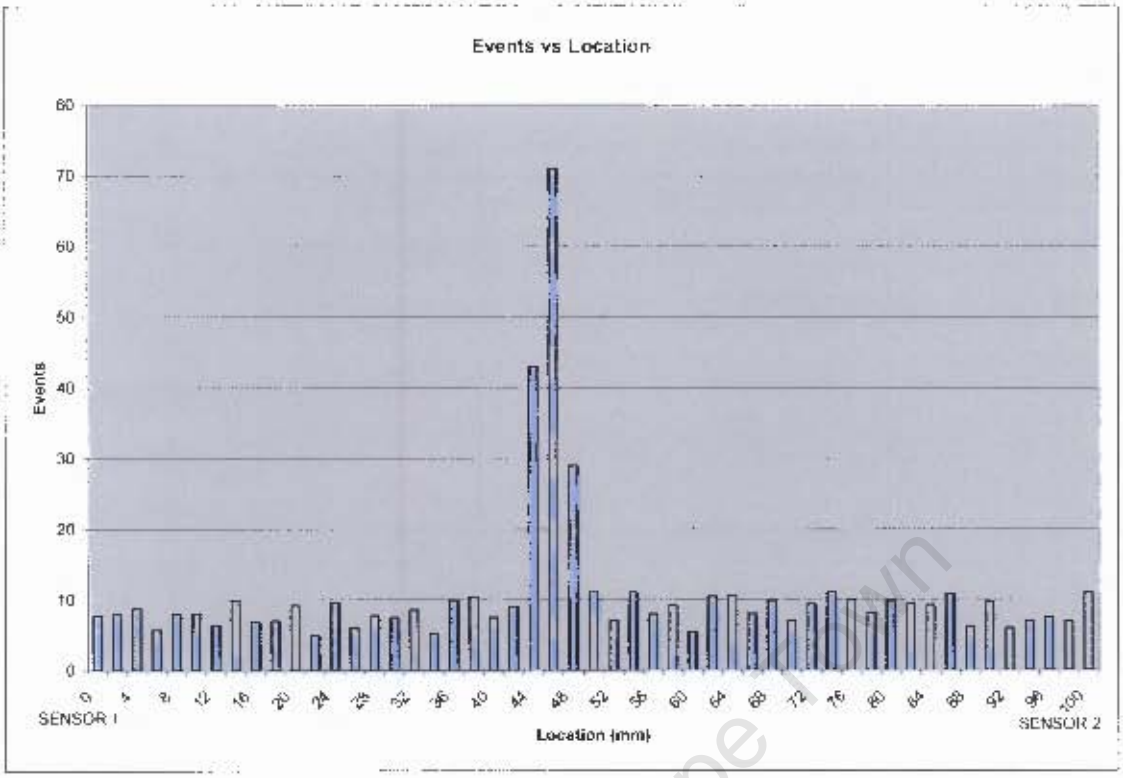

Figure 4.4 Graph of AE Events vs. Location (Stage 4)

In the figures above it is shown that there is noise, as expected, associated with localized plastic deformation across the test area [29, 33]. As the load is increased, the flaw/defect propagates and is shown to be the site of most activity, whilst the rate of activity across the test area decreases. Therefore, after approximately 2 minutes of testing, the defect or flaw distinguishes itself from the background noise.

4.1.2 AE Monitoring of the Filament Wound Composite Vessels

Sensors were placed 140mm apart.

The AE monitoring parameters for the loading programme were as follows:

Gain (dB)	Threshold (dB)	PDT (µs)	HDT (µs)	HLT(µs)
30	45	500	1000	2000

The pressurization regime that was applied was as follows:

Pressure (kPa)	0-500	500-0	0-800	800-0	0-1000	1000-0	0-1200
Time Elapsed (s)	0-50	50-88	88-120	120-145	145-186	186-216	216-240

In the figure below, it can be seen that the energy released from the vessel's material and the flaw increases with every incremental increase in pressure.

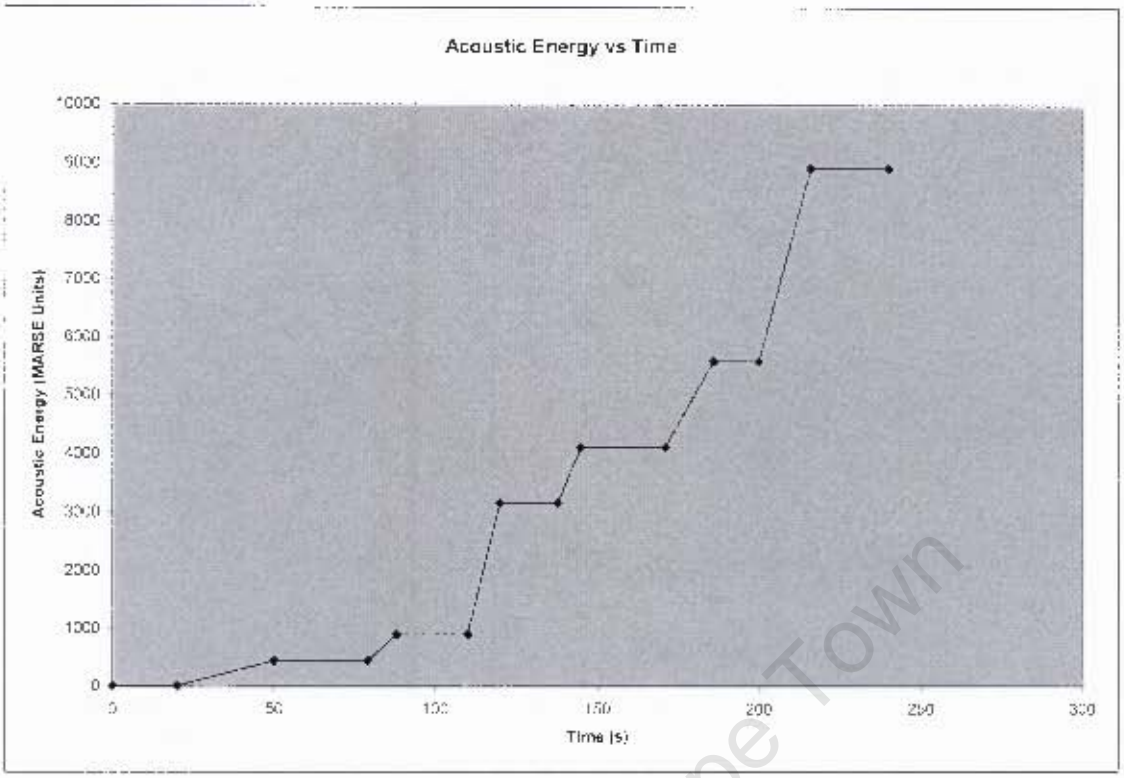

Figure 4.5 Graph of Acoustic Energy vs. Time during the Loading of the Composite Pressure Vessel

During the first 2 stages of pressurization, there is no clear indication of the location of the flaw, since events are registered across the test area due to noise associated with material strain or due to the testing procedure. It should be noted that composite materials are noisy by the nature of their composition [30-32].

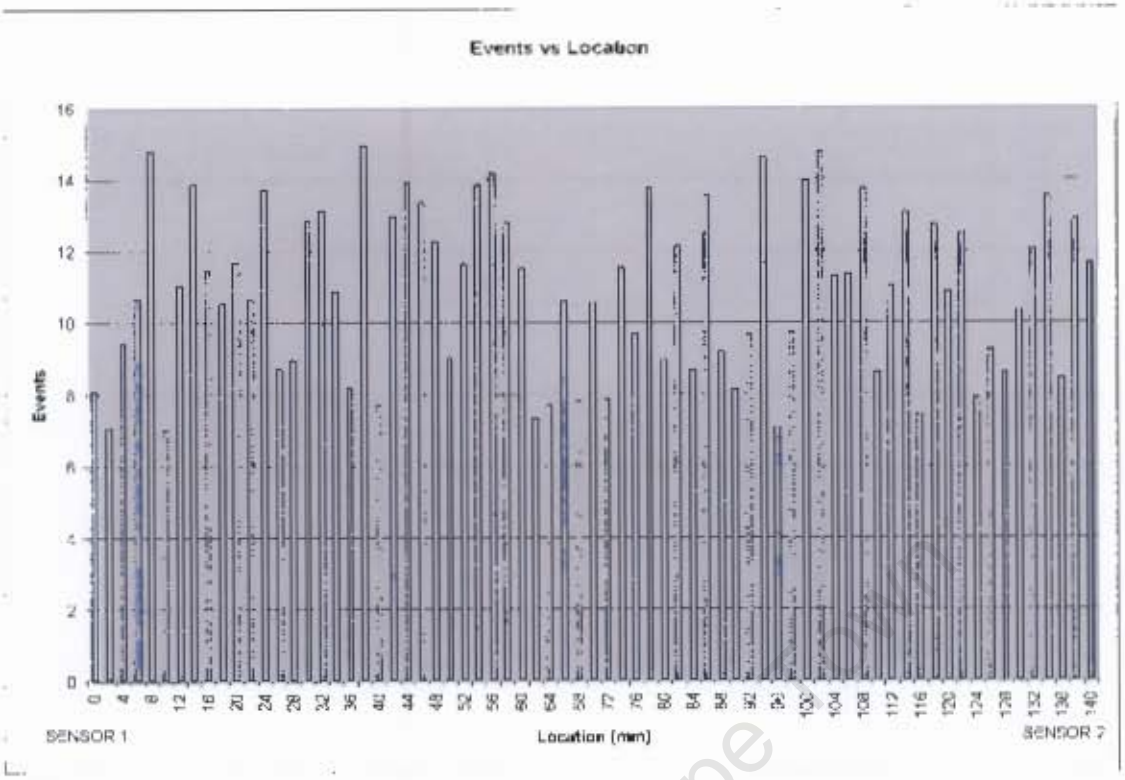

Figure 4.6 Graph of AE Events vs. Location (Stage 2)

Subsequent loading however shows the location of the defect as the emissions associated with defect propagation exceed the background noise significantly, particularly at stage 4.

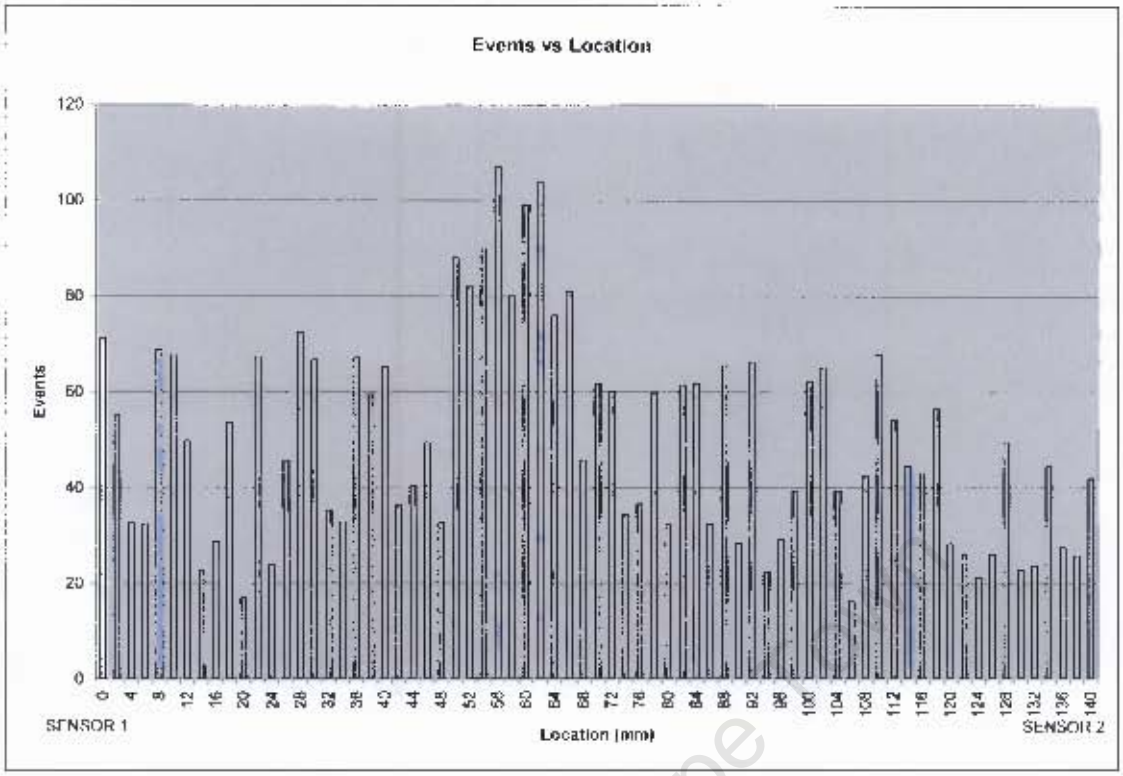

Figure 4.7 Graph of AE Events vs. Location (Stage 3)

At the final stage of the loading programme the location of the flaw is clearly indicated. The graph below shows that the flaw is clearly situated 56 ± 10mm from the left hand side sensor (at the zero position). The larger uncertainty in the location as opposed to the steel vessel shows that the composite is noisier in the area of the flaw due possibly to the sources of matrix cracking, fibre breakage or interfacial friction. These mechanisms are not present in the steel vessel.

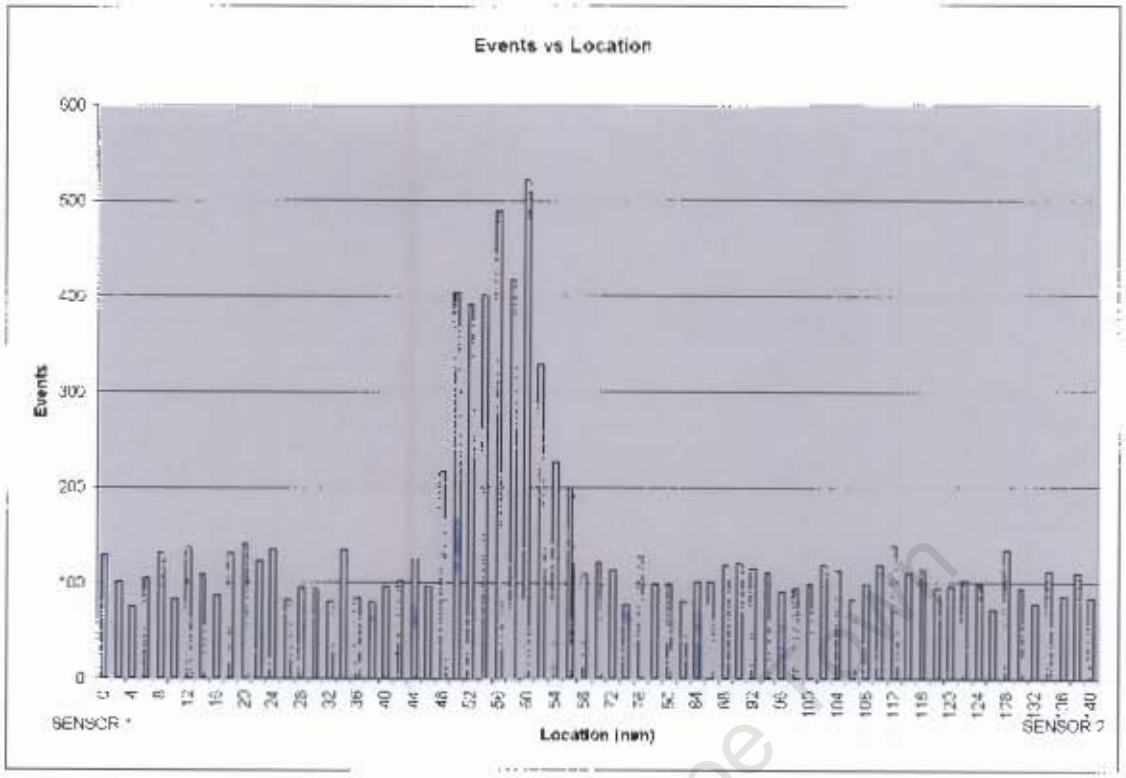

Figure 4.8 Graph of AE Events vs. Location (Stage 4)

A triangulation algorithm would be used to locate flaws/defects across a two dimensional surface. In this case, a set of four sensors are placed in a parallelogram formation. The active site is located when the AE equipment registers the difference in the time it takes for the signal to reach each of the sensors in turn [2].

4.2 Fracture Toughness Testing of ROQTUF AD690

A full record of the results obtained from the fracture toughness tests is shown in Appendix 1. A summary of the data is listed below.

The physical attributes of each specimen as well as the maximum load attained and the plastic component of notch opening displacement are necessary for the calculation of the fracture toughness [8]. These are shown in Appendix 1.

Table 4.5: Summary of data

Specimen #	Thickness, B mm	Width, W mm	Initial Crack Length, a_o mm	Crack Length ao+da mm
B	15.066	30.068	15.360	15.935
C	15.073	30.118	16.581	16.845
E	15.065	30.070	16.412	16.412
F	15.078	30.028	15.719	15.814
H	15.088	30.095	15.385	16.212
I	15.095	30.075	15.243	16.002
J	15.073	30.068	15.090	15.998
K	15.103	30.023	15.384	16.165
L	15.085	30.023	14.874	15.475
M	15.020	30.080	15.659	15.988
N	15.083	30.098	14.966	15.228

Table 4.6: Fracture Toughness and Tear size

Specimen #	COD (mm)	Tear size (mm)
B	0.199	0.575
C	0.183	0.264
E	0.140	0
F	0.151	0.094
H	0.188	0.827
I	0.186	0.759
J	0.210	0.908
K	0.208	0.781
L	0.173	0.601
M	0.257	0.329
N	0.253	0.262
Average Value	**0.188**	

Values for the Fracture Toughness are tabulated above and can be viewed graphically in Figure 4.9.

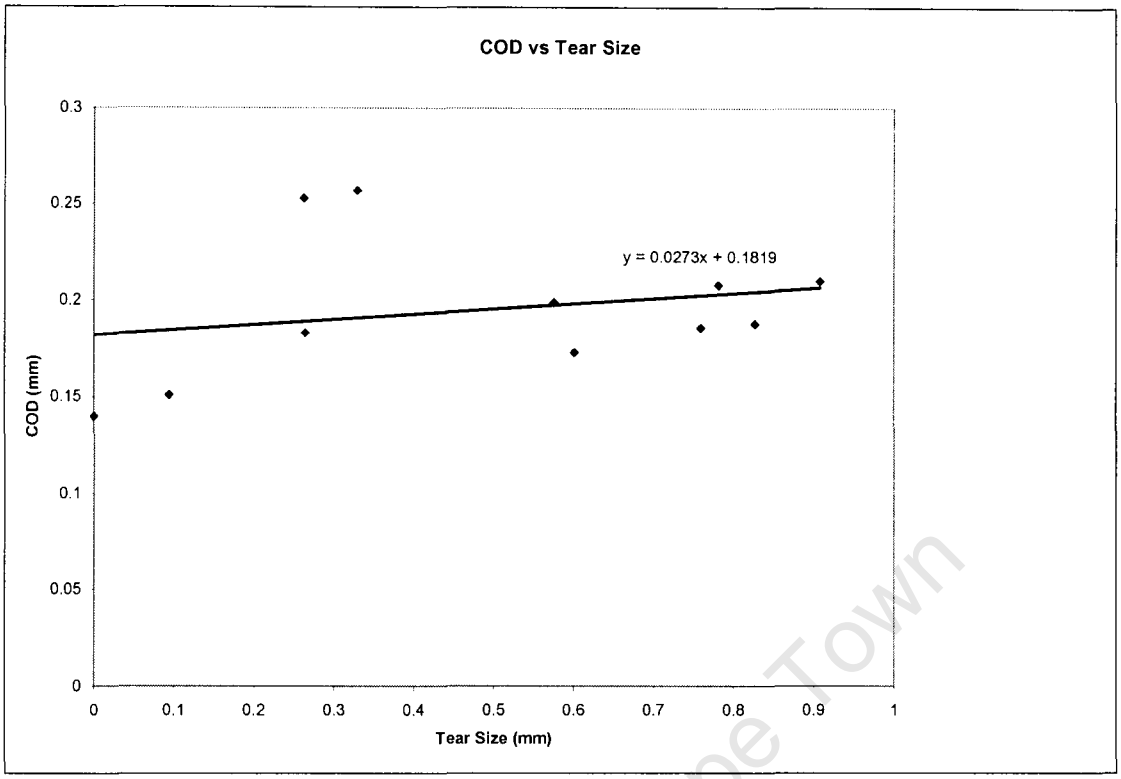

Figure 4.9 Graph of COD vs. Tear size

4.2.1 Determination of Crack Blunting and Crack Tearing Initiation

Crack blunting occurs prior to tearing initiation as explained in the literature review. This means that the tear size during this phase of flaw development is negligible. Tearing Initiation can be determined through plotting values of COD calculated for each specimen against their respective crack tear sizes. These points are shown in Table 4.6. A trend line is added to the graph and from that it is possible to determine the value of COD at tearing initiation.

From the Figure 4.9, the point of crack tearing can be approximated as the intersection of the trend line with the Y-axis. This point is obtained from the trend line formula. For a negligible tear size, the corresponding COD is equal to 0.1819mm

A record of the Load vs. the Clip Gauge Deflection was kept for each specimen and is included in Appendix 1.

When the preliminary test was conducted on the steel pressure vessel, the active flaw was located. However, no information was garnered on the development of that flaw at the microscopic level.

During each of the COD tests, the fracture process was monitored using AE. The results showed a repeatable trend for AE activity during the fracture process of a structural steel, ROQ-tuf AD 690.

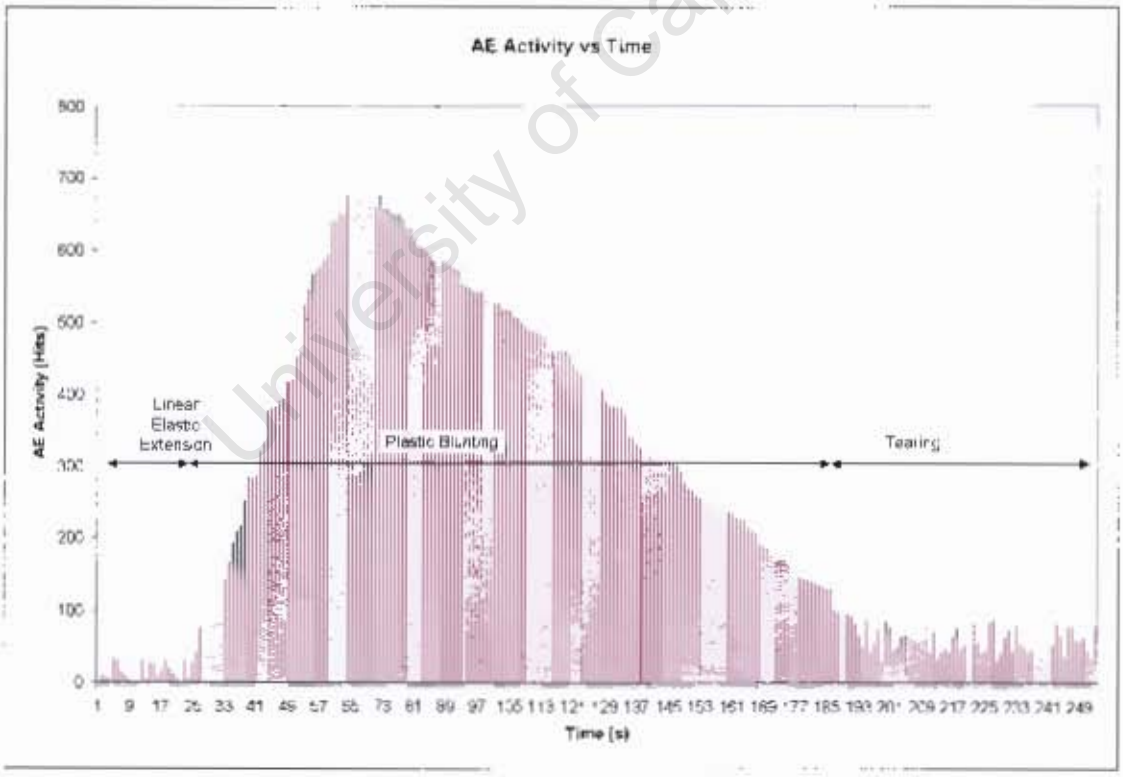

Figure 4.10 AE Activity vs. Time for Fracture Toughness Specimen J

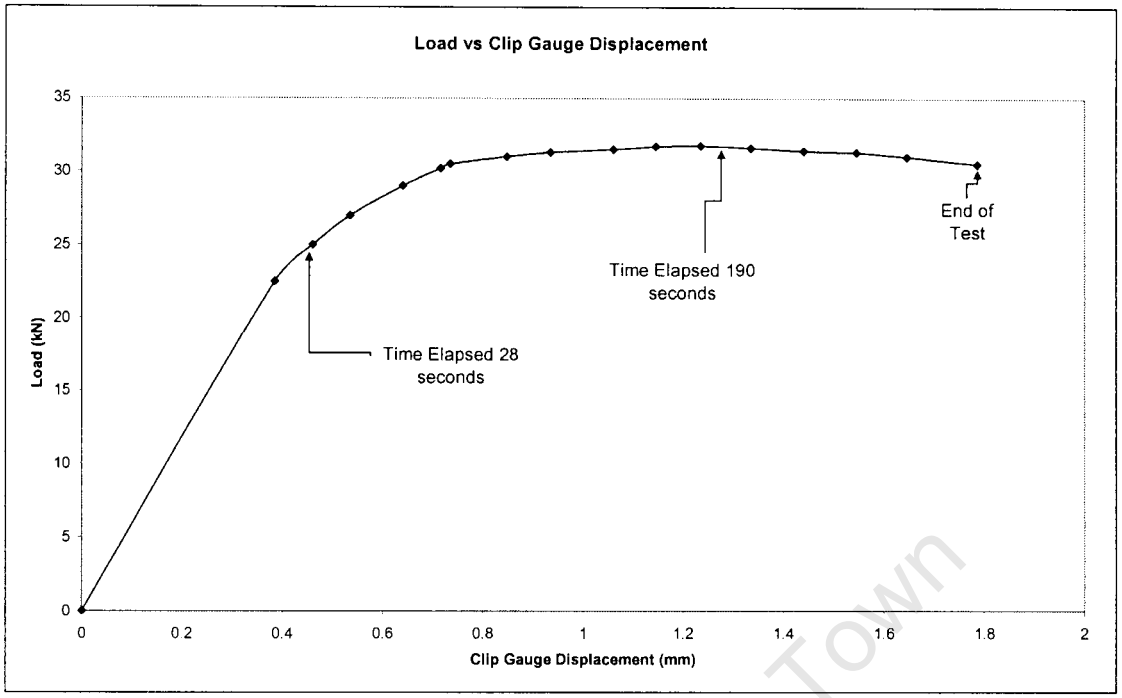

Figure 4.11 Force vs Clip Gauge Displacement for Fracture Toughness Specimen J

The figures above are typical of all the fracture toughness tests and show the correlation between the AE activity and the stages of crack growth development. In figure 4.10 there is a marked increase in the AE activity after 28 seconds into the test. This corresponds to a deviation in from linearity in figure 4.11. AE activity further increases to a maximum and then steadily declines until the 190 seconds have passed. This corresponds to the time at which the maximum load is reached. At this point, a steady rate of AE is observed i.e. in the area designated as "Tearing". This suggests that the tearing phase of crack propagation is quiet (less AE activity) compared to the blunting phase.

These results compare favourably with the studies done by Dunegan, Khan et al [11-23], i.e. that there is an increase in AE activity during plastic deformation. In ductile

metals, tensile failure occurs by microvoidal coalescence. According to the results shown, this process produces less activity at the frequency to which the sensors are tuned, viz., 150 kHz. The level of activity is strongly influenced by the threshold and gain settings mentioned in Chapters 2 and 3. However, the trend will not change with a change in these settings, only the intensity of the signals e.g. energy, is affected.

4.3 Testing on Laminate Composite Specimens

Two different lay-up configurations were chosen in order to generate different failure modes. Matrix cracking transverse to the load direction was studied using $[90°]_{6s}$ specimens. The $[0°]_{6s}$ specimens were used to show the type of failure that occurs in a composite loaded in the direction of fibres, viz. fibre breakage. The force and displacement data collected during the tensile tests is used to study and compare the AE response of the $[0°]_{6s}$ and $[90°]_{6s}$ specimens.

4.3.1 Longitudinal Lay-up $[0°]_{6s}$

These types of specimens were loaded to failure. The stress vs. strain graphs for the six LFVF & HFVF specimens, plotted on the same axis, are shown in figures 4.12 and 4.13 respectively. The stress-strain curves are not linear; this is not due to plastic deformation but due to microscopic damage, in this case mainly fibre breakage. Fibre breakage initiates at low stresses and grow in size as the stress is increased [25].

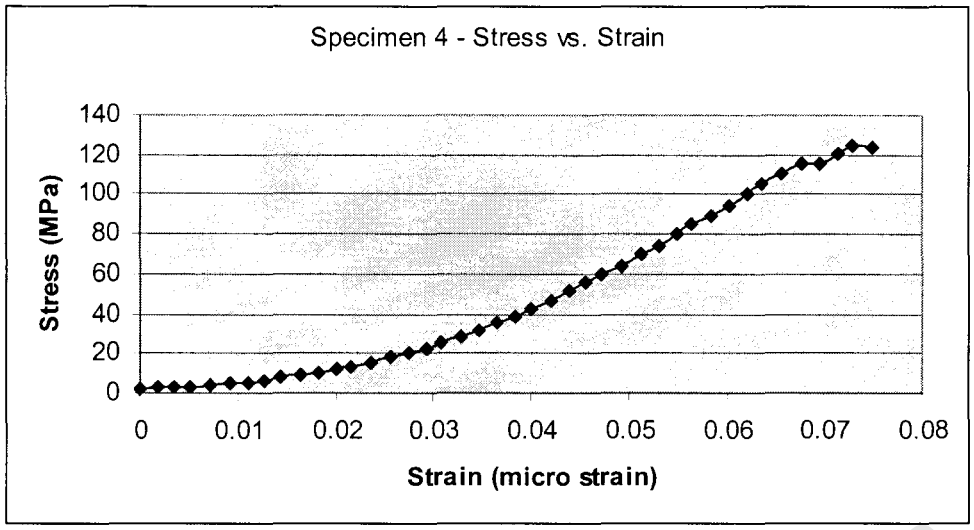

Figure 4.12 Graph of Stress vs. Strain for the LFVF specimen 4

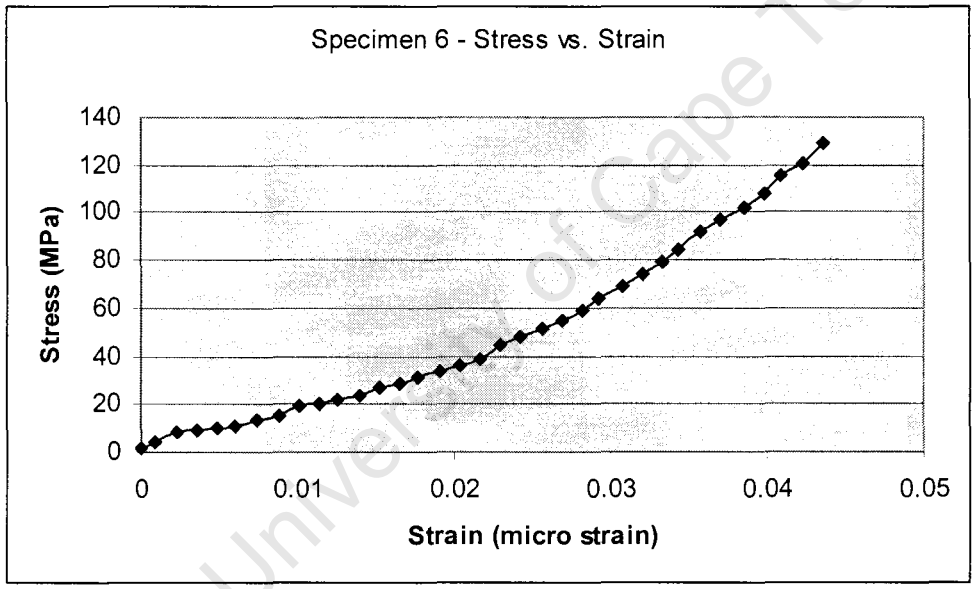

Figure 4.13 Graph of Stress vs. Strain for the HFVF specimen 6

The tested specimens were visually inspected and fibre breakage was observed in the 0° direction. Not all the fibres had ruptured and the fracture surface was also examined with a scanning electron microscope, which confirmed that fibre breakage occurred.

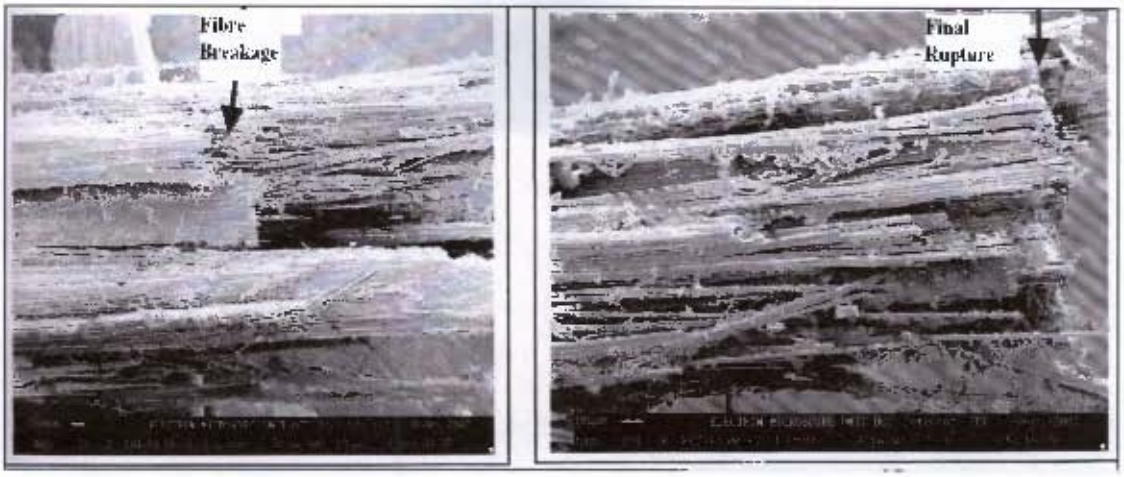

Figure 4.14 Micrograph of Fibre breakage

The average final failure stress and strain, for LFVF specimens, are 88 MPa and 0.055 $\mu\epsilon$ respectively. On the other hand the average failure stress and strain, for HFVF specimens, are 97 MPa and 0.040 $\mu\epsilon$ respectively. The specimens that failed at the highest stress is LFVF specimen 4, with stress of 129 MPa and strain of 0.044 $\mu\epsilon$ and HFVF specimen 6, with stress of 124 MPa and strain of 0.075 $\mu\epsilon$. For clarity, we will use these specimens to compare tensile tests results to AE results.

The energy emission associated with the failure of specimen 4 and 6, are shown by the energy *vs.* time. From the graphs, we are able to see that the energy released when the specimens finally fail is approximately 60 x 10^3 *MARSE*, for specimen 4 (LFVF) and 80 x 10^3 *MARSE* (HFVF), for specimen 6.

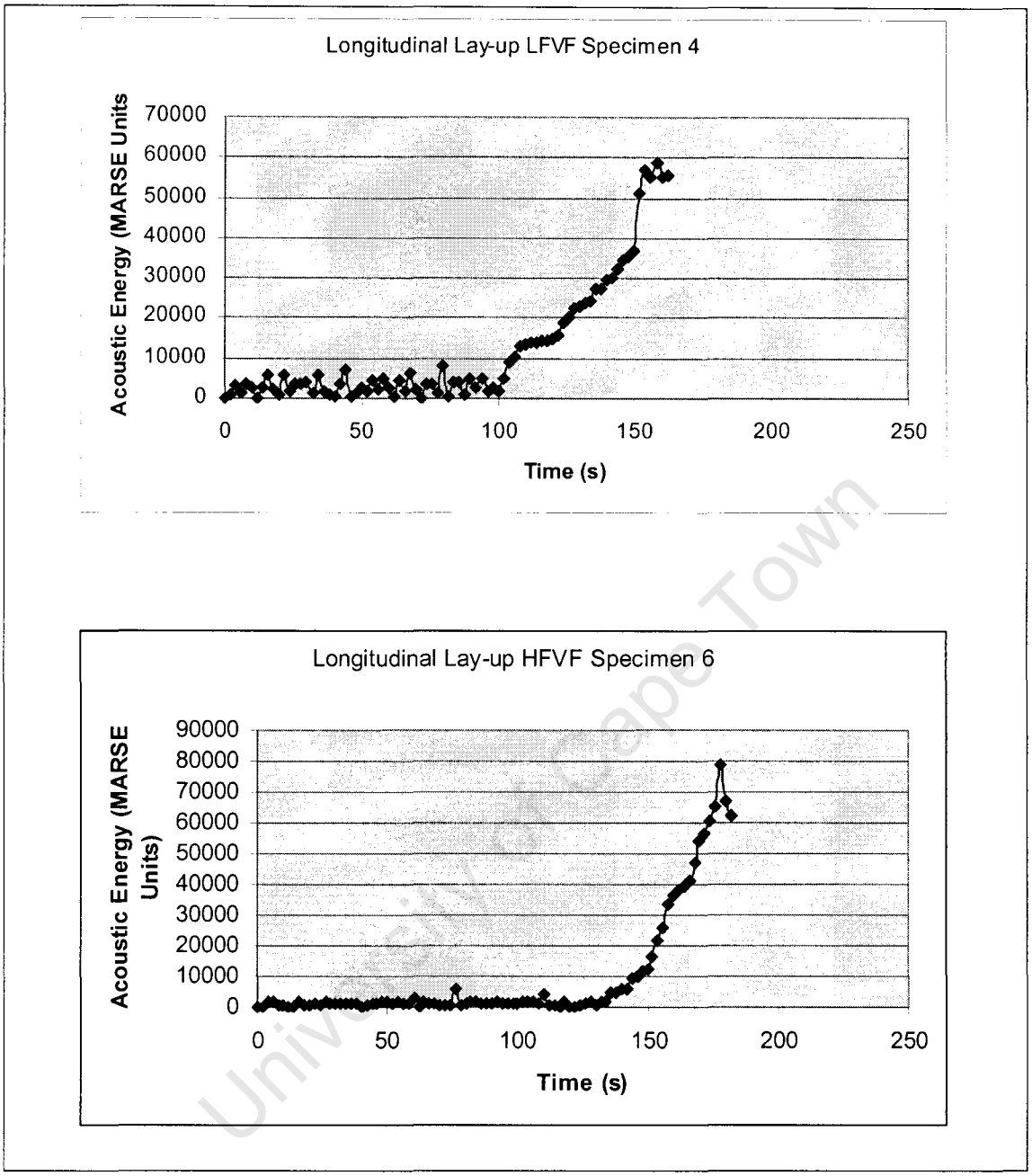

Figure 4.15 Graph of Acoustic Energy vs. Time for Specimens 4(LFVF) and 6(HFVF)

The energy-time graphs for other specimens are available in the appendix. It can be seen from the included stress-strain curves that all the specimens failed at different stress levels indicating a difference in their strength and modulus. Due to differences in stiffness, different sound intensities are released by each specimen when it fails.

This is in agreement with the findings of Narisawa [35], who showed the density dependence of activity in a composite. Even though all the LFVF specimens are made of the same material (epoxy/glass reinforced), irregularities that occurred during the laminate lay-up and specimen machining resulted in the mechanical properties of the laminate being different in all directions along the laminate plane. Irregularities that may have arisen during lay-up and specimen preparation include:

- formation of bubbles in the lamina, which results in the formation of voids in the material
- uneven resin application

The Energy-Time graphs for the longitudinal lay-up show a similar trend for both LFVF and HFVF specimens (figures 4.16, 4.17). They indicate that AE activity is limited initially but a rapid increase of activity is noted with increasing fibre failure. This trend is noted by Narisawa [35] as well.

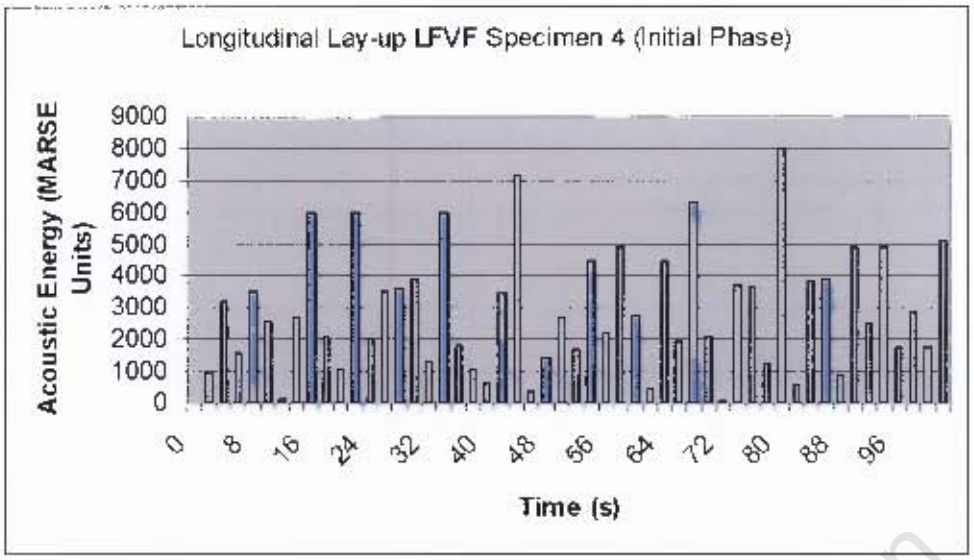

Figure 4.16 Graph of Acoustic Energy vs. Time for the Initial phase of fracture for LFVF Specimen 4

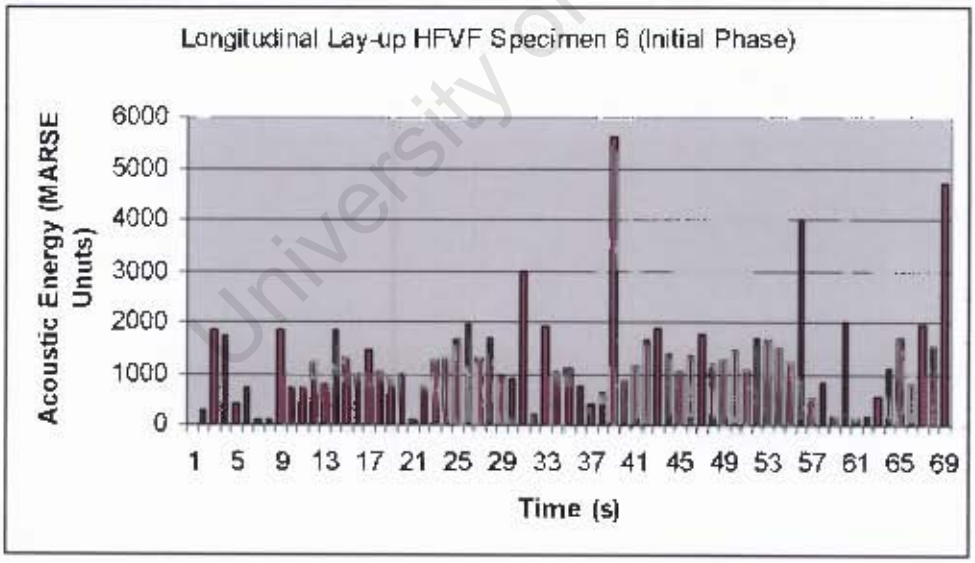

Figure 4.17 Graph of Acoustic Energy vs. Time for the Initial phase of fracture for HFVF Specimen 6

An interesting difference between the traces in specimens 4 and 6 is that the LFVF specimens exhibit a higher average in AE activity during the first phase of fracture development. On average the HFVF activity is ***1113 MARSE*** for all specimens whereas the average for LFVF is ***2430 MARSE*** during the first phase of fracture development.

This may be a result of the higher resin content in LFVF specimens; therefore matrix cracking is more prevalent in these specimens initially.

4.3.2 Transverse Lay-up [90°] $_{6s}$

These specimens were also loaded to failure. The stress vs. strain curves for the LFVF & HFVF specimens are also non-linear due to microscopic damage that initiated in the material [25]. In this case, the specimens experienced transverse matrix cracking. Scanning electron microscopy was also used to study the fractured surface, which confirmed that matrix cracking had occurred, figure 4.18 shows clearly that the fibres stayed intact and only the matrix failed.

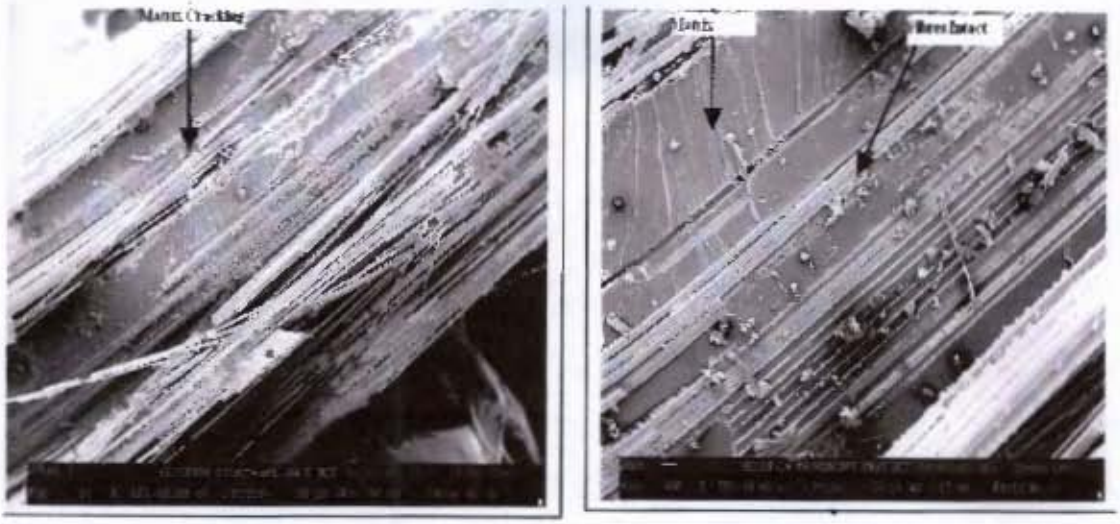

Figure 4.18 Micrograph of Matrix cracking

Figures 4.19 and 4.20 show the stress-strain curves for LFVF and HFVF specimens respectively. These defects as mentioned in 4.3.1 also have a significant effect on the mechanical properties (e.g., strength & modulus) of the material.

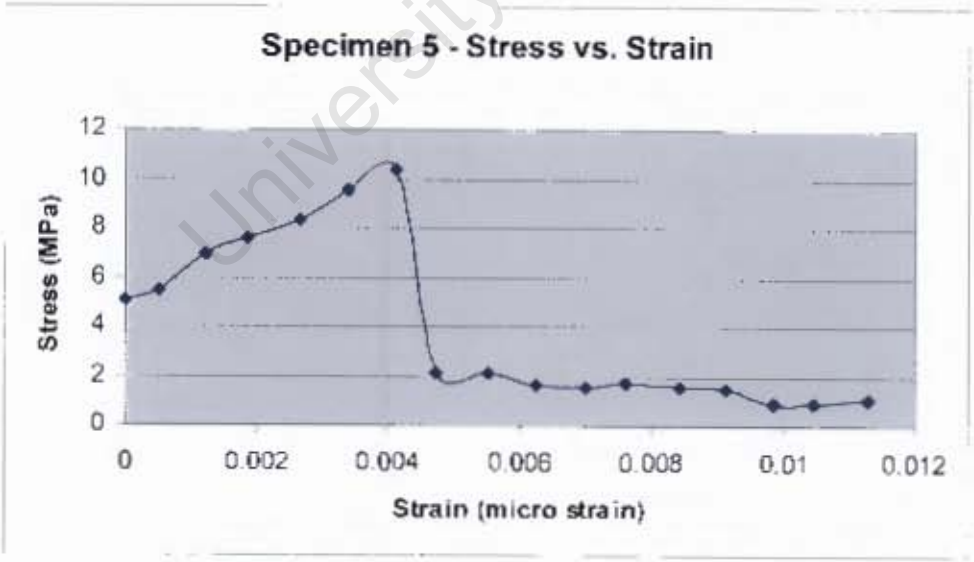

Figure 4.19 Graph of Stress vs. Strain for the LFVF specimen 5

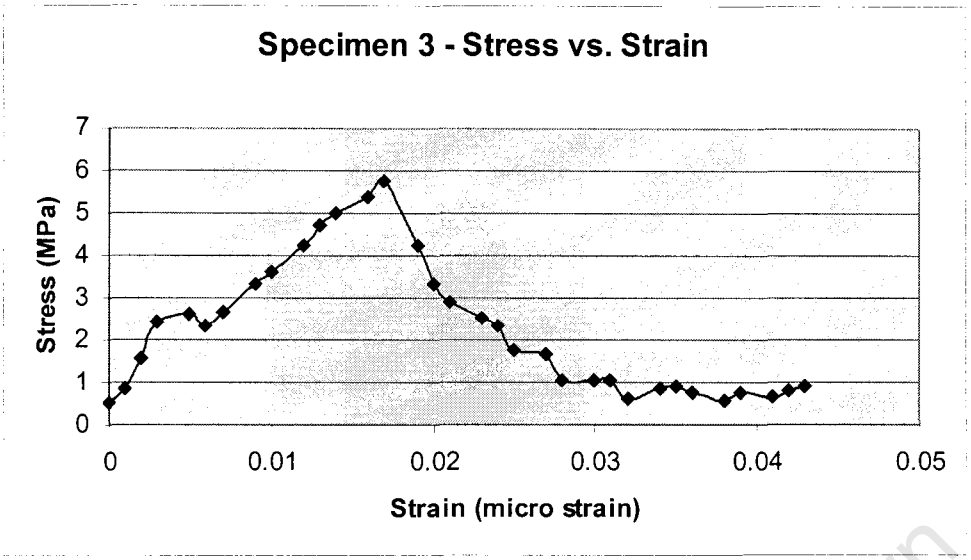

Figure 4.20 Graph of Stress vs. Strain for the HFVF specimen 3

Due to the nature of the lay-up i.e. $[90°]_{6s}$ specimens, the matrix is the load bearing component. It therefore does not behave in a predictable way. Hence we see the irregular load traces as above (Figures 4.19 and 4.20).

The energy emissions associated with the failure of specimens 3 and 5, are shown by the energy - time graph in figures 4.21 and 4.22. From the graphs, we are able to see that the maximum energy released is approximately 7.5 x 10^3 *MARSE*, for specimen 3 (HFVF) and 0.450 x 10^3 *MARSE*, for specimen 5 (LFVF).

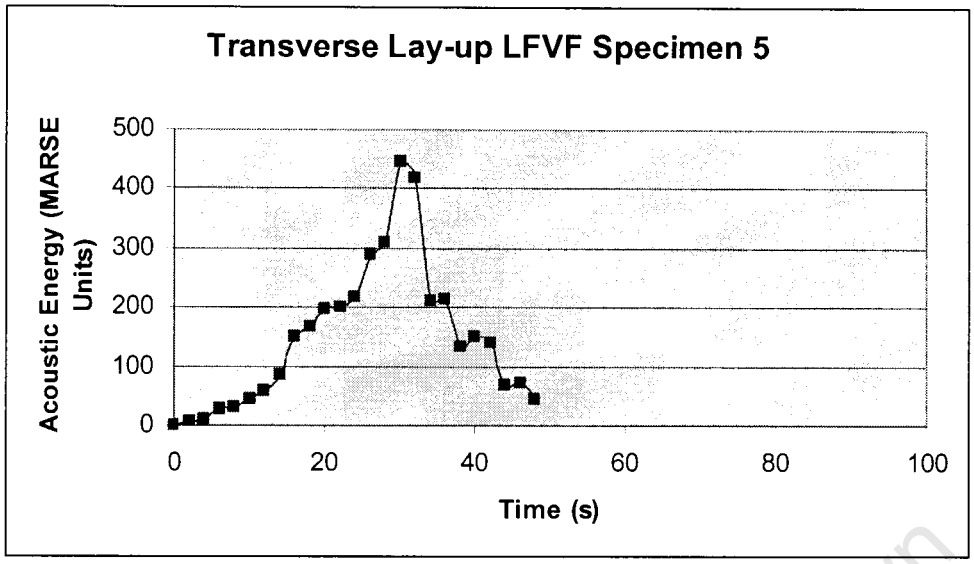

Figure 4.21 Graph of Acoustic Energy vs. Time for Specimens 5(LFVF)

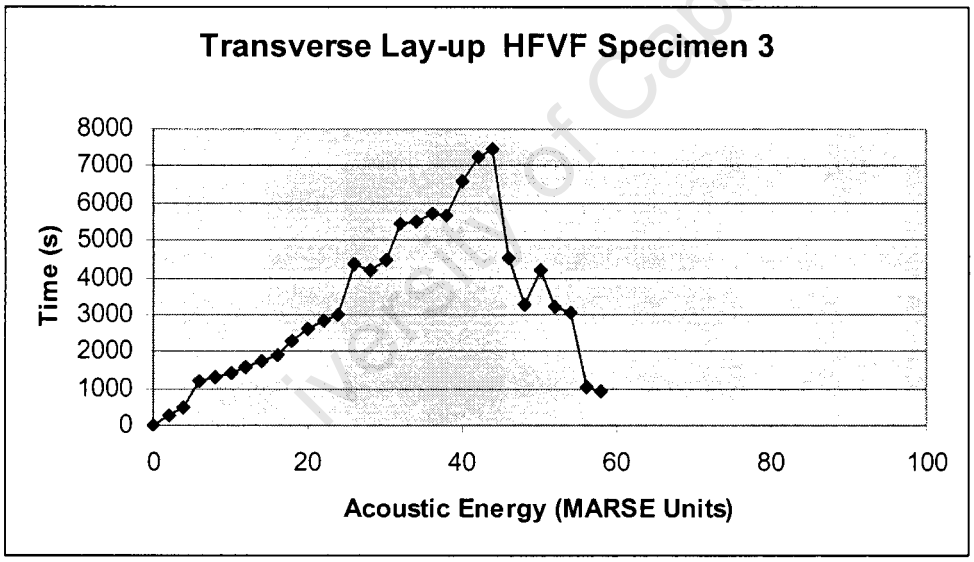

Figure 4.22 Graph of Acoustic Energy vs. Time for Specimen 3(HFVF)

The energy-time graphs for other specimens can be seen in Appendix 2. From the graphs we are able to see that the maximum energy released by transverse matrix cracking by HFVF specimens, ranges between 0.62-7.5 x 10^3 *MARSE* and by LFVF specimens, ranges between 0.109-0.450 x 10^3 *MARSE*.

5. Conclusions

5.1 Detection of Acoustic Emissions

The 8000 Spartan AT system proved to be a reliable instrument to monitor and detect flaws in both steel and composite pressure vessels. The Spartan clearly shows the Kaiser Effect by showing an increase in AE activity after an increase in load (section 4.1).

Flaws were located in both steel and composite pressure vessels using a linear location algorithm. In the steel pressure vessel, the flaw was located 46 ± 4mm from one of the sensors. The location of the flaw became apparent after the flaw's activity exceeded the background noise.

In the composite vessel testing, the technique showed the location of the flaw to be 56 ± 10 mm from the left-most sensor. There is a scatter of 20mm due to the fact that composites produce more acoustic activity due to their composition. The background noise is significantly higher, of the order of five times, than in the steel vessel. This is due to the fact that the composite is noisier in the area of the flaw where sources of matrix cracking, fibre breakage or interfacial friction may occur.

5.2 AE Monitoring of Fracture toughness testing

The critical fracture toughness of the ROQ-tuf AD 690 steel was determined as 0.1819 mm. This value was arrived at with multi-specimen testing. Each test was successfully monitored with the 8000 Spartan AT.

The Acoustic Emission trace for each specimen shows a repeatable trend. The three stages of crack development in a steel exhibiting ductile behaviour are clearly identifiable. The process of crack blunting is the noisiest reaching maximum levels of between 500 and 700 Hits. Tearing is by microvoidal coalescence (ductile failure). This process shows considerably lower AE activity, of the order of seven times less, than the maximum AE activity associated with blunting.

The inference is therefore, that AE can be used as a preventative tool in avoiding catastrophic failure of steel alloys such as ROQ-tuf AD 690 by identifying the stages of flaw development in the material.

5.3 AE Monitoring of Composite Test Specimens

The failure modes of Fibre Breakage and Matrix Cracking in the composite specimens were successfully monitored with the 8000 Spartan AT.

In the [0°] specimens, the average final failure stress and strain, for LFVF specimens, were 130 MPa and 0.1 $\mu\epsilon$ respectively. On the other hand the average failure stress and strain, for HFVF specimens, were 273.3 MPa and 0.104 $\mu\epsilon$ respectively.

The energy released by fibre breakage in HFVF specimens, ranges between 30 and 80 x 10^3 *MARSE* and by LFVF specimens, ranges between 20 and 60 x 10^3 *MARSE*.

The average final failure stress and strain in [90°] specimens, for LFVF specimens, were 8 MPa and 0.002 $\mu\epsilon$ respectively. On the other hand the average failure stress and strain, for HFVF specimens, were 4 MPa and 0.01 $\mu\epsilon$ respectively.

The energy released by transverse matrix cracking by HFVF specimens, ranges between 0.62-7.5 x 10^3 *MARSE* and by LFVF specimens, ranges between 0.230-0.450 x 10^3 *MARSE*.

Failure by fibre breakage produces AE activity of the order of ten times more than that of matrix cracking for the maxima. Also HFVF specimens produce 1.3 times more activity than LFVF in [0°] specimens, whilst it is more significant in the [90°] specimens, viz. 16 times.

In both the lay-up configurations the acoustic energy released steadily increases to the maximum. There are no discernable differences in the traces other than the maxima. The distinguishing factor may be that each failure mode exhibits a dominant frequency at failure. This characteristic cannot be measured by the 8000 Spartan AT. It may be necessary to include this parameter for measurement in future investigations.

Laminates will fail by a mixture of modes. The most likely mode of failure to occur initially is matrix cracking. AE monitoring would indicate this. Subsequent AE activity of the order of 10 times the initial activity would indicate the onset of fibre failure. Catastrophic damage could be averted by evaluating the structure at this stage.

6. List of References

1. ASM Handbook, Nondestructive Evaluation and Quality Control, Volume 17
2. Physical Acoustics Corporation, 8000 Spartan AT User's Manual
3. Williams, R.V., Acoustic Emission, Elsevier Applied Science Publications, 2nd Edition, 1984
4. Spanner, J.C., Acoustic Emission – Techniques and Applications, Intex Publishing Co., 1988
5. Wadley, H.N.G., Scruby, C.B., Speake, J.H., Acoustic emission for physical examination of metals, Int'l Metals Reviews, 1980
6. Raj, B., Jayakumar, T., Acoustic Emission: Current Practices and Future Directions, ASTM STP 1077, American Society for Testing and Materials, Philadelphia, 1990
7. Tait, R.B., Materials Selection in the Mining Industry, Butterworth & Co., 1987
8. British Standard, BS 7448: Part 1: 1991, Fracture Mechanics toughness tests, 1991
9. Anderson, T.L., Fracture Mechanics – Fundamentals and Applications, 2nd Edition, CRC Press, 1995
10. Latzko, D.G.H., et al., Post Yield fracture Mechanics, 2nd Edition, Elsevier Applied Science Publishers Ltd., 1984
11. Mukhophadhyay, C.K., Ray, K.K., Jayakumar, T., Raj, B, Acoustic emission from tensile deformation of unnotched and notched specimens of AISI type 304 Stainless Steels, Material Science and Engineering, A255, 1998
12. Dunegan, H.L., Harris, D.O., Tatro, C.A., Fracture Analysis by Use of Acoustic Emission, Engineering Fracture Mechanics Vol 1, 1968

13. Palma, J.M., Stafford, Stafford, S.W., edited by McGonnagle, W.J., International Advances in Non-destructive testing, 1979
14. Lambert, A., et al, Application of Acoustic Emission to the study of Cleavage fracture mechanism in a HSLA steel, Scripta Materialia Vol 43, 2000
15. Heipe, C.H., Carpenter, S.H., Journal of Acoustic Emission Vol 6, p117, 1987
16. Long, Q.Y., Huazi, Y., Metall. Transactions Vol 21A, p373,1990
17. Hartbower, C.E., Gerberich W.W., Liebowitz H., Investigation of Crack-Growth Stress-Wave Relationships, Engineering Fracture Mechanics Vol 1, 1968
18. Long, X., Guangjun, C., Svensson, L.E., Investigation of fracture and determination of fracture toughness of modified 9Cr-1Mo steel weld metals using AE Techniques, Material Science and Engineering A270, 1999
19. Khan, M.A., et al., Acoustic Emission Rating parameter for prediction of tearing instability in structural materials, Engineering Fracture Mechanics Vol 16, 1982
20. Khan, M.A., Characterisation of the Crack Toughness behaviour of structural steels by the Tearing modulus parameter and Acoustic emission, Journal of Testing and Evaluation, 1982
21. Camerin, C.S., Rebello, J.M.A., Soares, S.D., NDT & E Int. 25, 1992
22. Baker, G.S., Acoustic Emissions and pre fracture processes in high strength steels, AFML TR 67-266, Aero-jet General Corporation, Sacramento, CA, 1968
23. Jones, M.H., Brown, W.F., Acoustic detection of crack initiation in sharply notched specimens, Materials Research and Standards Vol 4, 1964
24. Zimcik, D.G., et al., Real-time monitoring of carbon-epoxy composites using acoustic emission NDE, SAMPE Quarterly 19, 1988

25. Johnson, M., Gudmunson, P., Broadband transient recording and characterization of acoustic emission events in composite laminates, Composite Science & Technology Vol 60 Issue 15, 2000

26. Mallick, P.K.(ed), Composites Engineering Handbook, Marcel Dekker, New York, 1997

27. Karam, G.K., Effect of fibre volume on tensile properties of real unidirectional fibre-reinforced composites, Composites Vol 22 no. 2, 1991

28. Baker, A.R., Sachse, W., Measurement of composite interface failure by quantitative AE, Ultrasonics Vol 34, 1996

29. Barthelemy, H., Periodic inspection of compressed gas cylinders and tubes – Flaw detection using acoustic emission testing, Journal of Pressure Vessel Technology, 1988

30. Hill, E.v.K., Lewis, T.J. Acoustic Emission Monitoring of a Filament wound Composite Rocket Motor Case during Hydroproof, Materials Evaluation, 43, 1985

31. Hill, E.v.K, Predicting Burst Pressures in Filament Wound Composite Pressure Vessels by using Acoustic Emission Data, Materials Evaluation, 1992

32. McNally, D.J., Inspection of Composite Rocket Motor Cases Using Acoustic Emission, Materials Evaluation, 43, 1985

33. Guang Dai, et al., AE monitoring and data analysis for large spherical tanks, NDT&E International, Vol 26 No. 6, 1993

34. Physical Acoustics Corporation, Sclected Standard Practices and Codes – Acoustic Emission

35. Narisawa, I., Oba, T., An Evaluation of acoustic emission from fibre-reinforced composites, Journal of Material Science, 20, 1985

APPENDIX 1 -Fracture Toughness Tests and Acoustic Emission Responses

Three Point Bend Specimen

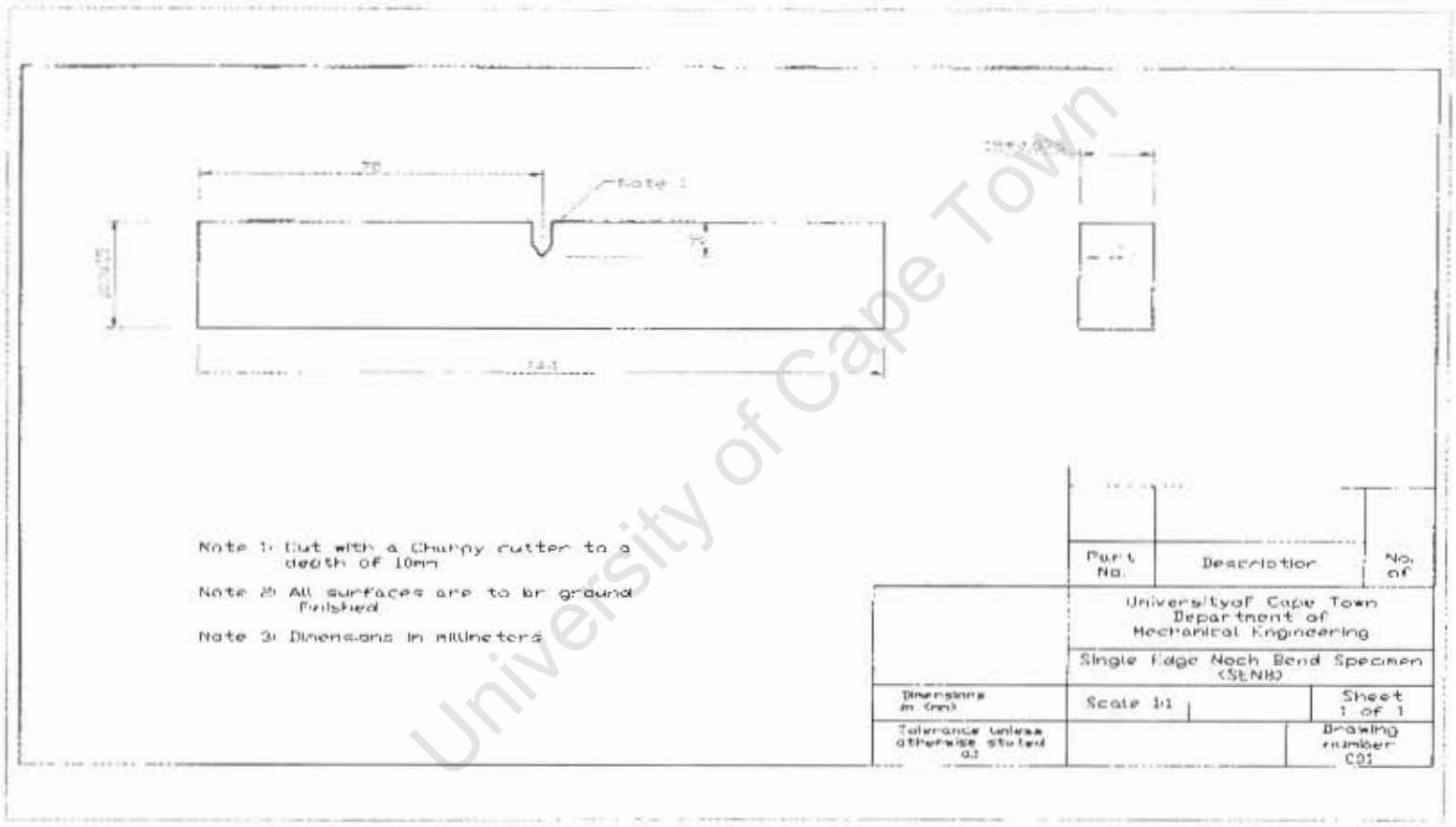

Load vs. clip gauge displacement curves

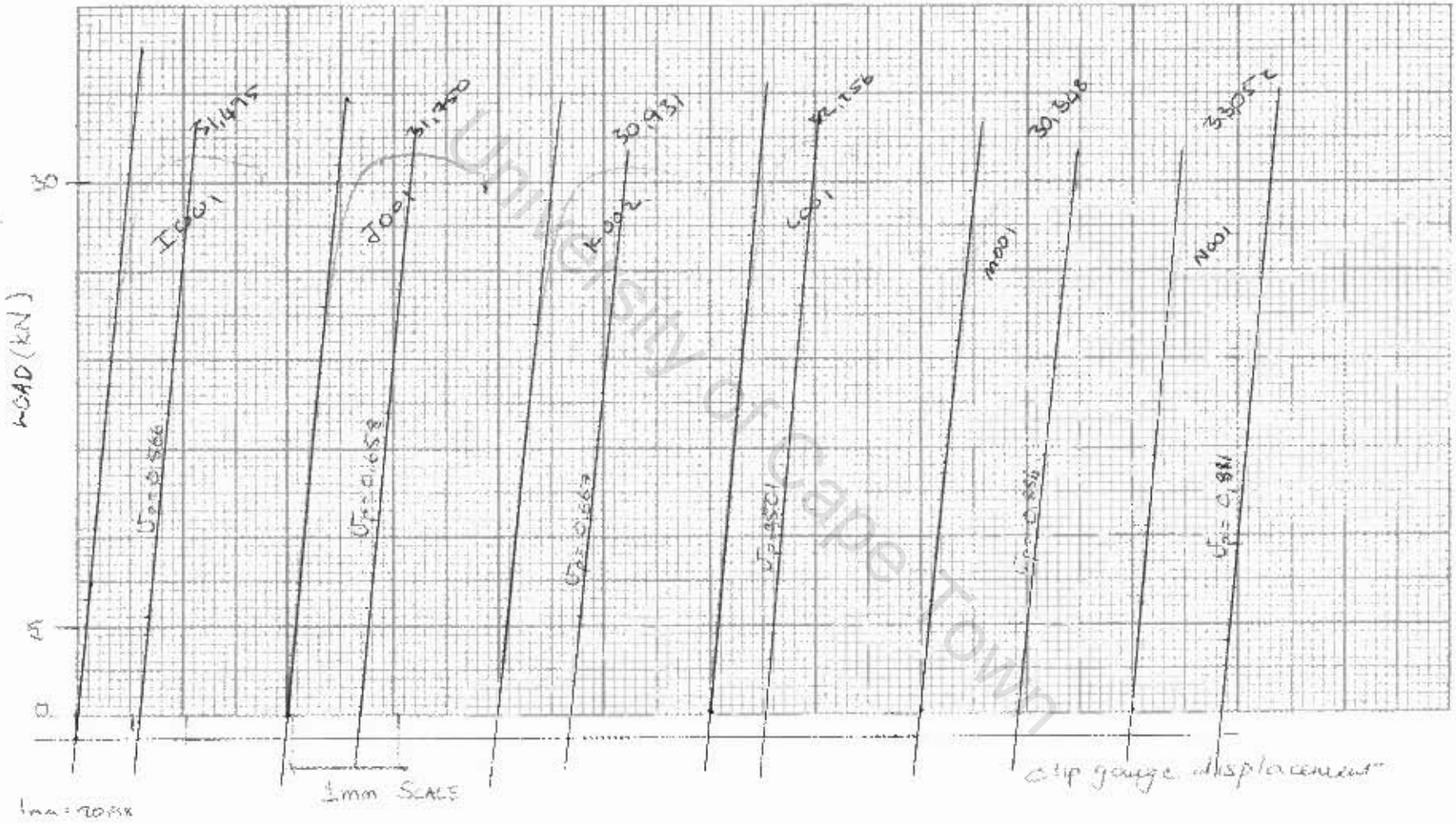

Load vs. clip gauge displacement curves

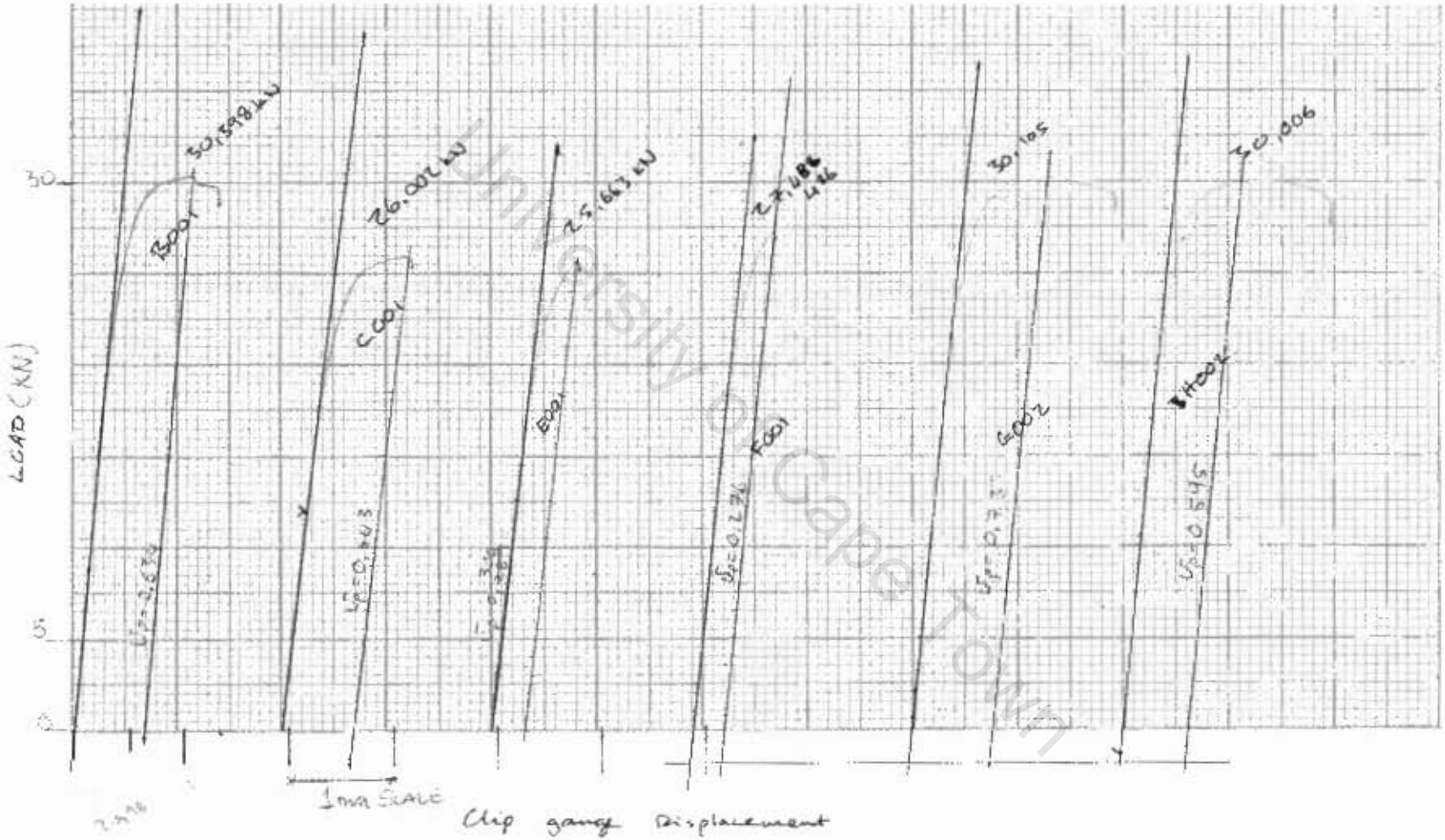

Fracture Toughness Test

Specimen	B										
Material Details											
Test Temperature	Ambient										
Yield Stress at test temperature	8.60E+08	Pa									
Young's Modulus, E	2.00E+11	Pa									
Poisson's ratio, v	0.24										
Specimen Dimensions	1	2	3	4	mean(m)						
Thickness, B (mm)	15.05	15.085	15.1	15.02	0.015066						
Width, W (mm)	30.06	30.07	30.1	30.08	0.030068						
Height of clip gauge, z (mm)	3	3	3	3	0.003						
Span					0.12043						
Test Details											
Loading Rate											
Full Scale load											
Extension rate	0.025	mm/s									
Full Scale stroke											
Max load											
Load Pq	3.04E+04	N									
Clip gauge displacement, Vp	6.35E-04	m									
Crack length	0	1/8B	2/8B		3/8B	4/8B	5/8B	6/8B	7/8B	B	mean(m)
total crack length, a0+Δa (mm)	14.68	15.41	15.88		16.5	17.01	16.67	16.01	15.32	14.68	0.015935
Fatigue precrack lenth, a0 (mm)	14.82	15.27	15.52		15.59	15.59	15.55	15.41	15.2	14.68	0.01536
Crack growth increment, Δa (mm)	0.14	0.14	0.36		0.91	1.42	1.12	0.6	0.12	0	0.000575
Ratio a0/W	valid crack ratio										0.510851
f(a0/W)	2.756626										
Kq (Mpa.m^0.5)	1.28E+08										
Valid Thickness	0.05579										
Elastic	4.52E-05										
Plastic	0.000154										
COD (mm)	0.199										
Tear size (mm)	0.575										

Fracture Toughness Test

Specimen	C										
Material Details											
Test Temperature	Ambient										
Yield Stress at test temperature	8.60E+08	Pa I									
Young's Modulus, E	2.00E+11	Pa I									
Poisson's ratio, v	0.24										
Specimen Dimensions	1	2	3	mean(m)							
Thickness, B (mm)	15.04	15.08	15.09	0.0150725							
Width, W (mm)	30.12	30.12	30.1	0.0301175							
Height of clip gauge, z (mm)	3	3	3	0.003							
Span				0.12043							
Test Details											
Loading Rate											
Full Scale load											
Extension rate	0.025	mm/s									
Full Scale stroke											
Max load											
Load Pq	2.60E+04	N									
Clip gauge displacement, Vp	6.48E-04	m									
Crack length	0	1/8B	2/8B	3/8B	4/8B	5/8B	6/8B	7/8B	B	mean(m)	
total crack length, a0+Δa (mm)	15.39	16.62	17.12	17.32	17.28	17.25	17.16	16.52	15.59	0.016845	
Fatigue precrack lenth, a0 (mm)	15.39	16.45	16.82	16.96	16.98	16.94	16.71	16.3	15.59	0.016581	
Crack growth increment, Δa (mm)	0	0.17	0.3	0.36	0.3	0.31	0.45	0.22	0	0.000264	
Ratio a0/W	valid crack ratio									0.550552	
f(a0/W)	3.148396										
Kq (Mpa.m^0.5)	1.25E+08										
Valid Thickness	0.052939										
Elastic	4.29E-05										
Plastic	0.00014										
COD (mm)	0.183										
Tear size (mm)	0.264										

Fracture Toughness Test

Specimen	E									
Material Details										
Test Temperature	Ambient									
Yield Stress at test temperature	8.60E+08	Pa I								
Young's Modulus, E	2.00E+11	Pa I								
Poisson's ratio, v	0.24									
Specimen Dimensions	1	2	3	4	**mean(m)**					
Thickness, B (mm)	15.06	15.08	15.07	15.1	0.015065					
Width, W (mm)	30.07	30.08	30.07	30.1	0.03007					
Height of clip gauge, z (mm)	3	3	3	3	0.003					
Span					0.12043					
Test Details										
Loading Rate										
Full Scale load										
Extension rate	0.025	mm/s								
Full Scale stroke										
Max load										
Load Pq	2.57E+04	N								
Clip gauge displacement, Vp	3.00E-04	m								
Crack length	0	1/8B	2/8B		3/8B	4/8B	5/8B	6/8B	7/8B	B	mean(m)
total crack length, a0+Δa (mm)	15.47	16.23	16.53		16.77	16.87	16.82	16.53	16.21	15.2	0.016412
Fatigue precrack lenth, a0 (mm)	15.47	16.23	16.53		16.77	16.87	16.82	16.53	16.21	15.2	0.016412
Crack growth increment, Δa (mm)	0	0	0		0	0	0	0	0	0	0
Ratio a0/W	valid crack ratio										0.545789
f(a0/W)	3.097										
Kq (Mpa.m^0.5)	1.22E+08										
Valid Thickness	0.050185										
Elastic	4.07E-05										
Plastic	6.59E-05										
COD (mm)	0.107										
Tear size (mm)	0										

Fracture Toughness Test										
Specimen	F									
Material Details										
Test Temperature	Ambient									
Yield Stress at test temperature	8.60E+08	Pa								
Young's Modulus, E	2.00E+11	Pa								
Poisson's ratio, v	0.24									
Specimen Dimensions	1	2	3	4	mean(m)					
Thickness, B (mm)	15.06	15.09	15.1	15.1	0.0150775					
Width, W (mm)	30.04	30.04	30.03	30	0.0300275					
Height of clip gauge, z (mm)	3	3	3	3	0.003					
Span					0.12043					
Test Details										
Loading Rate										
Full Scale load										
Extension rate	0.025	mm/s								
Full Scale stroke										
Max load										
Load Pq	2.75E+04	N								
Clip gauge displacement, Vp	2.76E-04	m								
Crack length	0	1/8B	2/8B		3/8B	4/8B	5/8B	6/8B	7/8B	B	mean(m)
total crack length, a0+Δa (mm)	14.83	15.62	16.02		16.2	16.2	16.1	15.96	15.59	14.81	0.015814
Fatigue precrack lenth, a0 (mm)	14.83	15.62	15.92		16.07	16.07	15.99	15.86	15.43	14.76	0.015719
Crack growth increment, Δa (mm)	0	0	0.1		0.13	0.13	0.11	0.1	0.16	0.05	9.44E-05
Ratio a0/W	valid crack ratio										0.523499
f(a0/W)	2.872899										
Kq (Mpa.m^0.5)	1.21E+08										
Valid Thickness	0.049666										
Elastic	4.03E-05										
Plastic	6.46E-05										
COD (mm)	0.105										
Tear size (mm)	0.094										

Fracture Toughness Test

Specimen	H									
Material Details										
Test Temperature	Ambient									
Yield Stress at test temperature	8.60E+08	Pa l								
Young's Modulus, E	2.00E+11	Pa l								
Poisson's ratio, v	0.24									
Specimen Dimensions	1	2	3	mean(m)						
Thickness, B (mm)	15.1	15.11	15.1	0.0150875						
Width, W (mm)	30.09	30.09	30.1	0.030095						
Height of clip gauge, z (mm)	3	3	3	0.003						
Span				0.12043						
Test Details										
Loading Rate										
Full Scale load										
Extension rate	0.025	mm/s								
Full Scale stroke										
Max load										
Load Pq	3.00E+04	N								
Clip gauge displacement, Vp	5.95E-04	m								
Crack length	0	1/8B	2/8B	3/8B	4/8B	5/8B	6/8B	7/8B	B	mean(m)
total crack length, a0+Δa (mm)	14.56	15.37	16.31	17.53	17.22	16.86	16.39	15.41	14.65	0.016212
Fatigue precrack lenth, a0 (mm)	14.49	15.23	15.56	15.62	15.69	15.69	15.56	15.27	14.43	0.015385
Crack growth increment, Δa (mm)	0.07	0.14	0.75	1.91	1.53	1.17	0.83	0.14	0.22	0.000827
Ratio a0/W	valid crack ratio									0.511214
f(a0/W)	2.75987									
Kq (Mpa.m^0.5)	1.27E+08									
Valid Thickness	0.054186									
Elastic	4.39E-05									
Plastic	0.000144									
COD (mm)	0.188									
Tear size (mm)	0.827									

Fracture Toughness Test

Specimen	I									
Material Details										
Test Temperature	Ambient									
Yield Stress at test temperature	8.60E+08	Pa I								
Young's Modulus, E	2.00E+11	Pa I								
Poisson's ratio, v	0.24									
Specimen Dimensions	1	2	3	**mean(m)**						
Thickness, B (mm)	15.07	15.11	15.1	0.015095						
Width, W (mm)	30.07	30.07	30.09	0.030075						
Height of clip gauge, z (mm)	3	3	3	0.003						
Span				0.12043						
Test Details										
Loading Rate										
Full Scale load										
Extension rate	0.025	mm/s								
Full Scale stroke										
Max load										
Load Pq	3.15E+04	N								
Clip gauge displacement, Vp	5.66E-04	m								
Crack length	0	1/8B	2/8B	3/8B	4/8B	5/8B	6/8B	7/8B	B	mean(m)
total crack length, a0+Δa (mm)	14.26	15.21	16.09	16.67	17	16.83	16.41	15.39	14.57	0.016002
Fatigue precrack lenth, a0 (mm)	14.26	15.06	15.34	15.51	15.51	15.51	15.44	15.23	14.43	0.015243
Crack growth increment, Δa (mm)	0	0.15	0.75	1.16	1.49	1.32	0.97	0.16	0.14	0.000759
Ratio a0/W	**valid** crack ratio									0.506837
f(a0/W)	2.721229									
Kq (Mpa.m^0.5)	1.31E+08									
Valid Thickness	0.058096									
Elastic	4.71E-05									
Plastic	0.000139									
COD (mm)	0.186									
Tear size (mm)	0.759									

Fracture Toughness Test

Specimen	J									
Material Details										
Test Temperature	Ambient									
Yield Stress at test temperature	8.60E+08	Pa I								
Young's Modulus, E	2.00E+11	Pa I								
Poisson's ratio, v	0.24									
Specimen Dimensions	1	2	3	4	mean(m)					
Thickness, B (mm)	15.04	15.09	15.1	15.1	0.0150725					
Width, W (mm)	30.06	30.07	30.07	30.1	0.0300675					
Height of clip gauge, z (mm)	3	3	3	3	0.003					
Span					0.12043					
Test Details										
Loading Rate										
Full Scale load										
Extension rate	0.025	mm/s								
Full Scale stroke										
Max load										
Load Pq	3.18E+04	N								
Clip gauge displacement, Vp	6.58E-04	m								
Crack length	0	1/8B	2/8B	3/8B	4/8B	5/8B	6/8B	7/8B	B	mean(m)
total crack length, a0+Δa (mm)	14.23	15.16	16.27	17.21	17.21	16.75	15.95	15.06	14.51	0.015998
Fatigue precrack lenth, a0 (mm)	14.23	15	15.3	15.38	15.38	15.34	15.16	14.9	14.29	0.01509
Crack growth increment, Δa (mm)	0	0.16	0.97	1.83	1.83	1.41	0.79	0.16	0.22	0.000908
Ratio a0/W	valid crack ratio									0.501871
f(a0/W)	2.678377									
Kq (Mpa.m^0.5)	1.30E+08									
Valid Thickness	0.057409									
Elastic	4.65E-05									
Plastic	0.000164									
COD (mm)	0.21									
Tear size (mm)	0.908									

Fracture Toughness Test

Specimen	K									
Material Details										
Test Temperature	Ambient									
Yield Stress at test temperature	8.60E+08	Pa I								
Young's Modulus, E	2.00E+11	Pa I								
Poisson's ratio, v	0.24									
Specimen Dimensions	1	2	3	mean(m)						
Thickness, B (mm)	15.11	15.11	15.11	0.0151025						
Width, W (mm)	29.98	30.03	30.04	0.0300225						
Height of clip gauge, z (mm)	3	3	3	0.003						
Span				0.12043						
Test Details										
Loading Rate										
Full Scale load										
Extension rate	0.025	mm/s								
Full Scale stroke										
Max load										
Load Pq	3.09E+04	N								
Clip gauge displacement, Vp	6.67E-04	m								
Crack length	0	1/8B	2/8B	3/8B	4/8B	5/8B	6/8B	7/8B	B	mean(m)
total crack length, a0+Δa (mm)	14.35	15.41	16.38	16.96	17.22	16.87	16.37	15.59	14.69	0.016165
Fatigue precrack lenth, a0 (mm)	14.35	15.17	15.47	15.64	15.7	15.72	15.6	15.32	14.55	0.015384
Crack growth increment, Δa (mm)	0	0.24	0.91	1.32	1.52	1.15	0.77	0.27	0.14	0.000781
Ratio a0/W	valid crack ratio									0.512407
f(a0/W)	2.770545									
Kq (Mpa.m^0.5)	1.31E+08									
Valid Thickness	0.05833									
Elastic	4.73E-05									
Plastic	0.000161									
COD (mm)	0.208									
Tear size (mm)	0.781									

Fracture Toughness Test

Specimen	L									
Material Details	Ambient									
Test Temperature	8.60E+08	Pa l								
Yield Stress at test temperature	2.00E+11	Pa l								
Young's Modulus, E	0.24									
Poisson's ratio, v										
Specimen Dimensions	1	2	3	4	**mean(m)**					
Thickness, B (mm)	15.06	15.1	15.1	15.1	0.015085					
Width, W (mm)	30	30.03	30	30	0.0300225					
Height of clip gauge, z (mm)	3	3	3	3	0.003					
Span					0.12043					
Test Details										
Loading Rate										
Full Scale load										
Extension rate	0.025	mm/s								
Full Scale stroke										
Max load										
Load Pq	3.23E+04	N								
Clip gauge displacement, Vp	5.01E-04	m								
Crack length	0	1/8B	2/8B		3/8B	4/8B	5/8B	6/8B	7/8B	B	mean(m)
total crack length, a0+Δa (mm)	13.97	14.92	15.53		16.34	16.39	16.2	15.5	14.84	14.19	0.015475
Fatigue precrack lenth, a0 (mm)	13.97	14.77	15.05		15.15	15.15	15.2	15.01	14.69	14.07	0.014874
Crack growth increment, Δa (mm)	0	0.15	0.48		1.19	1.24	1.05	0.49	0.15	0.12	0.000601
Ratio a0/W	valid crack ratio										0.49542
f(a0/W)	2.624227										
Kq (Mpa.m^0.5)	1.30E+08										
Valid Thickness	0.057043										
Elastic	4.62E-05										
Plastic	0.000127										
COD (mm)	0.173										
Tear size (mm)	0.601										

Fracture Toughness Test

Specimen	M									
Material Details										
Test Temperature	Ambient									
Yield Stress at test temperature	8.60E+08	Pa l								
Young's Modulus, E	2.00E+11	Pa l								
Poisson's ratio, v	0.24									
Specimen Dimensions	1	2	3	4	mean(m)					
Thickness, B (mm)	15.02	15	15	15	0.01502					
Width, W (mm)	30.08	30.1	30.1	30.1	0.03008					
Height of clip gauge, z (mm)	3	3	3	3	0.003					
Span					0.12043					
Test Details										
Loading Rate										
Full Scale load										
Extension rate	0.025	mm/s								
Full Scale stroke										
Max load										
Load Pq	3.03E+04	N								
Clip gauge displacement, Vp	8.86E-04	m								
Crack length	0	1/8B	2/8B	3/8B	4/8B	5/8B	6/8B	7/8B	B	mean(m)
total crack length, a0+Δa (mm)	14.85	15.7	16.19	16.5	16.54	16.4	16.06	15.62	14.85	0.015988
Fatigue precrack lenth, a0 (mm)	14.76	15.5	15.84	15.94	15.94	15.9	15.81	15.51	14.84	0.015659
Crack growth increment, Δa (mm)	0.09	0.19	0.35	0.56	0.6	0.52	0.25	0.11	0.01	0.000329
Ratio a0/W	valid crack ratio									0.52057
f(a0/W)	2.845314									
Kq (Mpa.m^0.5)	1.33E+08									
Valid Thickness	0.059533									
Elastic	4.82E-05									
Plastic	0.000209									
COD (mm)	0.257									
Tear size (mm)	0.329									

Fracture Toughness Test

Specimen	N									
Material Details										
Test Temperature	Ambient									
Yield Stress at test temperature	8.60E+08	Pa I								
Young's Modulus, E	2.00E+11	Pa I								
Poisson's ratio, v	0.24									
Specimen Dimensions	1	2	3	4	mean(m)					
Thickness, B (mm)	15.09	15.1	15.1	15.1	0.015083					
Width, W (mm)	30.09	30.1	30.1	30.1	0.030098					
Height of clip gauge, z (mm)	3	3	3	3	0.003					
Span					0.12043					
Test Details										
Loading Rate										
Full Scale load										
Extension rate	0.025	mm/s								
Full Scale stroke										
Max load										
Load Pq	3.31E+04	N								
Clip gauge displacement, Vp	8.11E-04	m								
Crack length	0	1/8B	2/8B	3/8B	4/8B	5/8B	6/8B	7/8B	B	mean(m)
total crack length, a0+Δa (mm)	14.13	15	15.43	15.64	15.74	15.5	15.42	14.94	14.19	0.015228
Fatigue precrack lenth, a0 (mm)	13.99	14.9	15.17	15.27	15.26	15.2	15.11	14.82	14.02	0.014966
Crack growth increment, Δa (mm)	0.14	0.12	0.26	0.37	0.48	0.28	0.31	0.12	0.17	0.000262
Ratio a0/W	valid crack ratio									0.497238
f(a0/W)	2.63932									
Kq (Mpa.m^0.5)	1.33E+08									
Valid Thickness	0.060153									
Elastic	4.88E-05									
Plastic	0.000204									
COD (mm)	0.253									
Tear size (mm)	0.262									

Acoustic Emission Responses for Fracture Toughness Specimens (ROQ-tuf AD 690)

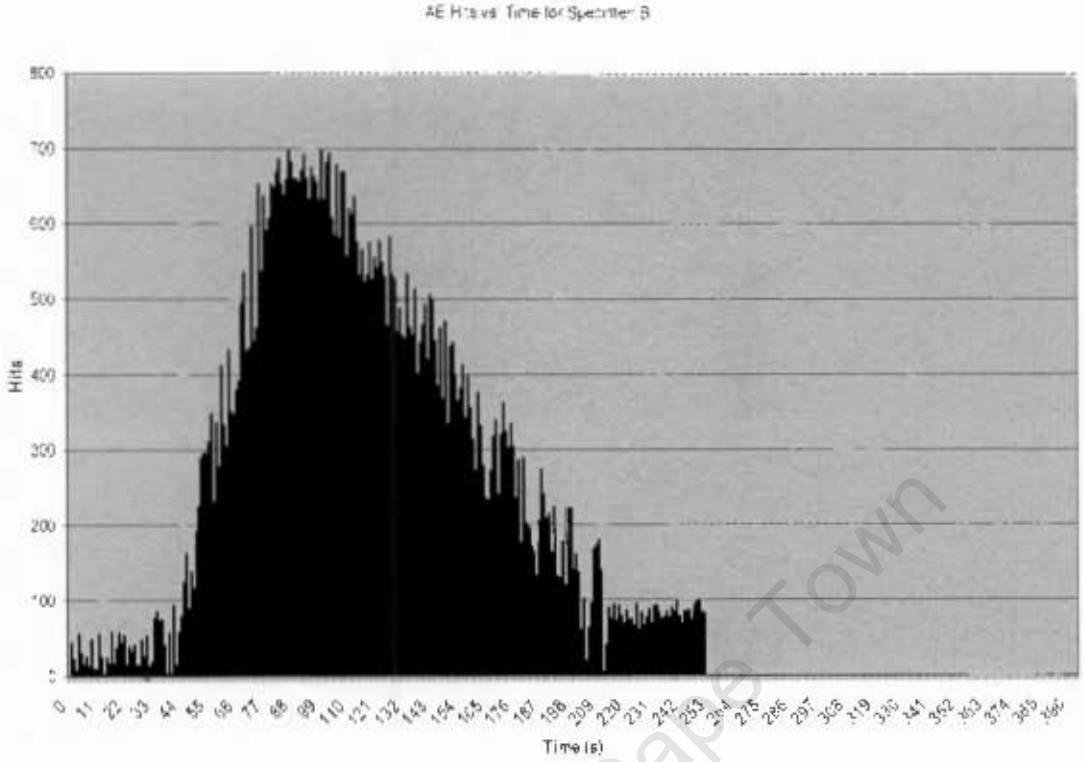

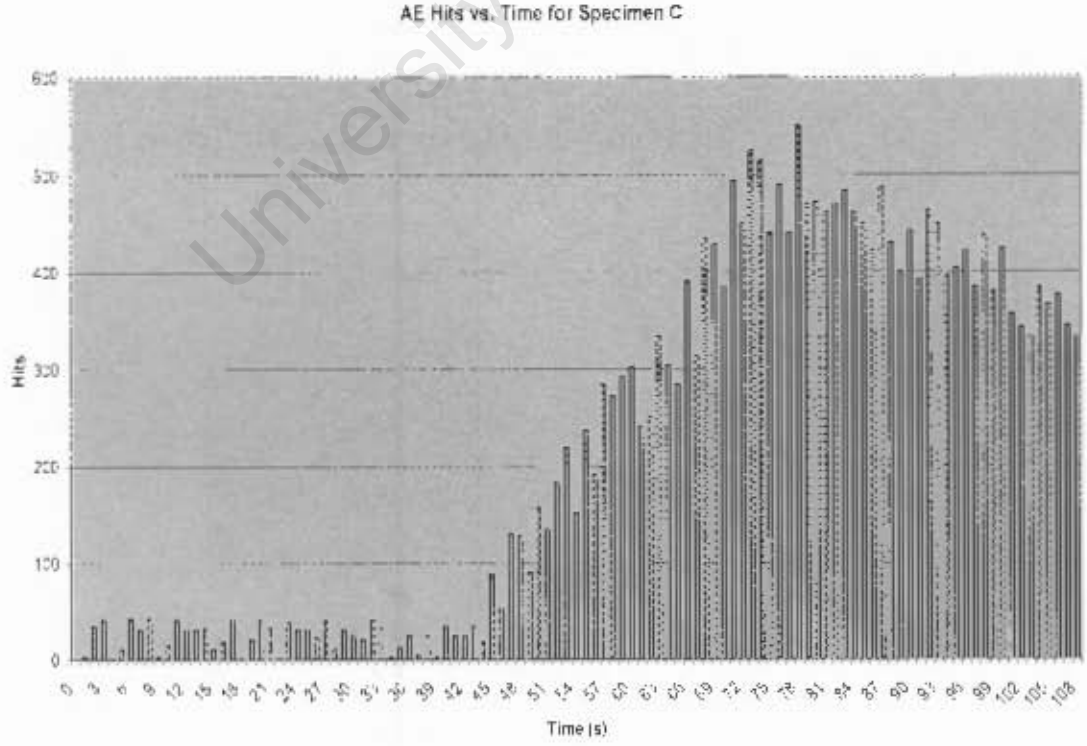

AE Hits vs. Time for Specimen E

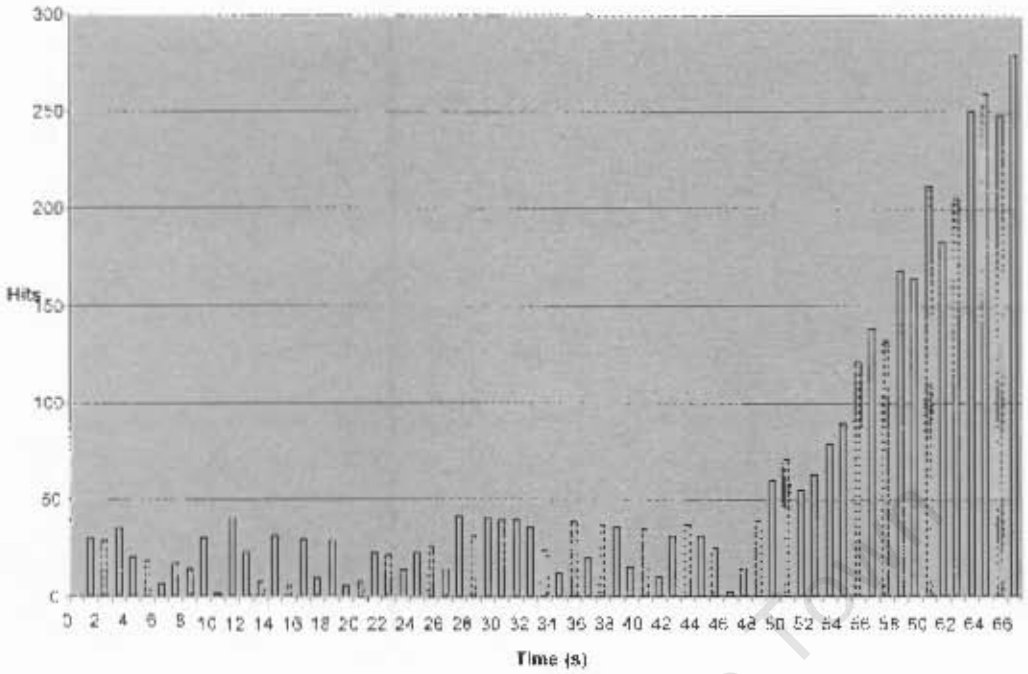

AE Hits vs. Time for specimen F

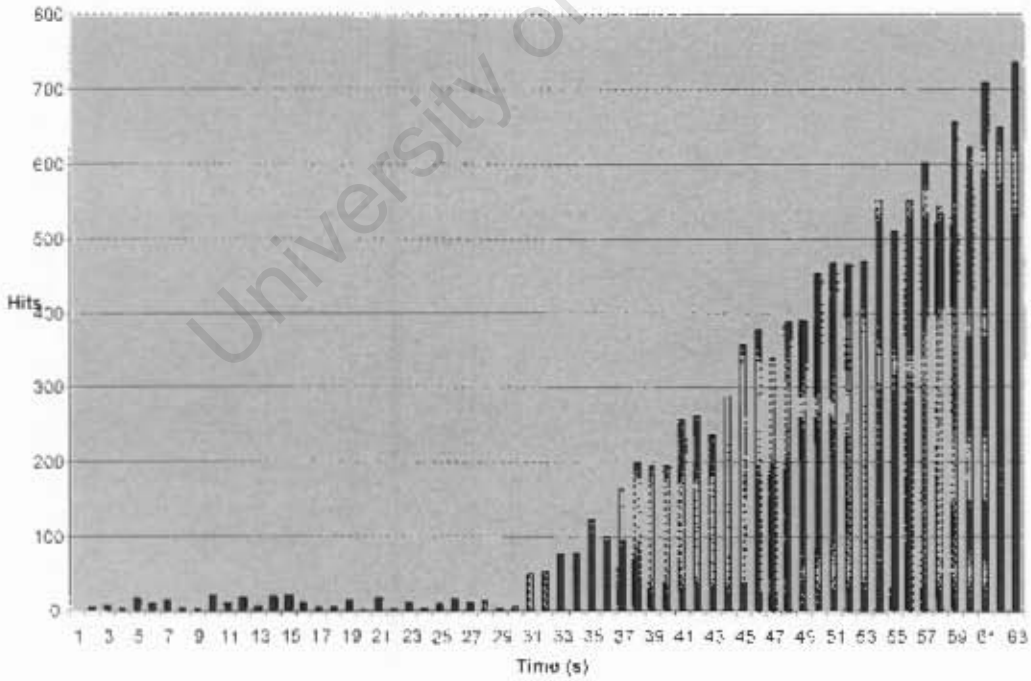

AE Hits vs. Time for Specimen H

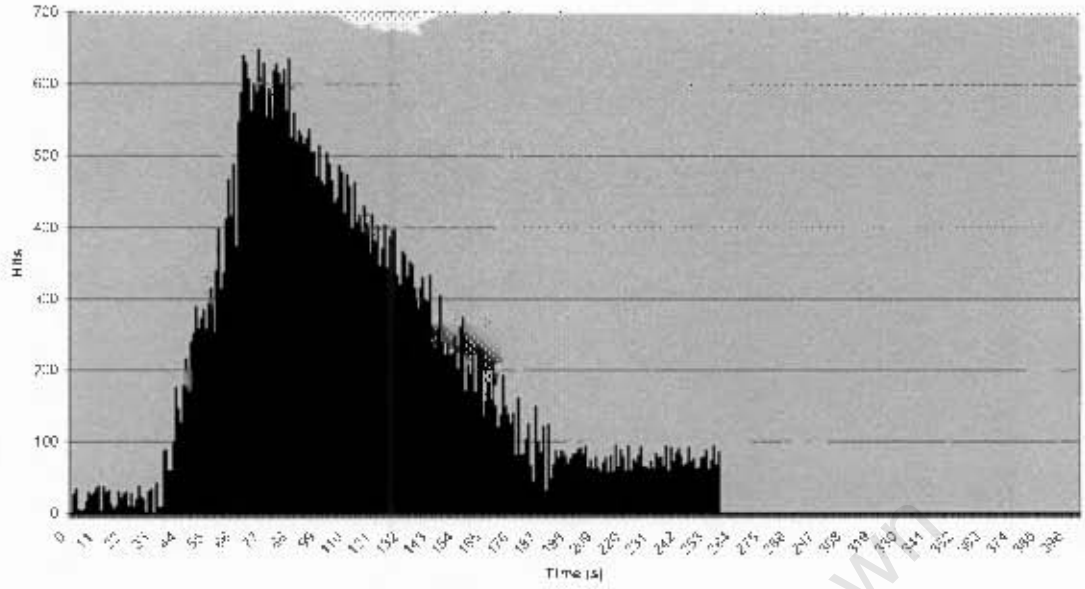

AE hits vs. Time for Specimen I

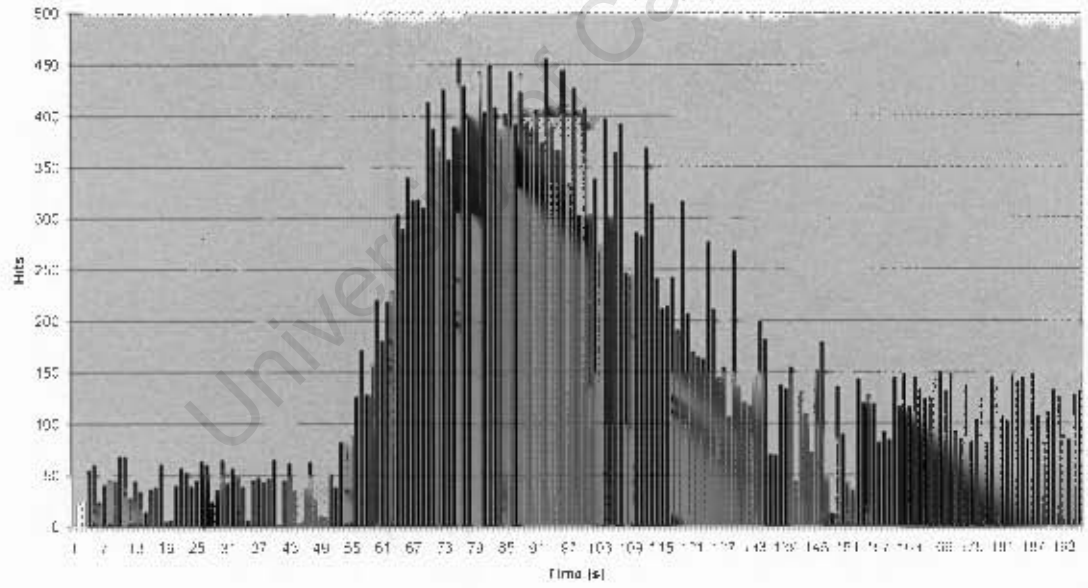

AE Hits vs. Time for Specimen K

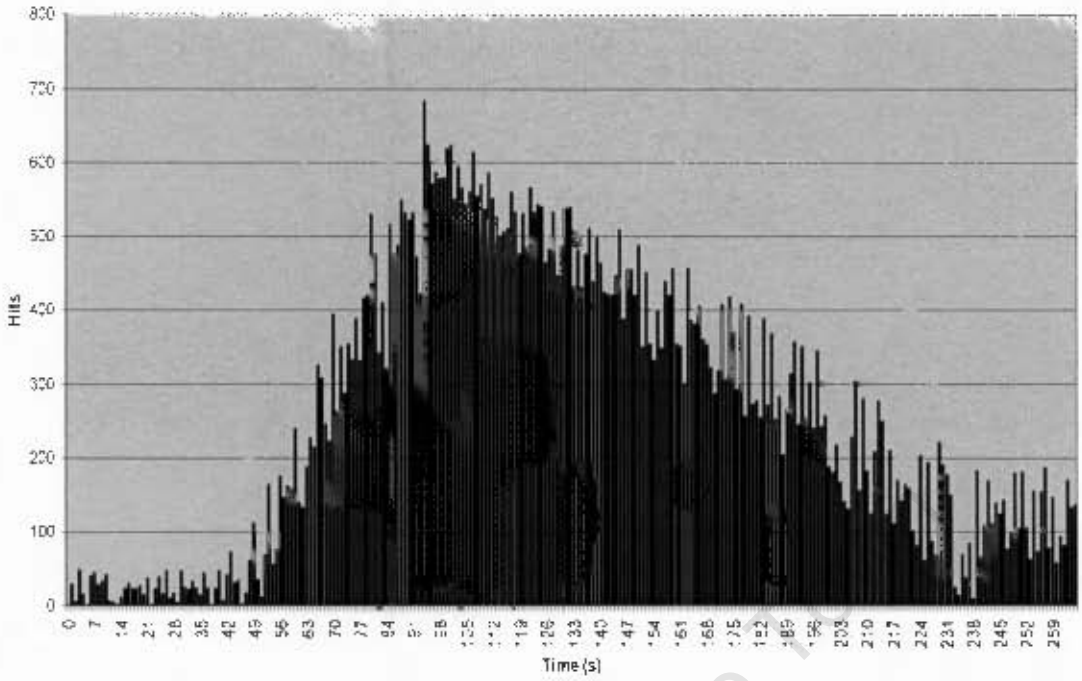

AE hits vs. Time for Specimen L

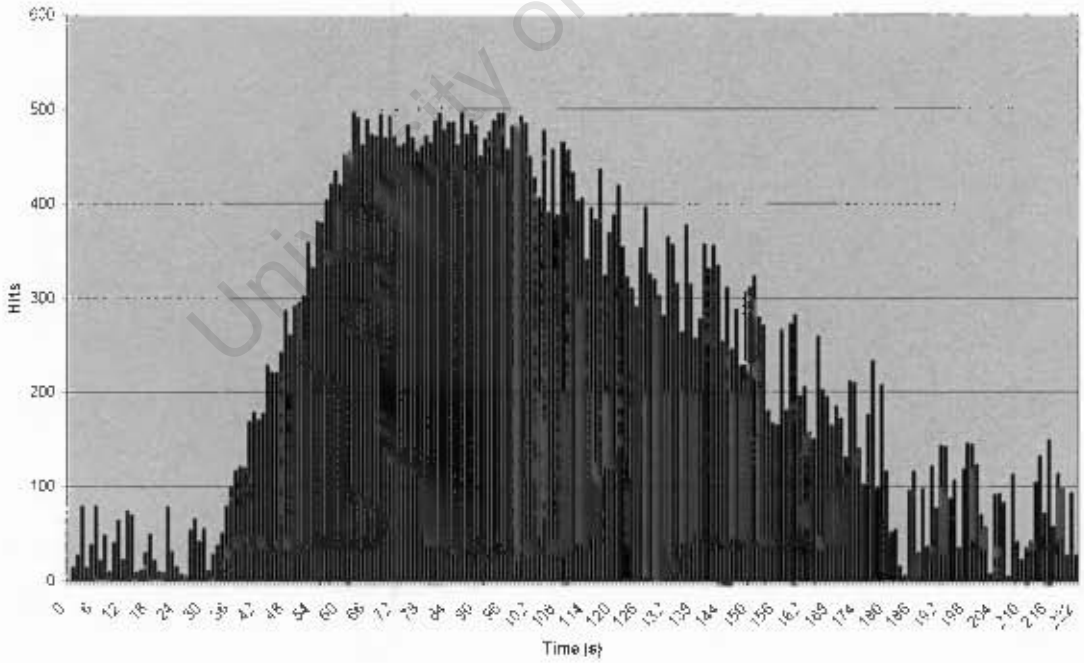

AE Hits vs time for Specimen M

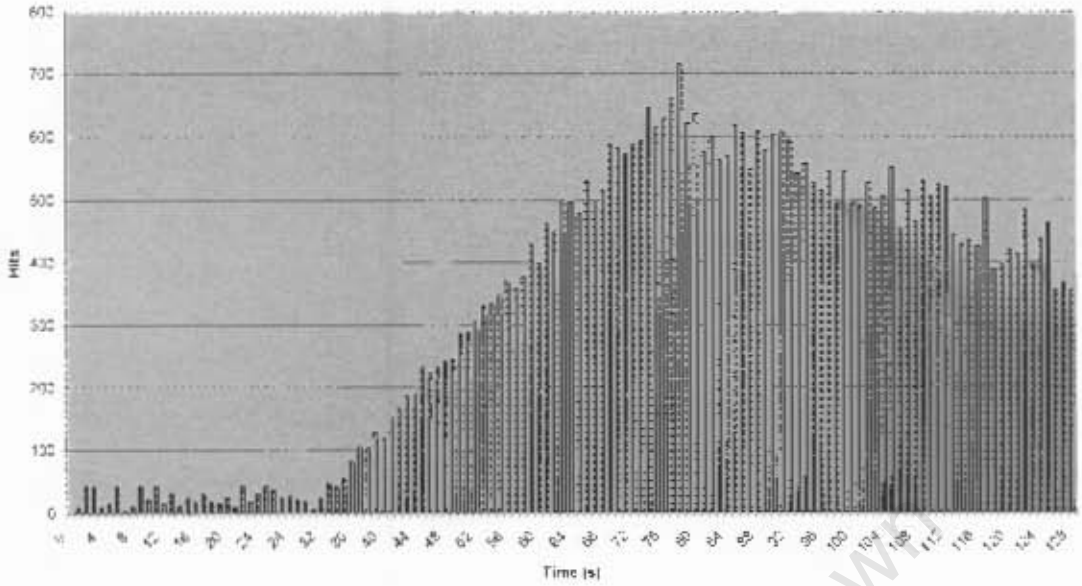

AE Hits vs. Time for Specimen N

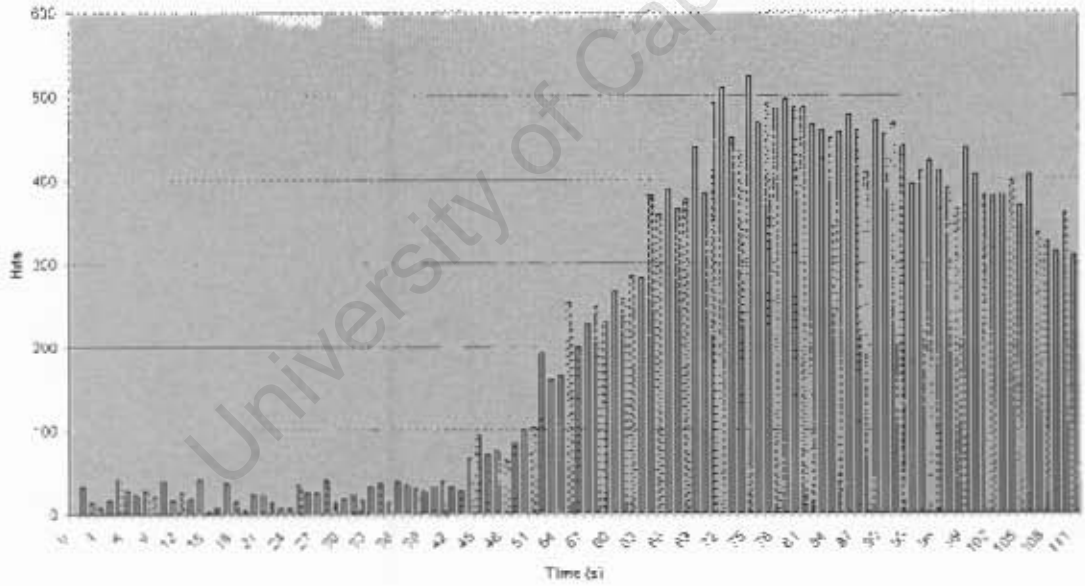

APPENDIX 2 -Composite Testing and Acoustic Emission Responses

Stress vs. Strain Curves for Longitudinal Lay-up

LFVF Specimens

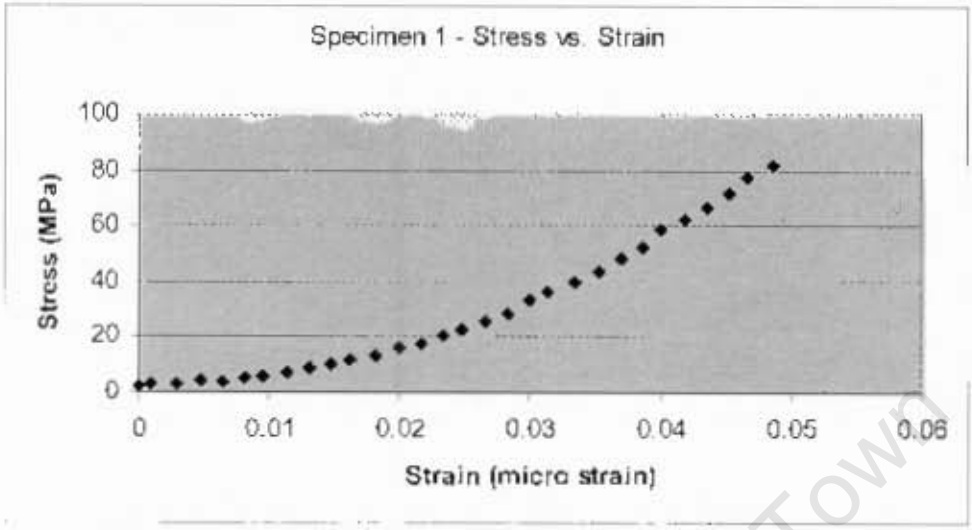

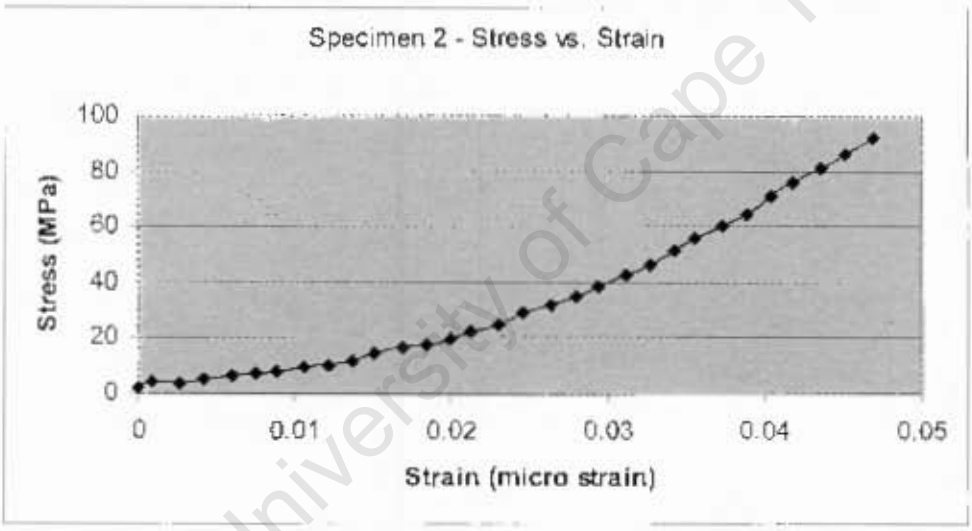

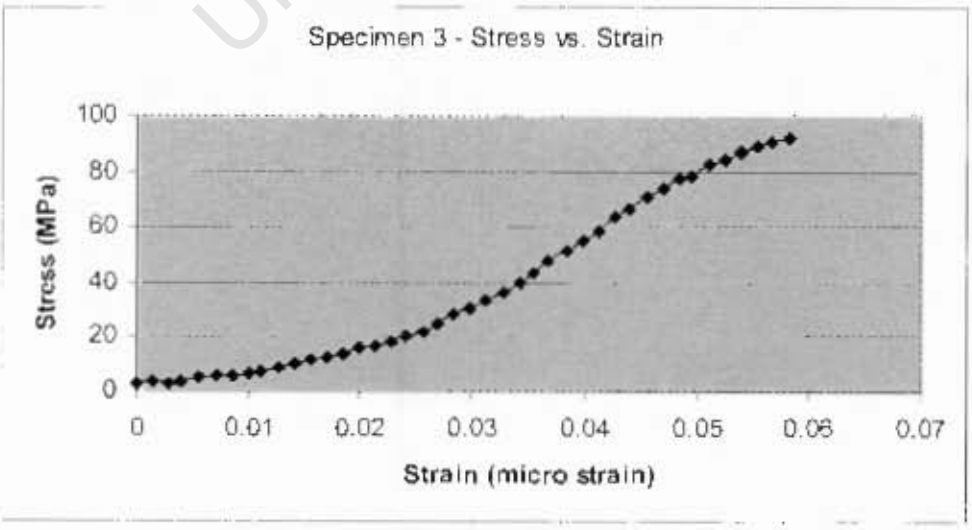

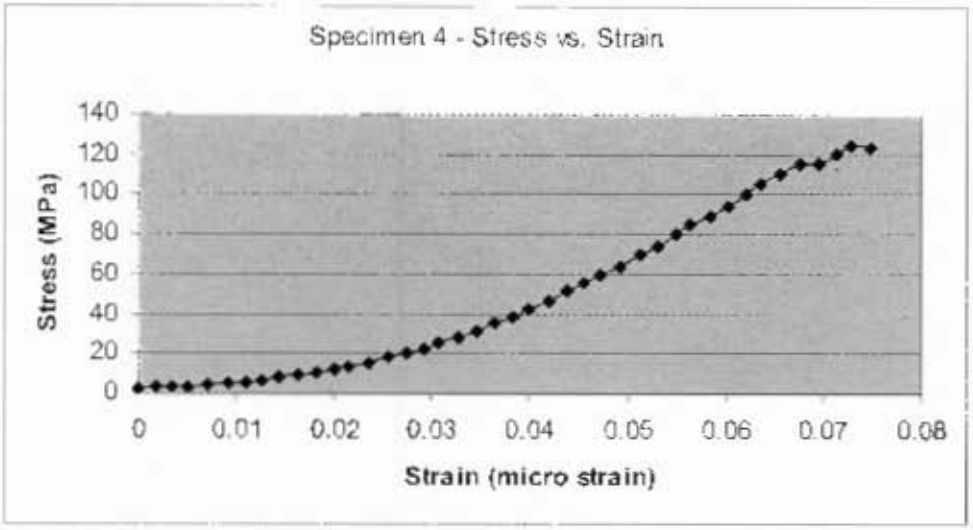

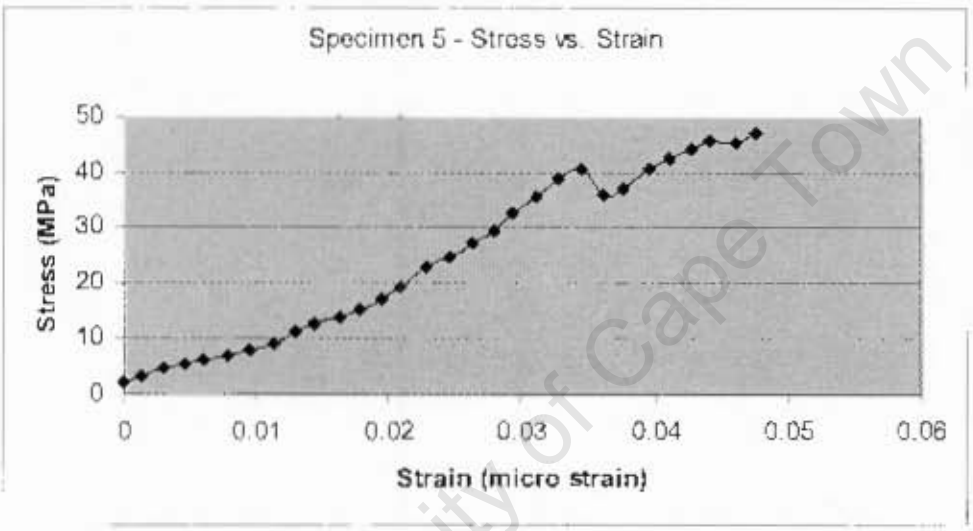

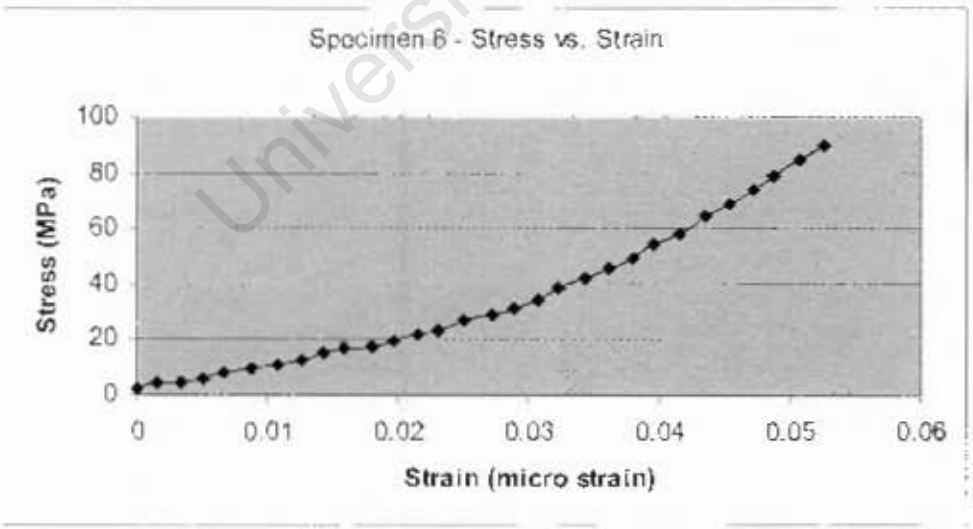

Acoustic Emission Responses for Longitudinal Lay-up LFVF specimens

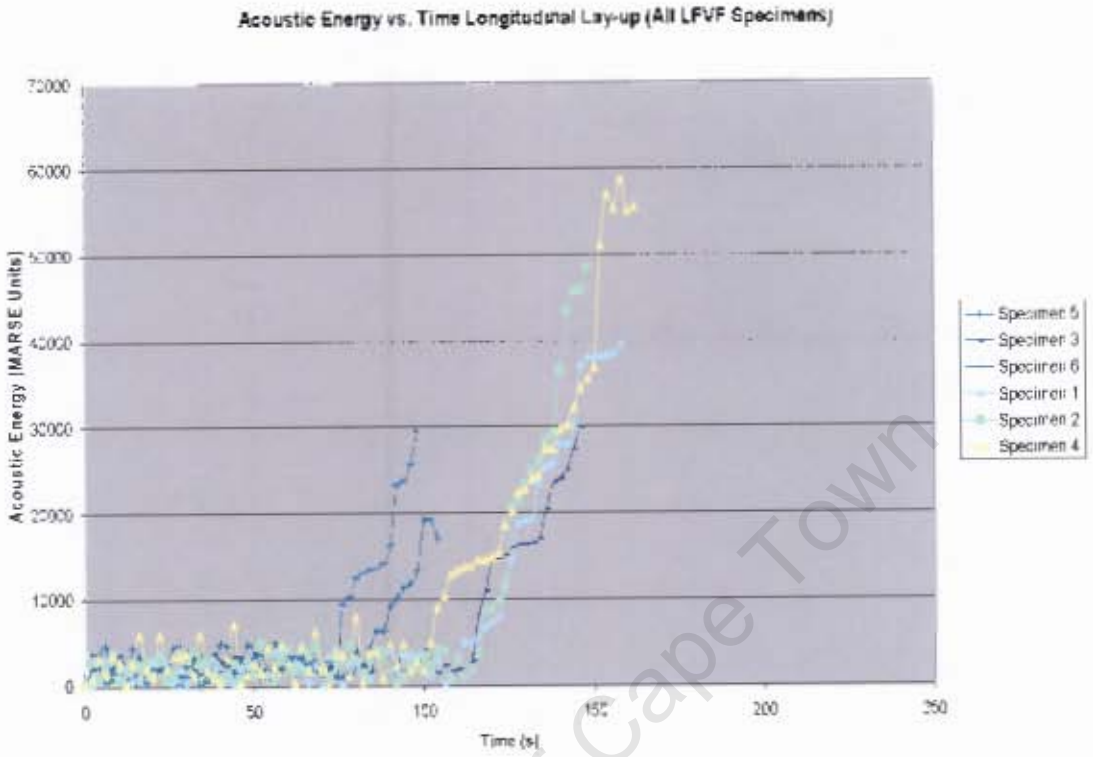

Stress vs. Strain Curves for Longitudinal Lay-up

HFVF Specimens

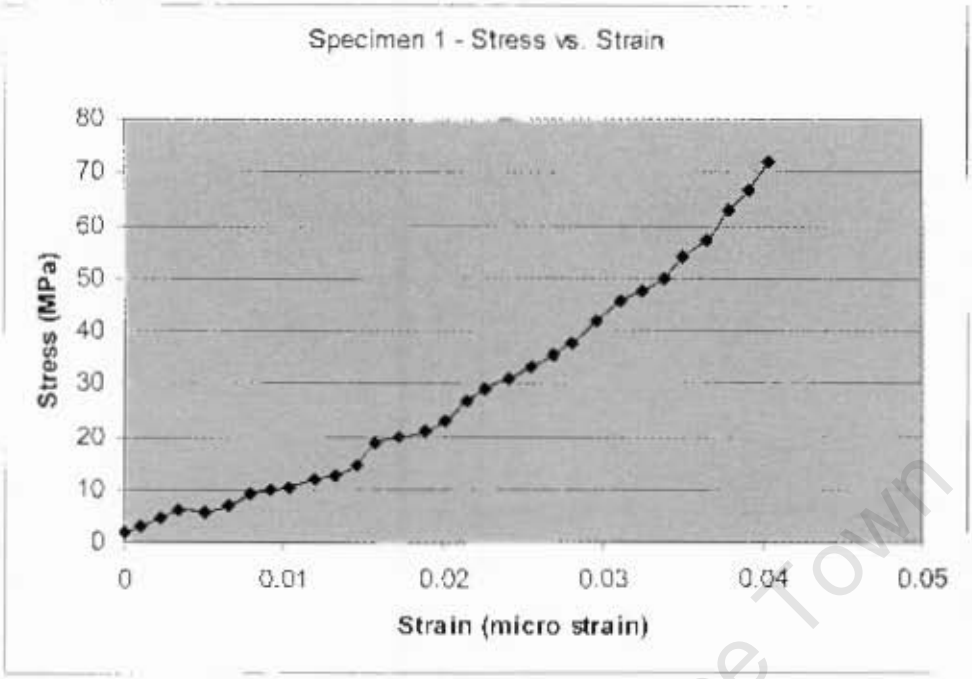

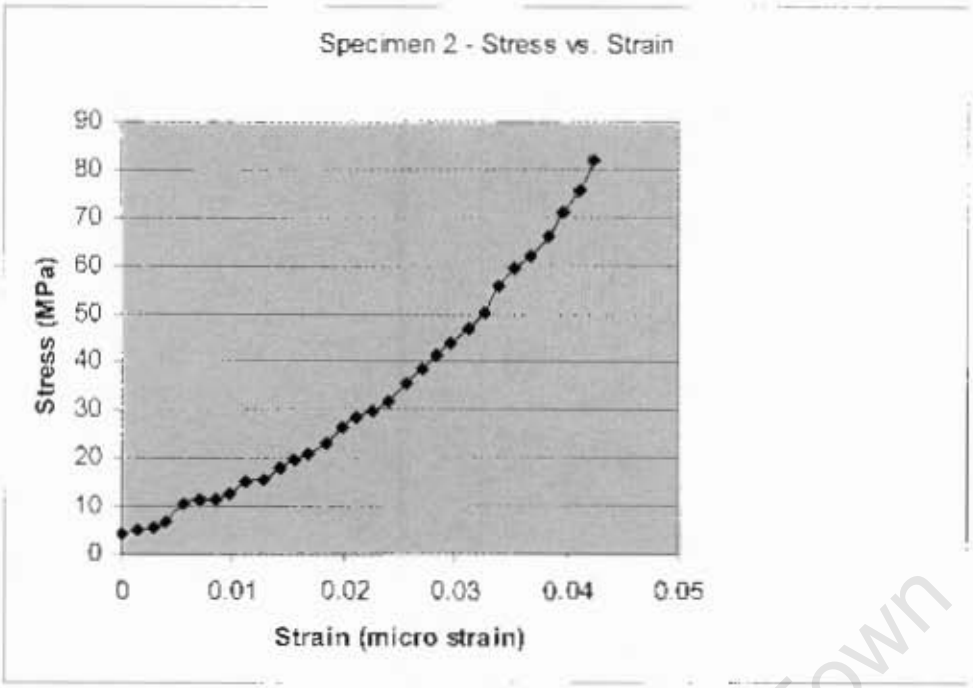

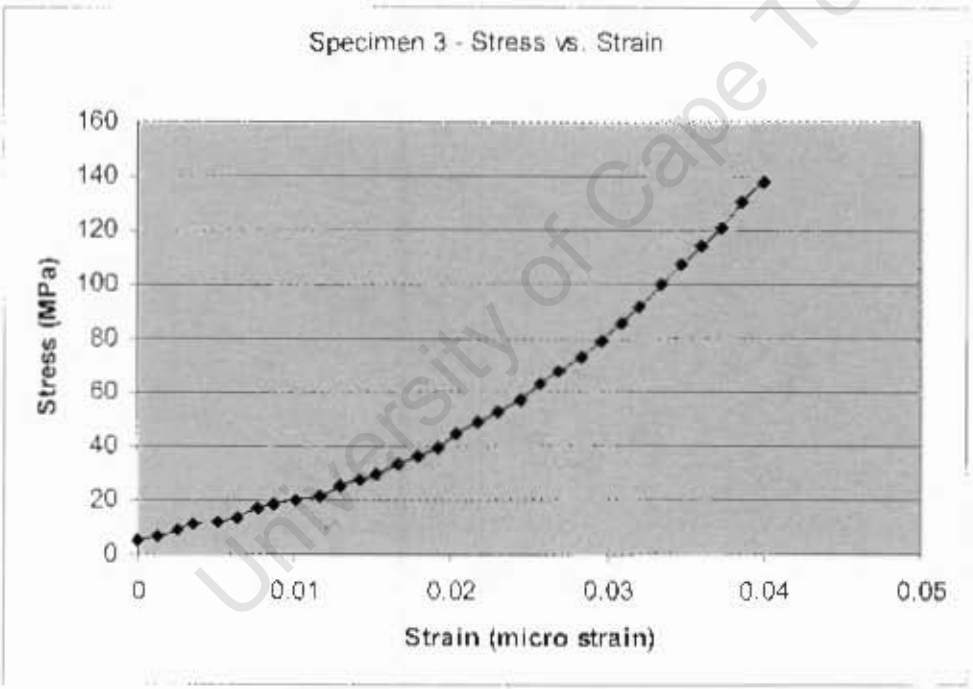

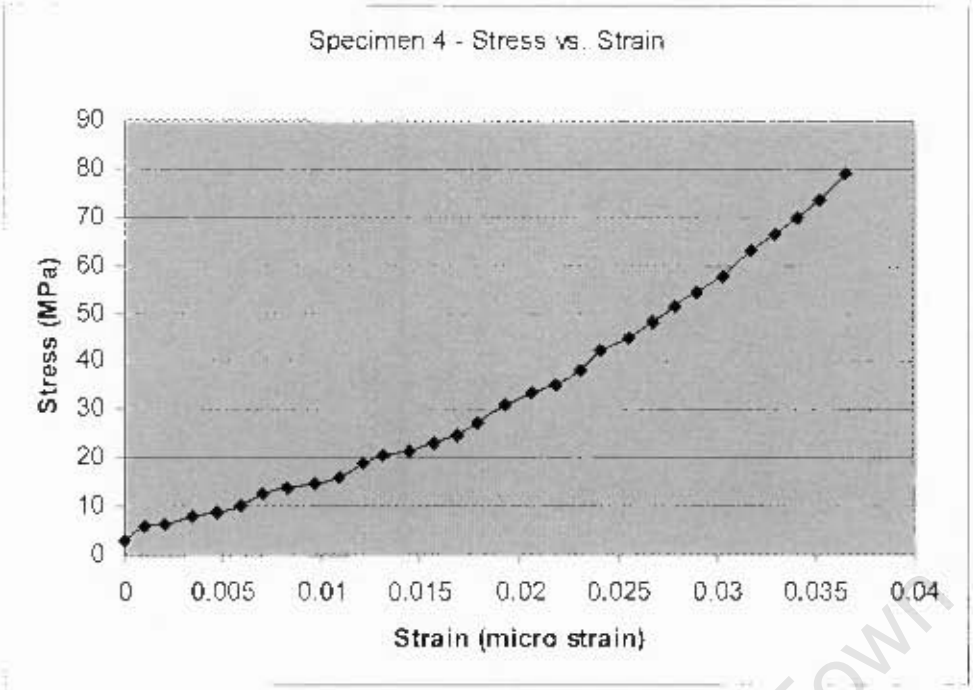

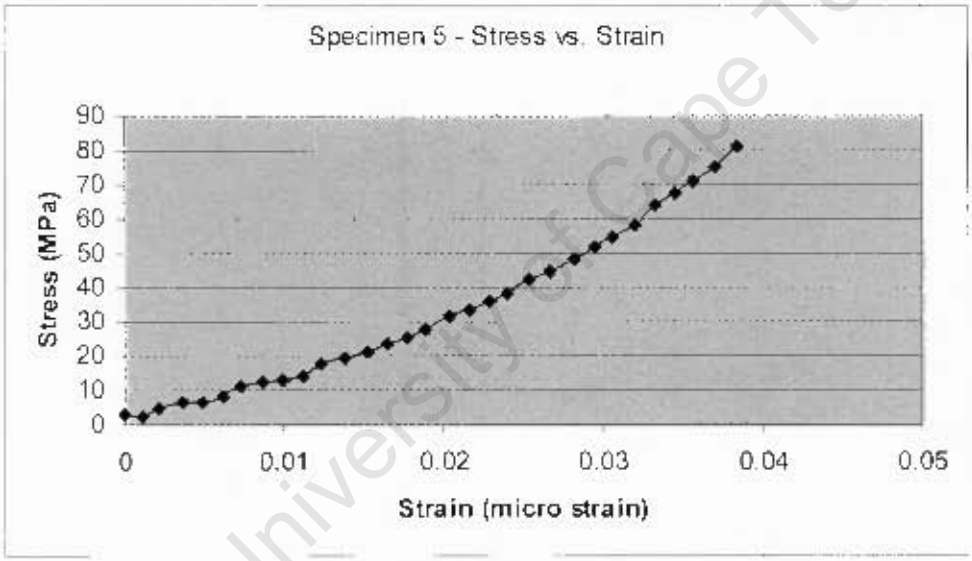

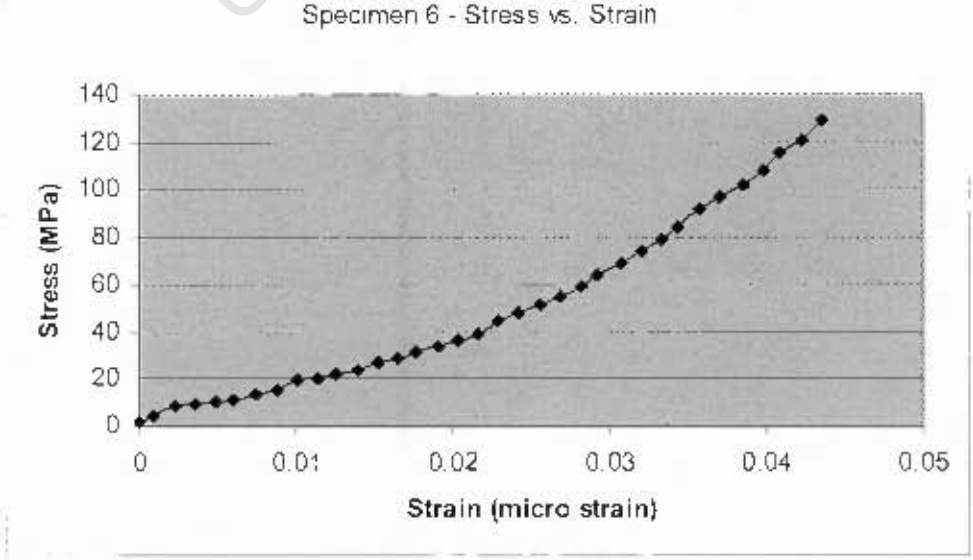

Acoustic Emission Responses for Longitudinal Lay-up HFVF specimens

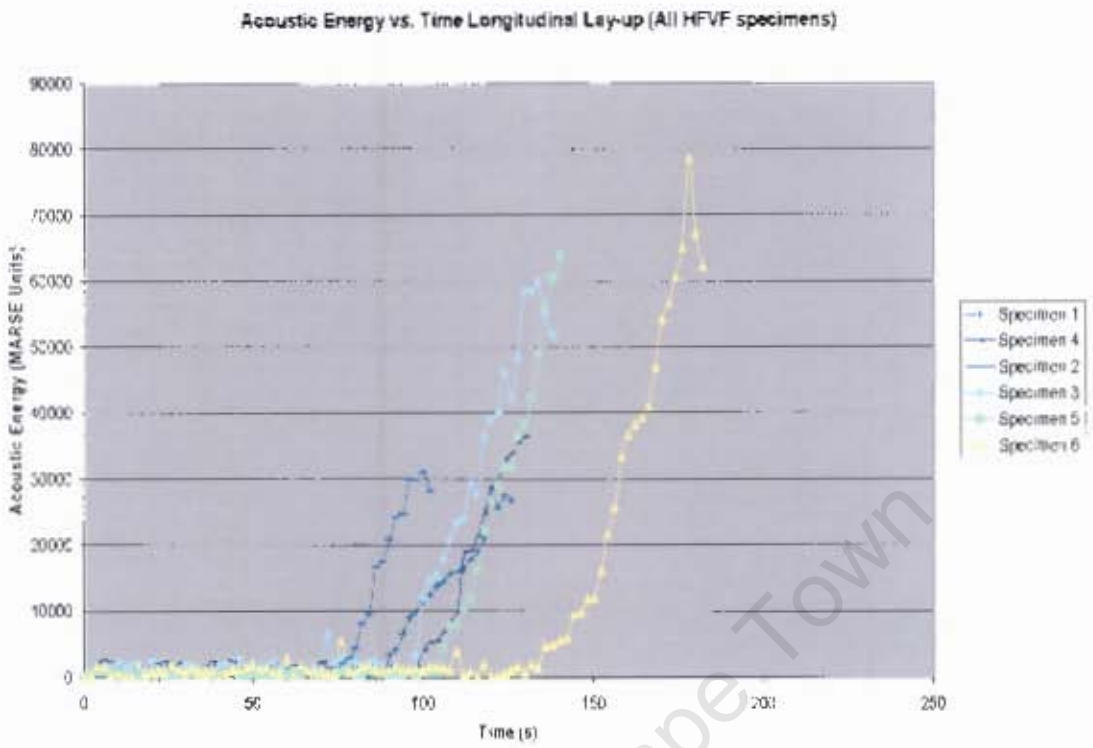

Stress vs. Strain Curves for Transverse Lay-up

LFVF Specimens

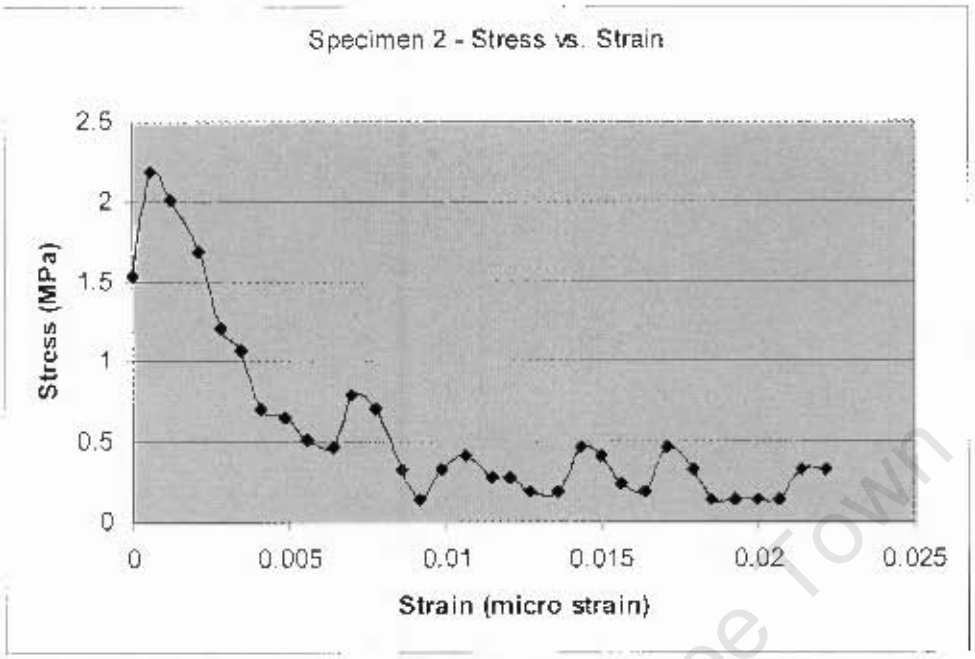

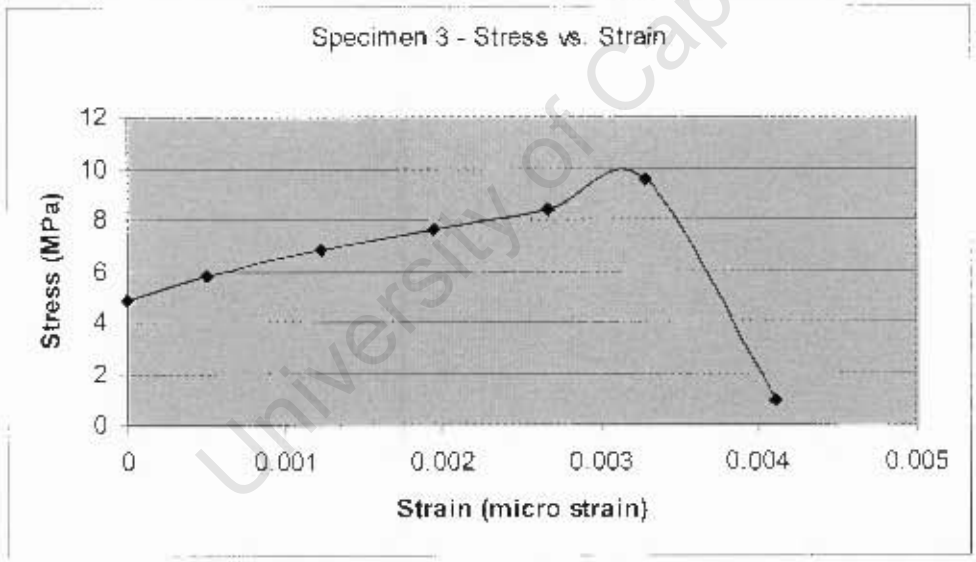

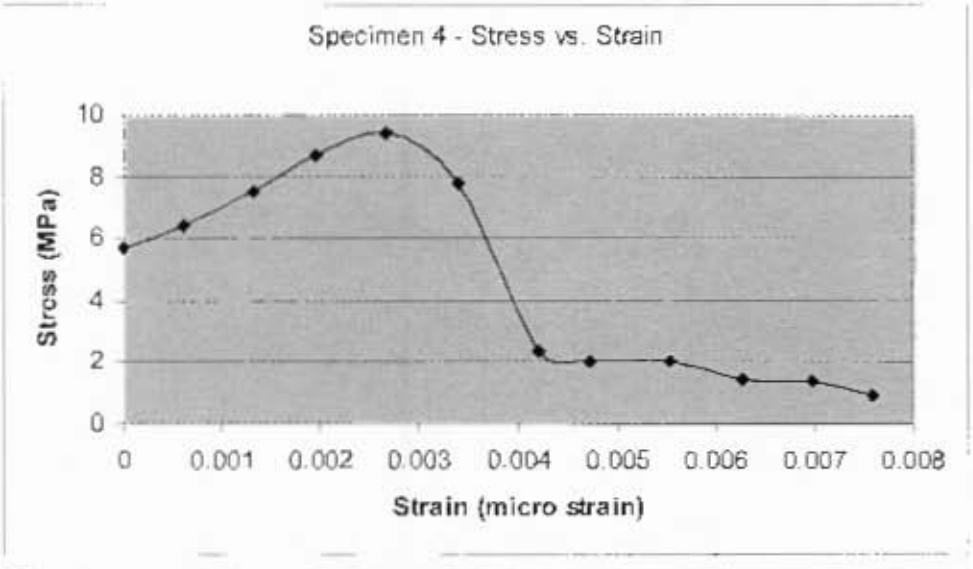

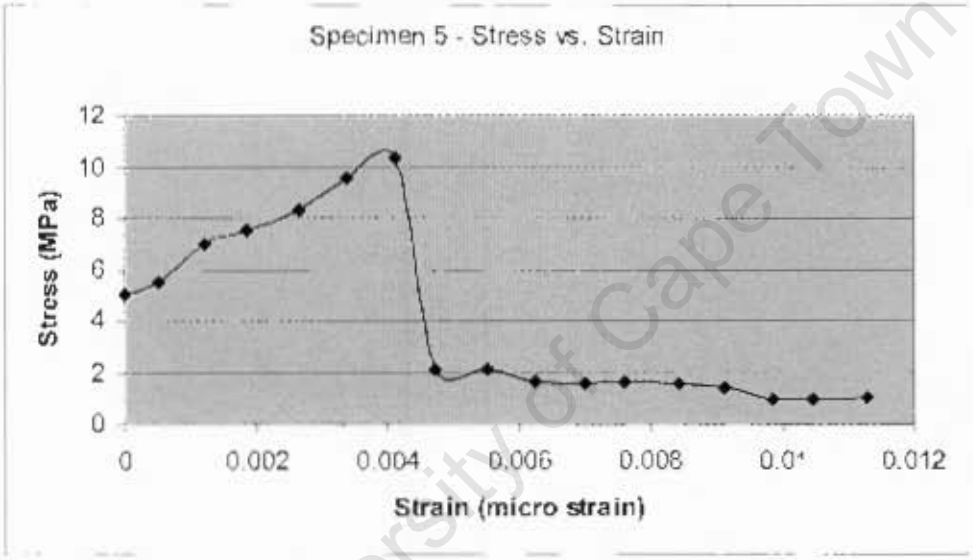

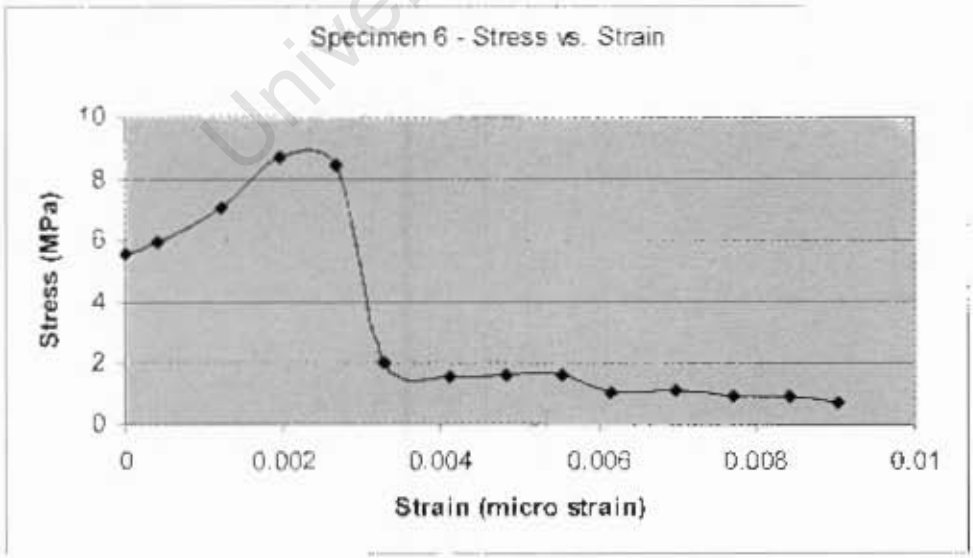

Acoustic Emission Responses for Transverse Lay-up LFVF specimens

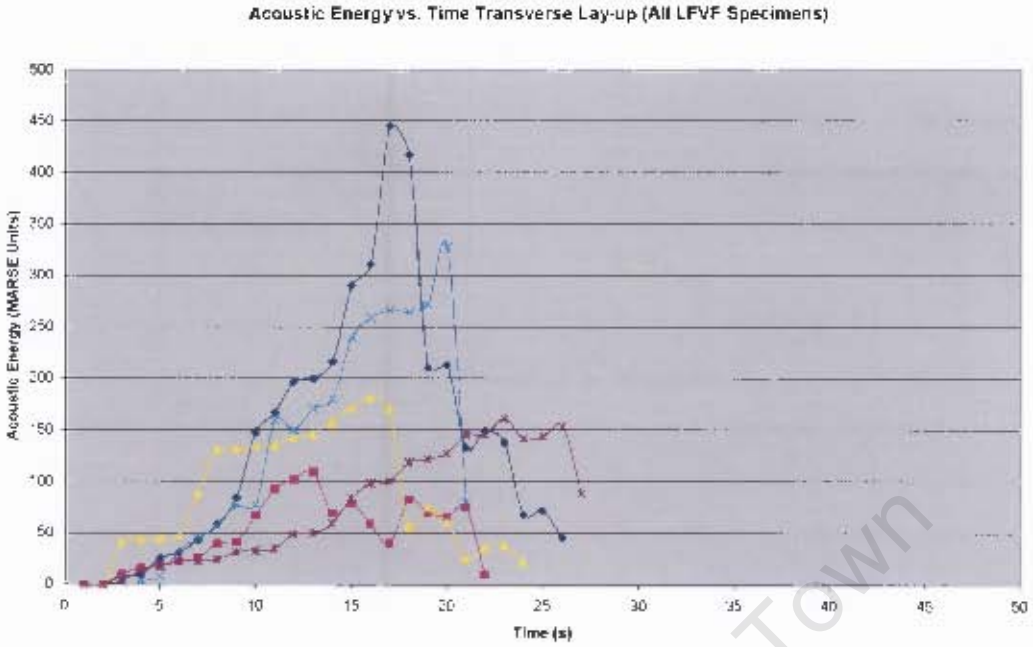

Stress vs. Strain Curves for Transverse Lay-up

HFVF Specimens

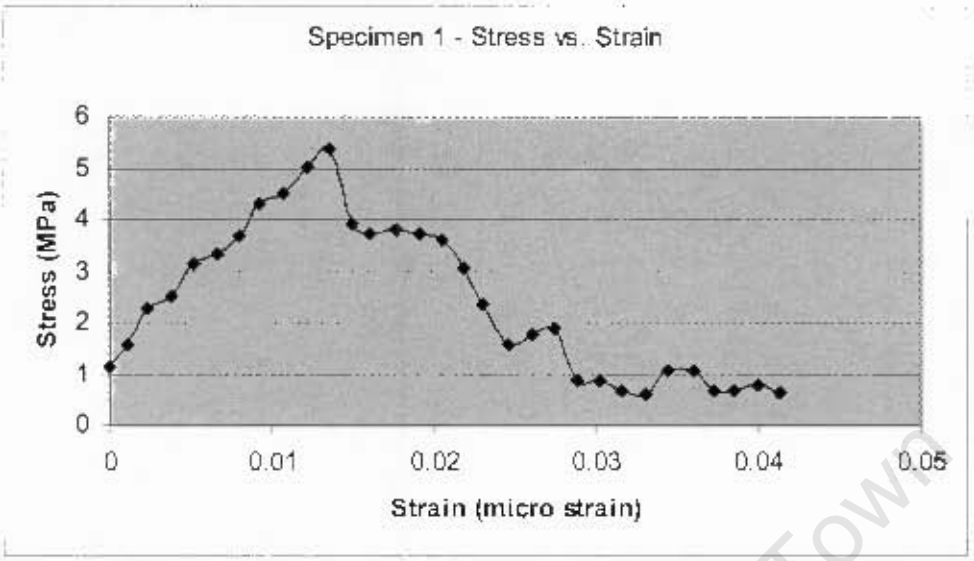

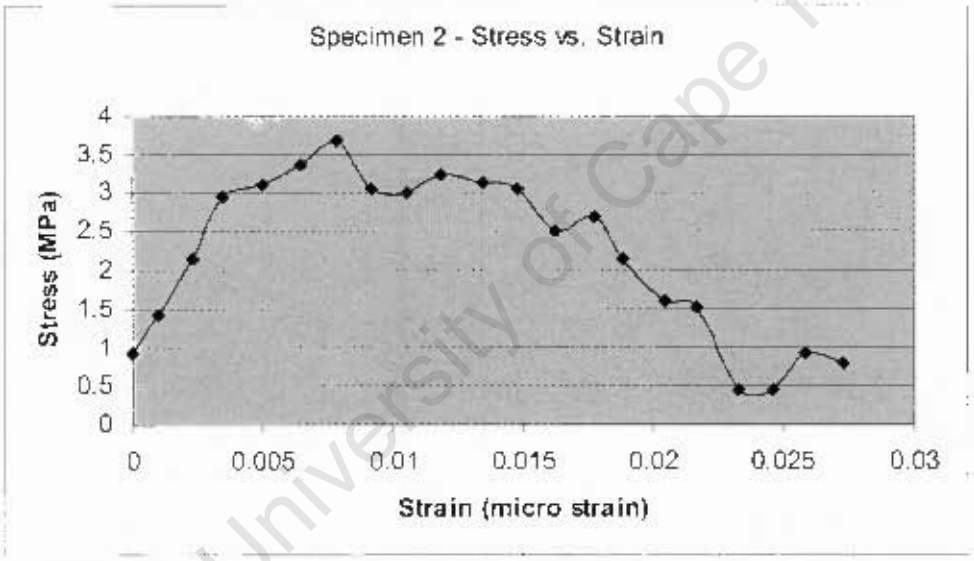

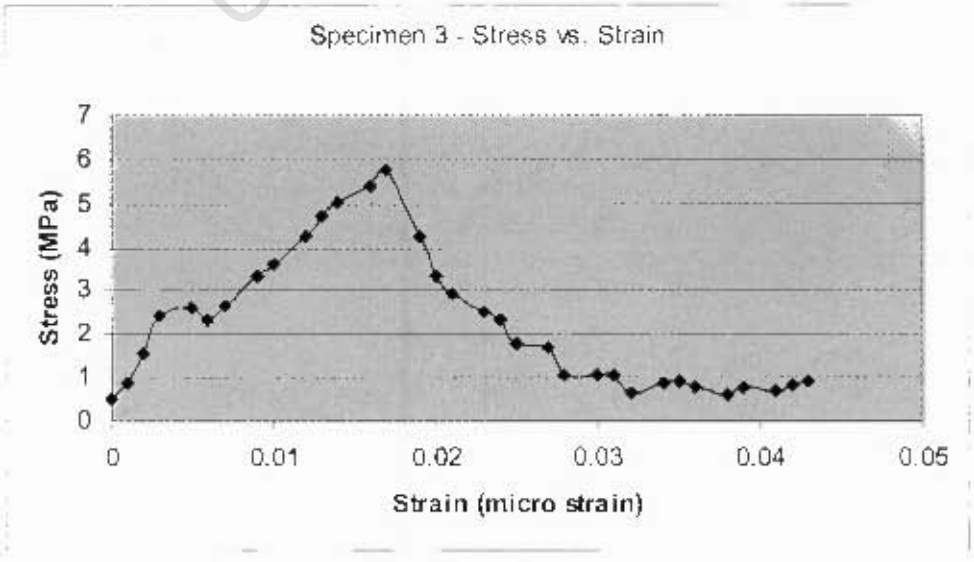

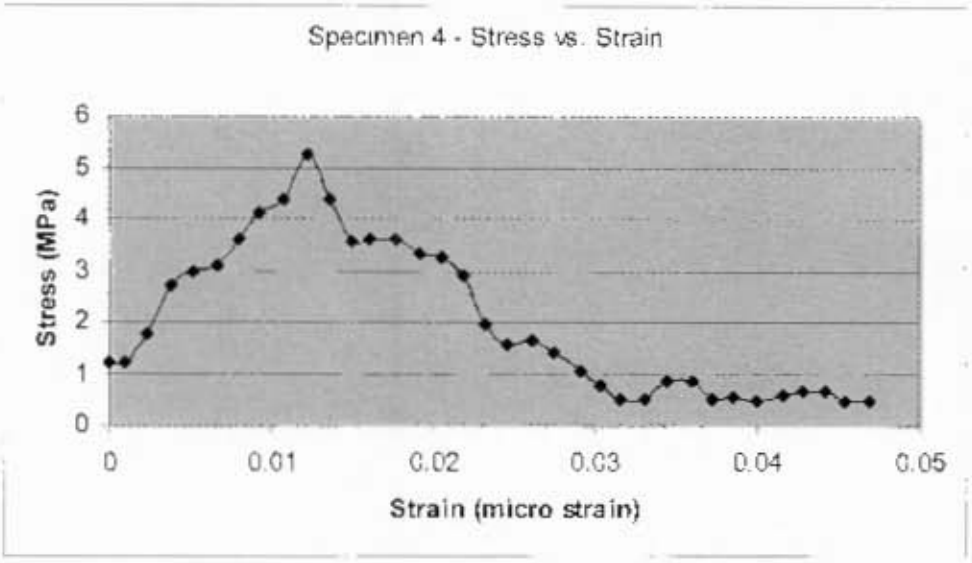

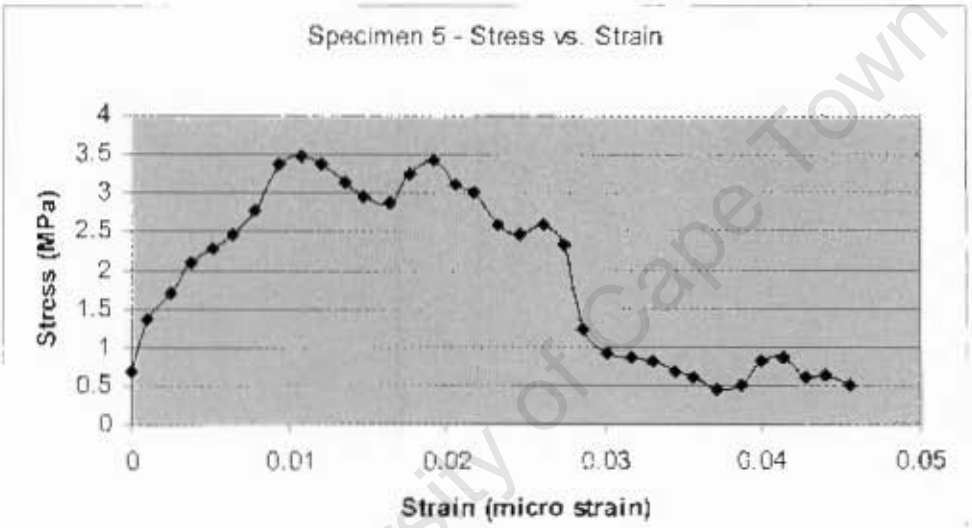

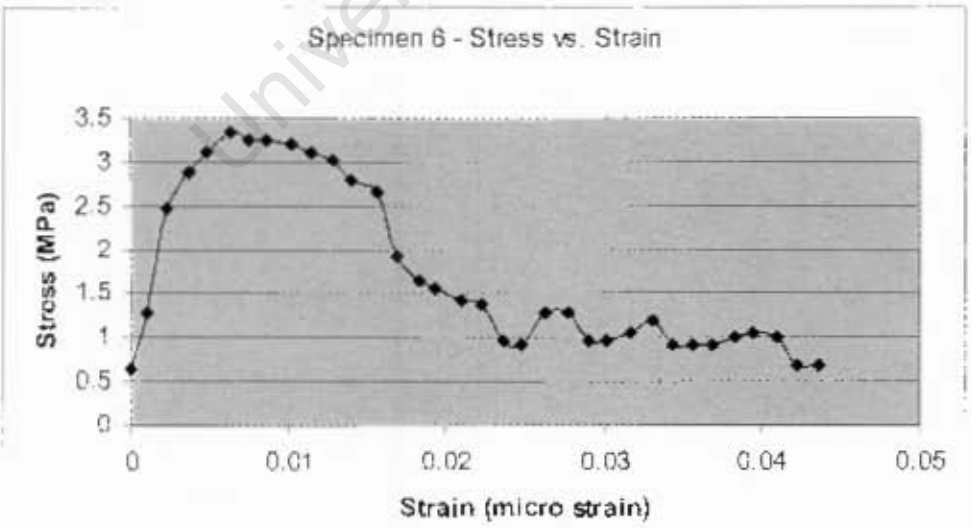

Acoustic Emission Responses for Transverse Lay-up HFVF specimens